Tampere University

Ville-Veikko Koskinen

WATER CONTACT ANGLE AND RELATED MEASUREMENTS TO QUALIFY SURFACE TREATMENTS

Master's Thesis
Faculty of Engineering and Natural Sciences
Examiners: Assoc. Prof. Mikko Kanerva,
D. Sc. Jarno Jokinen,
M. Sc. Pauli Hakala
01/2022

ABSTRACT

Ville-Veikko Koskinen: Water contact angle and related measurements to qualify surface treatments
Master's Degree
Tampere University
Master's Programme in Materials Science and Engineering
01/2022

The purpose of this work is to determine if water contact angle (WCA) and other measurements can be used to qualify the surface treatments for adhesive bonding in composites. In adhesive bonding, the surface condition is critical in order to form a good bond. This work will focus on adhesive bonding of carbon fibre reinforced plastic (CFRP) structures and the use of WCA to determine if the surface conditions are acceptable and the WCA measurement repeatable and reliable.

The first thing to consider is if WCA measurements can indicate distinguishable measure for differently treated surfaces. This was done by conducting contact angle (CA) measurements on surface treated CFRP surfaces with four different probe liquids. This provides information on the surface conditions such as the surface energy and its components.

For the WCA to be accurate, the aspects affecting WCA value should be scouted. This one was done using drop shape and time relation testing. Also, it was studied how does the measurement location affect WCA. This was done by changing the view angle on a selected sample surface and by increasing the measurement time – to see when the water droplets will evaporate from the surface at some point. In practice, the time between surface preparation and the actual bonding process can vary in reality. For this, laboratory environment contamination testing was used. WCAs were measured using eight hours of observation time in total.

Based on the results, CA measurements were able to distinguish the surface treatments from one another. The difference in the polar component of surface energy was substantial between untreated and treated surfaces. This made it possible to use water as probe liquid since water is affected by the change in polar component – noting that this is favoured for good bonding. Other tests proved that CA values depend on the view angle, proving unideal droplet shapes. The evaporation behaviour seemed to be linear and in line with standard surfaces, such as glass. A long observation time provided data with a slight fluctuation of CA values over time, but they were still in line with the standard deviation.

Keywords: Composite, Adhesive, Adhesive bond, Contact angle, Surface treatment

TIIVISTELMÄ

Ville-Veikko Koskinen: Veden kontaktikulman hyödyntäminen pinnan muokkauksien kelpuuttamiseksi
Ylempi korkeakoulu tutkinto
Tampereen yliopisto
Materiaalitekniikan DI-ohjelma
01/2022

Tämän työn tarkoituksena on määrittää, mikäli veden kontaktikulmaa tai muita mittauksia voidaan käyttää apuna pinnan muokkauksissa komposiittien liimaliitoksia varten. Onnistunut pinnanmuokkaus liimaliitosta varten on äärimmäisen tärkeää lujan liitoksen varmistamiseksi. Tämä diplomityö keskittyy hiilikuituvahvistettuihin komposiitteihin ja mahdollisuuteen käyttää veden kontaktikulmaa pinnan tilan varmistamiseksi liimausta varten.

Ensimmäiseksi varmistetaan, että veden kontaktikulmamittauksella voidaan erotella eri pintakäsittelyin muokattuja pintoja toisistaan. Tämä toteutettiin käyttämällä neljää eri mittausnestettä kontaktikulmien määrittämiseen. Näistä tuloksista voitiin myös määrittää pinnalle sen kokonaispintaenergia sekä pintaenergian komponenttien arvot, jotka antavat tarkkaa tietoa pinnan muokkauksen tilasta.

Oleellista on tarkastella, onko veden kontaktikulmamittaus tarpeeksi tarkka, toistettava ja luotettava menetelmä ja mitkä tekijät vaikuttavat sen absoluuttiseen lukuarvoon. Pisaran muodon sekä ajan vaikutusta mittauksiin tutkittiin seuraavaksi. Lisäksi pisaroiden mittauspaikat pinnalla taltioitiin mittauspaikan tarkan sijainnin (jolla eksakti karheus, materiaali) vaikutuksen määrittämiseksi. Mittauksen katselukulmaa varioitiin pisaran muodon ja kontaktikulman yhteyden löytämiseksi. Myös seuranta-aikaa tarkasteltiin, jotta nähtäisiin, millainen vaikutus sillä on kontaktikulmaan. Laboratorio-olosuhteissa seurattiin kahdeksan tunnin ajanjaksona kontaktikulman muuttumista olosuhteiden vaikutuksesta ja suhteessa pinnan muokkauksen tekemisestä.

Tulosten perusteella kontaktikulmamenetelmä pystyy erottelemaan eri hiilikuitukomposiittien pinnan muokkaukset toisistaan. Pinnan polaarikomponentti kasvaa työssä tehtyjen pinnanmuokkauksien seurauksena, mikä parantaa yleisesti liimaliitoksia. Vesi reagoi vahvimmin polaarikomponentin muutoksiin, joten vesi sopii nesteenä mittauksiin hyvin. Saadut kontaktikulman arvot riippuvat katselu- eli mittauskulmasta. Mitatuissa materiaaleissa, pinta ei näytä imevän vettä, vaan kulmamuutos johtuu lähinnä haihtumisesta, koska sen muutos ajan suhteen oli sama kuin lasipinnoilla.

Avainsanat: Komposiitti, Liima, Liimaliitos, Kontaktikulma, Pintakäsittely

PREFACE

I would like to acknowledge and give my thanks to my mentors and other personnel who have been a part of the thesis work. Special thanks to the Finnish Defence Forces Logistics Command for funding this thesis.

Tampere, 18 January 2022

Ville-Veikko Koskinen

CONTENTS

LIST OF FIGURES

LIST OF SYMBOLS AND ABBREVIATIONS

AC	Advisory circulars
ATL	Automatic tape laying
CA	Contact angle
CA(r)	Right contact angle
CA(l)	Left contact angle
CA(m)	Average contact angle of the right and left
CF	Carbon fibre
CFRP	Carbon fibre reinforced plastics
BF_3	Boron trifluoride
DDS	Diaminodiphenyl sulfone
DGEBA	Diglycidyl ether of Bisphenol A
EVA	Ethylene vinyl acetate
FRP	Fibre reinforced plastics
MEK	Methyl ethyl ketone
NDT	Non-destructive testing
PAN	Polyacrylonitrile
PTFE	Polytetrafluoroethylene
Q-Q plot	Quantile-quantile plot
SFE	Surface free energy
SLJ	Single lap shear joint test
StDev	Standard deviation
TGMDA	Tetraglycidyl methylenedianiline
WBL	Weak boundary layer
WLP	White-light profilometry
XPS	X-ray photoelectron spectroscopy

G	Fracture energy release rate
G_C	Fracture energy
K	Fracture stress intensity factor
K_C	Fracture toughness
θ	Static contact angle
θ_{eq}	Equilibrium contact angle
θ_A	Advancing contact angle
θ_R	Receding contact angle
γ	Total surface energy
γ^d	Dispersive component of surface energy
γ^p	Polar component of surface energy
γ_{LV}	Surface energy of liquid-vapour interface
γ_{SL}	Surface energy of solid-liquid interface
γ_{SV}	Surface energy of solid-vapour interface
γ_{LV}^d	Dispersive component of liquid-vapour interface
γ_{LV}^h	Hydrogen-bond component of liquid-vapour interface
γ_{LV}^p	Polar component of liquid-vapour interface
γ_{LV}^{LW}	Lifshitz-van der Waals component of liquid-vapour interface
γ_{LV}^+	Lewis acid component of liquid-vapour interface
γ_{LV}^-	Lewis base component of liquid-vapour interface
γ_{SV}^d	Dispersive component of solid-vapour interface
γ_{SV}^h	Hydrogen-bond component of solid-vapour interface
γ_{SV}^p	Polar component of solid-vapour interface
γ_{SV}^{LW}	Lifshitz-van der Waals component of solid-vapour interface
γ_{SV}^+	Lewis acid component of solid-vapour interface

γ_{SV}^{-}	Lewis base component of solid-vapour interface

1. INTRODUCTION

Composite adhesive bonding

The use of composites has become prominent in the transportation industry. This has been a trend in the aircraft manufacture for years, but a shift to the automotive and rail manufacture can be seen. Composites provide attractive strength and stiffness to weight ratio, which is beneficial in many different products. Lighter products use less energy during their service life, for example, a lighter car gets better mileage. The replacement of traditional materials with composites brings a new set of challenges. A challenge when using composites is joint design. Adhesive bonding and adhesive joints are common for composite structures due to their lightness. Adhesive bonding has decisive strengths when compared to more traditional mechanical joints. The ability to bond dissimilar materials and the possibility to have a smoother stress distribution are the strengths of adhesive bonding. As with all technologies, adhesive bonding is not without problems. The uncertainty of good bonding brings up the need to find new methods of ensuring successful surface treatments.

The quality of an adhesive bond is difficult to determine via non-destructive methods. This is because there is not a single non-destructive testing (NDT) method that could indicate all of the possible flaws. A so-called kissing bond is an example of a flaw that cannot be indicated by current NDT methods. A kissing bond seems like a good bond but, in reality, fails at a low load. Kissing bonds can be the result of poor surface conditions at the time of bonding. Surface conditions at the time of bonding activities are critical in creating a good adhesive bond. Surface conditions and the possibility to ensure and qualify that the results are acceptable is the key point for this M.Sc. thesis work. Surface energies can give valuable information about the surface condition in general. At the time of ideal adhesive failure, the fracture energy is the same as the work of adhesion. Work

of adhesion can be calculated in theory using the CA measurements. Surface energies can also be determined using a CA of a liquid drop on the solid surface.

Thesis objective

CA measurements can be performed using a drop shape analyser, which is utilized in this thesis. The research objectives for this thesis are:

1. Experiments to determine surface energies and its components of differently surface treated carbon fibre reinforced plastic (CFRP) laminates.
2. The experimental sensitivity analysis of factors affecting water contact angle (WCA) on CFRP laminates.

Firstly, this thesis will cover adhesive bonding and composite structures and materials used in the current literature as the background of the thesis. In my case, CFRP composites will be the main focus of the adherend materials. In general, the curing of the (epoxy) resin is an important part of composite manufacturing as well as adhesive bonding. Different failure types (in adhesive bonds) will be discussed as they reveal information on which part has been the weakest link in a bonded structure. Before going into the CAs, the theories and forces behind adhesion will be covered. The theory behind CAs and their link to adhesive bonding and joints are the last sections in the background chapter before the Experimental chapter. Results and analysis will cover the results from the experiments and analyse the findings. The Discussion chapter goes over the findings from the Results and Analysis chapter and summarizes its key points. The conclusion will gather the most important points of the work and cover if the thesis objectives were achieved.

2. ADHESIVE BONDING OF COMPOSITE STRUCTURES

Adhesive can be defined as material, which joins surfaces together and resists separation (1). The principal substance in adhesives is a certain organic polymer, or several compounds, which can chemically react to produce the 'polymeric system' in adhesive. The adhesive product must be able to form an intimate or direct contact at the time of application. This is to ensure wetting of surface by adhesive. Then, adhesive either solidifies (meltable polymers), cures (thermosets) or polymerizes (reactive polymerization) and finally becomes a solid. An exception to this is the group of the so-called pressure-sensitive adhesives that remain in the solid state in all the stages of operation. (1,2)

2.1 Needs and advantages

Mechanical joints are popular in engineering applications. However, for some materials, their usage is disadvantageous, or they simply cannot be used. This can be because of functional design requirements, e.g. transparency to electromagnetic signals for radomes. Materials may not be suitable for particular joining methods, such as welding. Also, costs or the long-term durability of might limit the type of joining technology. (1-3)

Adhesively bonded joints are used as an alternative and have gained popularity. The advantages of adhesive joints are numerous. The main ones are the uniform distribution of stresses and a larger stress-bearing area when compared to mechanical joints. The possibility to join dissimilar materials and different shapes easily although some material limitations still apply. Possibility to use additives to improve properties such as electrochemical corrosion resistance, insulation against heat transfer and electrical conductance. Vibration and shock absorption are inherent due to the elastic nature of adhesive

bonds. Adhesive bonds do not require a lot of added material which benefits the attractive strength to weight ratio they have compared to mechanical joints. (1,2)

The aeronautical industry is one of the precursors in the usage on adhesively bonded joints in advanced structures. The automotive and rail industry have started to use composite adhesive bonding to reduce the weight of the vehicles. (1-3)

2.2 Carbon fibre reinforced composites

Composite materials can be classified as a system of two or more materials working in combination resulting in better properties in the composite system than the individual materials have. Usually, an advanced composite system consists of a fibrous reinforcement and the matrix components distributing loads in the system. Fibres can be various, for example, glass, aramid or carbon, and they might be continuous or discontinuous depending on the application. The matrix component can be polymer, metal, or ceramic. (4,5) This work will focus on specific epoxy-based polymeric matrix and carbon fibres.

2.2.1 Carbon fibre

Carbon fibres (CF) were used already in the late 1800s in lightbulbs. These fibres did not have the mechanical properties that the high-performance, structural CF have in composites nowadays. (4,6) In the 1960s, William Watt and colleagues discovered a technique for converting polyacrylonitrile (PAN) precursor fibres into carbonized fibres. This was a huge upgrade compared to CF produced from rayon a few years earlier. Rayon CF only contained 20% carbon, making the mechanical properties poor. Various fibre reinforced plastics (FRP) were known at the time, but the Watt's accomplishment made the structural composites a reality. (6) Currently, CF can be made from rayon, pitch, or PAN fibres. PAN is used extensively for structural CF because of the high carbon yield compared to rayon and high strength compared to pitch-based fibres. CF produced from pitch can have an ultrahigh modulus (values from 340 to over 1000 GPa). (4)

In Figure 1, the processes to make CF from PAN and pitch are shown. The PAN process starts with the stretching of the fibres to orient the molecules and maintain the tension of the fibres through the process. The oxidation process cross-links the PAN fibres to stabilize them preventing the melting during the carbonization process. The oxidation process temperature is usually between 200-300 °C and atmospheric air is used. Carbonization is done between 980-1595 °C using an inert atmosphere like in nitrogen. During

this step of the process, the fibres reduce in diameter and lose up to 50% of their weight. (4-6)

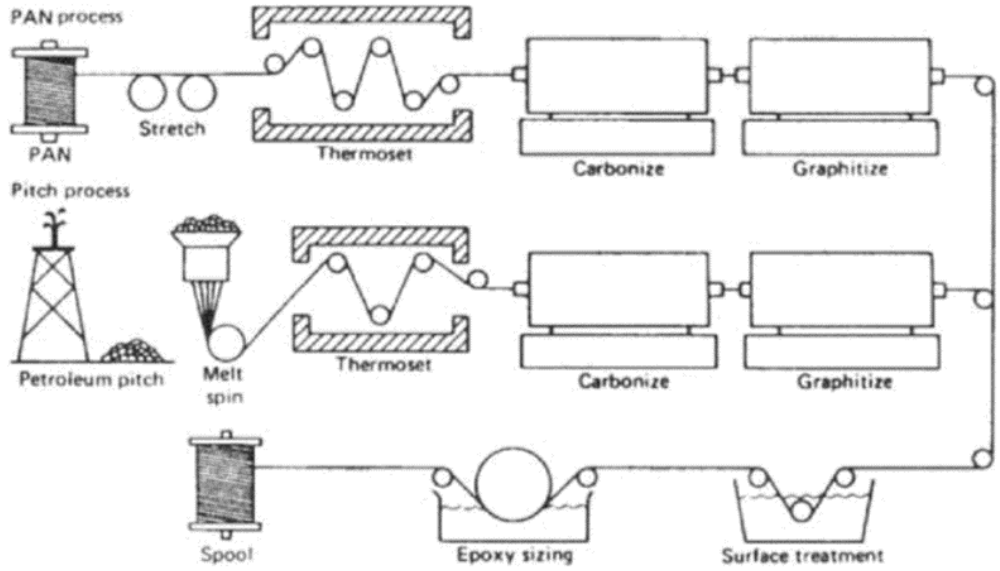

Figure 1. *Processes for manufacturing carbon fibres* ***(5)***

Carbonization results in carbon having a network of hexagonal ribbons. This type tends to align parallel to the fibre's long axis. The crystal structure is very small, which contributes to its high strength. (4)

After the desired carbon content has been reached, fibre surface treatment is applied. First surface treatment typically improves the processability of the fibres. This layer protects the fibres against mechanical abrasion and helps the handling of the fibres. (4,5) Sizing is the final step of the process. Sizing is critical for good interlaminar adhesion. Sizing chemicals can alter the surface characteristics of the fibre dramatically, increasing composites shear strength and shear stiffness. This is done by improving the fibre-to-matrix bonding. Typically, an electrolytic alkaline bath is used. Electrolytic oxidation removes the weak surface layers, etches the fibres and forms reactive or polar groups. These include carboxyl, carbonyl, and hydroxyl groups. The surface generated increases the adhesion to thermosets and some thermoplastic resins. (7) CF that will be woven, are usually protected with uncatalyzed epoxy. (4,5)

The other method of making CF is to use pitch, which is shown in Figure 1. Coal tar pitch is heated up to 40 hours at 425 °C. This forms a highly viscous liquid with a high degree of molecular order, also known as mesophase. A small orifice is used to spin the

mesophase aligning the molecules along the fibre axis. After this, the process continues as with the PAN based fibres.

2.2.2 Prepreg system

Prepregs are reinforced laminae products, which have been pre-impregnated with a resin system. Protective layers are present on the laminae to avoid contamination and sticking while transportation or storage. Airtight bags can be used for storing, which must be in a refrigerator for most resins. Prepregs are commonly manufactured using epoxy resins and CF. (5,6)

Prepregs are very common in advanced composite manufacturing, which includes high-end materials such as CF composites. The first generations of prepregs required careful handling and packaging. The worker using the prepreg products needed lots of knowledge and practice to use them effectively. Currently, prepregs are much easier to transport and use, making manufacturing more accessible and lowering labour costs. Freezing temperatures are mandatory for storing the uncured materials within shelf-life. (6)

Currently, a prepreg product forms a single fibrous layer, which can be woven or unidirectional in its configuration. Custom fibre orientations can be used depending on the application. The resin embedded is in the so-called B-stage (or β-stage). This B-stage resin is partly cured and is capable of ‘flow’ during the cure cycle at elevated temperature. In room temperatures, prepregs are sticky and adhere on surfaces. This makes the lay-ups (stacks) of prepregs easier to compile. Prepregs are provided with specified resin contents. Some prepregs contain an excess of resin that bleeds out during the curing process. Other differences are fibre areal weight and cured per ply thickness. (4-6)

Prepreg manufacturing methods are hot melt impregnation, resin filming and solvent impregnation. Different methods provide different products which are supplied as narrow or wide unidirectional tape, roving or woven cloth. Figure 2 shows what unidirectional

and woven cloth type prepregs consist of. Both sides of the prepreg film are protected by a protective film. (4-6)

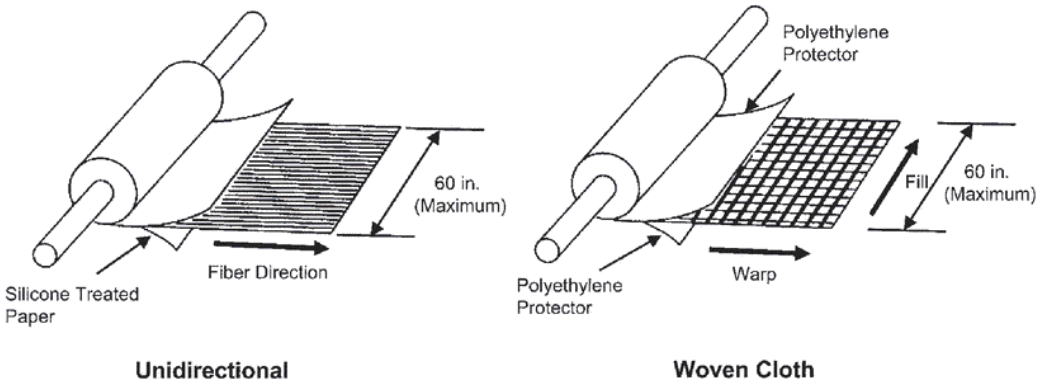

Figure 2. *Unidirectional and woven cloth prepreg films* ***(4)***

The hot melt process is shown in Figure 3. The fibres are fed from a creel, collimated, and impregnated with melted resin. The cooling is done immediately after impregnation before the prepreg film is spooled on a roll. The resin filming process is newer compared to the hot melt process. In Figure 4, the start of the resin filming process is shown. The resin system is applied to the backing paper, making it possible to control the thickness of the resin layer. The film is then spooled on a roll and can be used for prepreg products or frozen for later use (e.g., as interleaving or resin films).

Solvent impregnation is used on towpreg, woven fabrics and high temperature resins that must be dissolved in solvents and cannot be manufactured otherwise. There is a possibility that some of the solvent will remain in the prepreg. The remaining solvent can compromise the curing process when parts or laminae are manufactured. The fabric used is dipped in a tank of resin solution and then passed through roller nips to control

the amount of resin on the prepreg. The hot-air oven is used to get rid of the remnant solvent before the material is spooled up. (4-6)

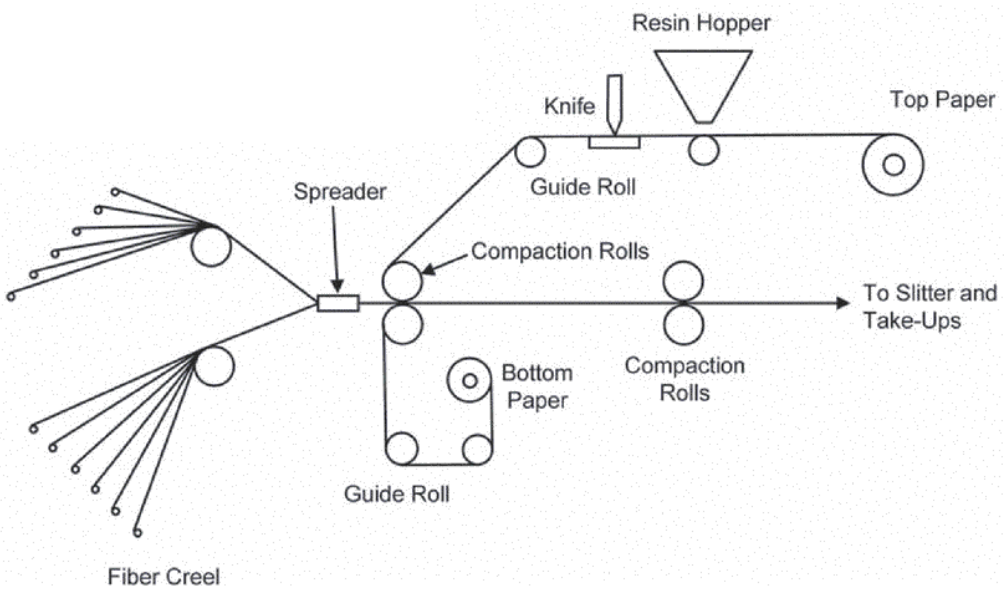

Figure 3. *Hot melt resin impregnation process* ***(4)***

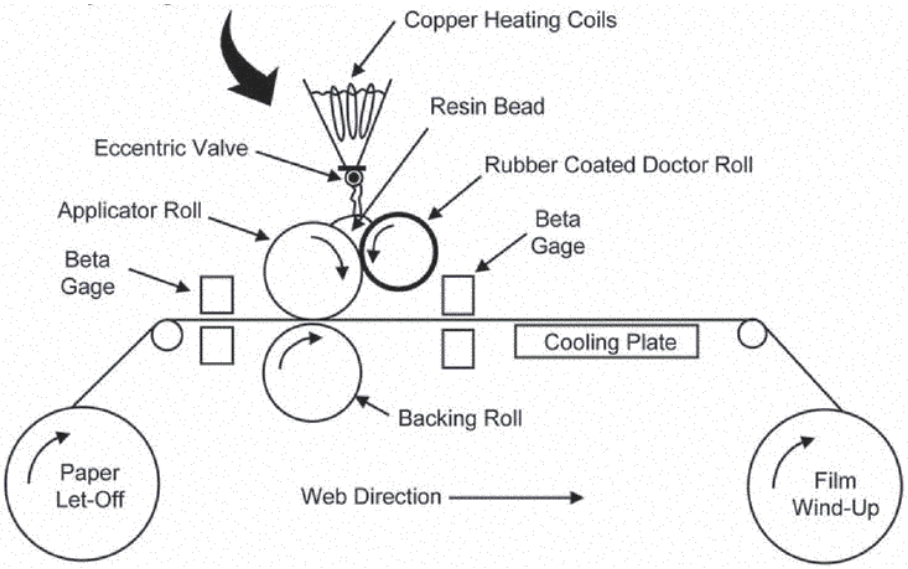

Figure 4. *Resin filming process* ***(4)***

2.2.3 Lay-up process of composite laminae

CFRP have usually limited structure, similar to other continuous-fibre composites. This means that the structure is created from individual layers of plies or laminae that have been stacked. The laminae are usually oriented in a designed way depending on the load direction of the component. The fibres in the laminae carry longitudinal tension and

compression load while the matrix material distributes the load between fibres. Interlaminar forces are carried by the matrix. The fibre strength can be around 3.4 GPa and the polymer matrix typically around 35-70 MPa. Therefore, the orientation of the fibres is very important. These strength values change greatly depending on the fibre and matrix material used. (4,5)

Lay-up processes are used to fabricate composite structures. Lay-up can be done using different techniques which are manual lay-up by hand, automated tape laying (ATL), filament winding, or fibre placement. Large prepregs are used in manual lay-up, but it is possible to do manual lay-up using raw goods. Tape prepregs are used in ATL and fibre placement. Each of the methods has different advantages and disadvantages, depending on the number of similar parts made and their complexity. (4,8)

For manual lay-up, the plies are usually pre-cut using an automated ply cutter or by hand for small scale applications. Automated machinery can label the plies for easier are more precise knitting operations. Bond tools are coated with mould release agent or release ply is used. The plies are then placed on the mould as the drawings specify, computer software can be used to define the right ply placement. The lay-up requires debulking by vacuum every few plies depending on the application. This helps to remove air and compact the laminae. For complex parts, prebleeding or hot debulking can be used, but with the current type of prepregs, these methods are needed much less than before. Figure 5 shows how laminae are placed into a mould using a manual lay-up process. (4,8)

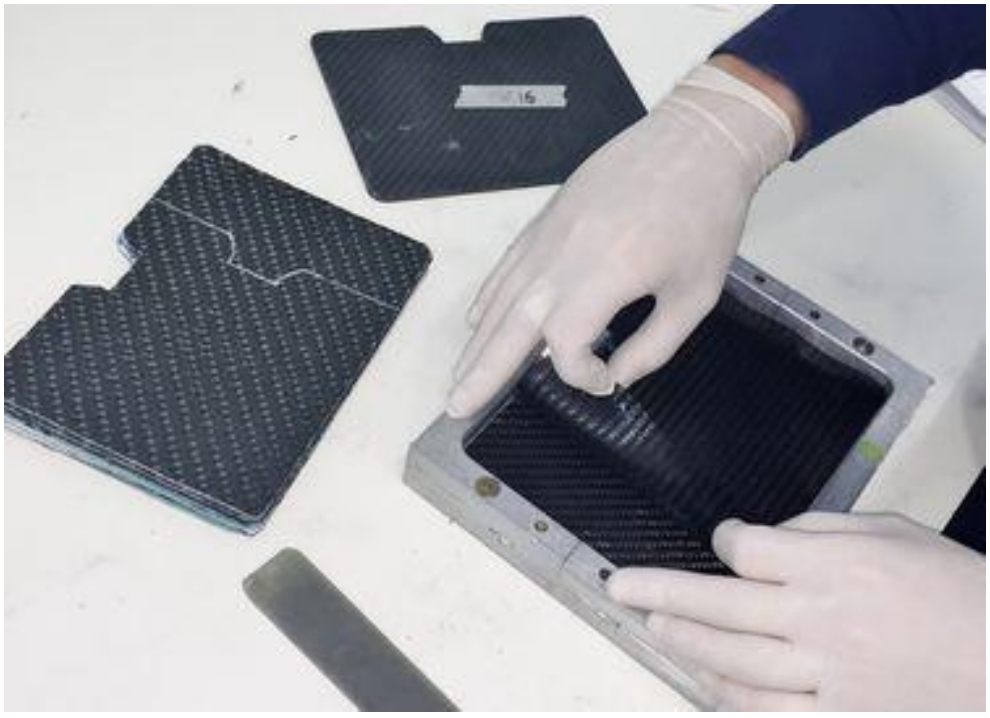

Figure 5. *Manual lay-up into a mould* ***(9)***

ATL is used for large flat parts such as aeroplane wing skins. ATL uses a unidirectional tape of different widths. ATL machinery is typically gantry based and can contain up to 11 axes of movements. The configuration depends on the mould shape and contours, which limits the width of the tape. The tape comes in spools, which are loaded into the delivery head supply reel. Modern ATL machines have optical sensors that detect faults during the tape laying process and inform the operator. The boundaries are tracked using laser systems. The ATL machine is software operated. The software records the plies applied and updates the surface geometry based on it. It can track the ply orientation and the gaps between adjacent courses. Figure 6 shows the TORRESLAYUP ATL machine which represents the modern ATL machines. It has 11 axes of movement and has been designed for high-speed tape laying. (4,5,8)

Figure 6. *TORRESLAYUP ATL machine with 11 axes of movement* ***(10)***

Filament winding is a high-speed process. There, a continuous fibre band is applied to a rotating mandrel. It is used for large, thick-walled structures of revolution like shafts, cylinders, and cones. The diameter may differ from a few centimetres to over six meters. Typical filament winding includes dry tows of fibres being drawn through a resin bath, collimated into a band, and then applied on a mandrel. There are three main variants: wet winding, wet rolled prepreg winding, and towpreg winding. There are limitations on the fibre orientation that can be used due to slippage that may occur on the mandrel ends. This can be controlled using temporary fibre pins. Dominant fibre placements patterns are helical winding, polar winding and hoop winding. After winding, the wet parts are usually B-staged before final curing. Most of these parts are cured in an oven without vacuum bags or pressure application. Only pressure comes from the mandrel expanding

due to heat, which helps avoid void and porosity from forming. Autoclaves can also be used but the part size is then limited by a greater amount. (4,5,8)

The fibre placement method is a crossover of filament winding and tape laying. It allows individual tows of prepreg to be used. The roller mechanism allows material laying to concave contours, and the compaction roller applies pressure to debulk the laminae during lay-up. Typical applications include pressure tanks, fuselage sections, nozzle cones, engine cowls, and fan blades for aerospace products. The mechanical properties achieved are similar to the hand lay-up process. The head of the machine can be steered, which makes it possible to create efficient load-bearing structures. Operation software is even more complex than in previous methods. (4,5,8)

Prepreg parts are typically cured in autoclaves. Autoclaves heat up to the curing temperature and apply pressure. A high pressure ensures the compaction of plies and suppresses void formation. Depending on the manufacturing process, autoclaves have different sizes. From laboratory use to the manufacturing of commercial aircraft parts. The largest autoclaves can be almost nine meters wide and 36 meters long. Figure 7 shows an autoclave curing set-up. The composite lay-up is in a vacuum sealed bag before entering the autoclave. Prepreg processes do not always use a vacuum bag. This is because these processes do not need added resin or have excess resin to be bled out. (3,5)

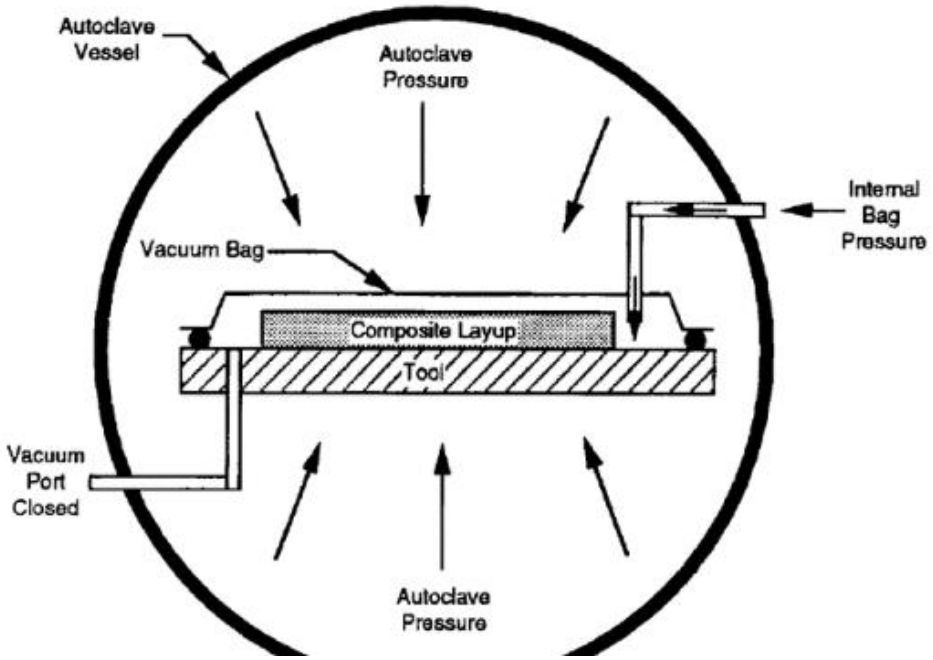

Figure 7. *Autoclave curing set-up illustration* ***(5)***

2.3 Structural adhesives

Structural adhesives are adhesive materials that have high strength and performance. Their primary function is to hold structures together and resist high mechanical loads. There are different types of structural adhesives, but the main materials used are epoxies, nitrile phenolics and bismaleimides. (2,4,5)

2.3.1 Epoxy systems

Epoxies are one of the most important groups of adhesives. They are widely used differing from basic consumer applications to high-end aerospace products. Epoxies are thermosets and crosslink during the curing cycle. Epoxies are defined by the epoxide group, shown in Figure 8. All epoxy compounds contain two or more of these groups. There are many types of epoxy resins, ranging from low-viscosity fluids to high melting point solids when compared to other thermosets. There are more than two dozen different epoxies known. (2)

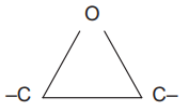

Figure 8. *Chemical structure of the epoxide group* ***(2)***

A curing agent is needed, for the cross-linking to occur. Commonly used curing agents are amines (primary and secondary) and anhydrides. Figure 9 shows the cross-linking of amine and epoxy during curing. The hydrogen atom in the amine can open the epoxide ring, creating a covalent bond. Diglycidyl ether of Bisphenol A (DGEBA) is one of the most used epoxies. It has an epoxy group on both ends of its chain, as shown in Figure 10. Epoxies can contain higher functionality, like three or four reactive epoxy groups.

Higher functionality increases the number of crosslinks, which results in high strength, rigidity, and elevated temperature resistance. (2,4)

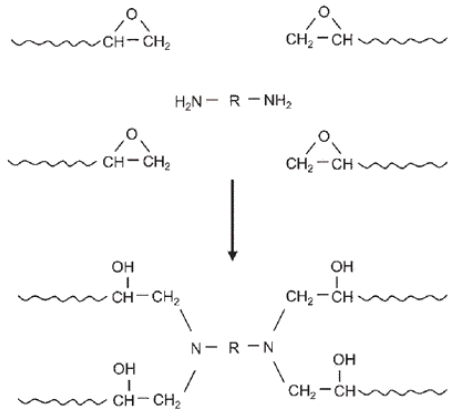

Figure 9. *Amine crosslinking reaction with epoxies* ***(4)***

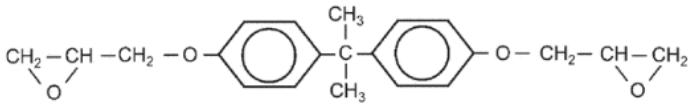

Figure 10. *Diglycidyl ether of Bisphenol A (DGEBA)* ***(4)***

2.3.2 Fillers and additives in the epoxy system

Fillers, additives, and minor epoxies are typically mixed into the epoxy resin depending on the application to adjust the properties needed. Minor epoxies are generally added to improve processability, elevated-temperature performance or other properties of cured resin. These minor epoxies include amine based phenols, novolacs, cycloaliphatics, and others. A typical composition of the epoxy matrix system is shown in Table 1. Tetraglycidyl methylenedianiline (TGMDA) is the primary epoxy and minor epoxies being Alicyclic diepoxy carboxylate and Epoxy cresol novolac. Diaminodiphenyl sulfone (DDS) is the curing agent and boron trifluoride amine complex (BF_3) is the catalyst. (2,4)

Table 1. *Typical composition of an epoxy matrix* ***(4)***

Component	Total percent (*wt*)
Tetraglycidyl methylenedianiline (TGDMDA)	56.4
Alicyclic diepoxy carboxylate	9.0
Epoxy cresol novolac	8.5
4,4' Diaminodiphenyl sulfone (DDS)	25.0
Boron trifluoride amine complex (BF_3)	1.1

Diluents are sometimes added to the resin system to reduce viscosity, improve shelf and pot life, lower the exotherm and reduce shrinkage. The amount for diluents is usually between three to five percent. Higher concentration can cause a decrease in mechanical properties. Common diluents include glycidyl ethers of butyl, cresyl, phenyl, and aliphatic alcohol. (2,4)

Curing agents are classified as additives, even when they are a requirement. The other additives which affect curing are the catalytic curing agents, as the BF_3, in Table 1. These agents promote epoxy-to-epoxy or epoxy-to-hydroxyl reaction. These catalytic curing agents do not serve as crosslinking agents, even if they produce highly crosslinked structures. They also have a long shelf life. Anhydride curing agents need high temperatures and long curing times to achieve full curing. Anhydrides generally have long pot life and low exotherm. They provide good high-temperature properties, chemical resistance, electrical properties and lower viscosity when blended with epoxy. (2,4)

2.3.3 Adhesive types

Adhesives come in different types, which are paste and film. Different pastes are common in different industries and are supplied for general use. Common paste adhesives include polyurethane construction adhesives. Adhesives are also supplied in film or tape form. The main benefits of film adhesives are uniform thickness and application process. Compared to paste adhesives, film adhesives are used in high end applications due to their precision and applicability. Film adhesives can be supported by a (knitted) fabric carrier. This fabric will carry part of the load and provide improved bond toughness. The fabric can be made from glass, polyester, nylon or paper. (2) Figure 11 presents a type of film adhesive used for the target application in this work.

Figure 11. *FM 300-2 film adhesive*

2.4 Adhesively bonded composite structures

Adhesive bonding can be used with different materials. It is common to bond composite structures and laminates to metals, such as aluminium and titanium. This practice is used commonly in aerospace manufacturing. This work will focus on the composite to composite adhesive bonding. Depending on the state of composites the bonding process can be done in several ways which will be discussed in the next sections. Composite to composite bonding can be used for difficult geometries and composite repairs. (1,4,5,8)

2.4.1 Surface treatments for adhesive bonding

To achieve a good adhesive bond, the condition of the surface at the time of bonding is critical. There are several techniques to prepare the surface for adhesive bonding in composites. The usage of peel plies is one of these methods and it has become quite popular. Peel ply is typically woven fabric made from nylon, polyester, or fibreglass. The exact material of the peel ply will depend on the resin used in the composite. It is applied on the outer surface of the composite at the lay-up process before curing. (1,4,5,11)

As the name suggests, peel ply is torn from the surface before adhesive bonding. The peeling will break the resin surface along the peel ply. This reveals a clean and roughened surface for adhesive bonding. Depending on the application, additional surface treatments, such as hand sanding can be used. This ensures that release agents that can be present on the surface are removed. For some applications, the removal of the thick epoxy layer is necessary to improve the mechanical properties of the adhesive bond. Nevertheless, peel plies are highly effective and easy to use in composite manufacturing to prevent surface contamination. (1,4,5,11) Plastic treatments such as flame and corona can be used on composites to improve adhesion. (2,3) In addition to peel ply, different surface treatments are applied. These include solvent cleaning (12), grinding (12), grit blasting (12,13), chemical etching (12,14), and plasma treatments (12-15). Different laser treatments are also being tested (16).

In the scope of this work, grinding (sanding) is the main surface treatment with solvent cleaning. Sanding can be done with a machine or by hand. The main point is to remove the epoxy layer left from the removal of the peel ply and reveal CFs. The amount of material removed will depend on the type of laminate and the surface preparation procedure. It is possible to visually approximate the state of material removal. Sanding epoxy will yield greenish coloured sanding dust and when CFs are being sanded, black

dust will appear. The level of sanding can be controlled by these visual indicators. Solvents can be used to clean the surface of the sanding residue and other contaminants. These types of surface preparation methods are used for aircraft composites.

2.4.2 Water-break test

Different methods have been used to ensure the quality of the surface treatment and possible surface contamination. One commonly used method is the water break test. It is a cheap and easy method to use, compared to more technical methods, such as the FTIR analysis. Water-break test can be used for different surface materials and is used by different industries for this reason. Figure 12 shows the principle of the water break test. Water is poured or spayed on the surface and contaminated areas can be seen where the water film is broken. The areas which are chemically active or polar will hold the water film. (10,17,18) The amount of water used and the angle the surface is depends on the operator. There is no global standard and different manufacturers will have their procedures. Depending on the material, the drying of the surface might be needed before adhesive can be applied on the surface. This drying process can give information on how the surface is prepared, by observing how the water evaporates from the surface when a heat gun is used to dry the surface. Water that is left on the surface, can compromise the curing process by evaporating and creating pressure. (10,17,19)

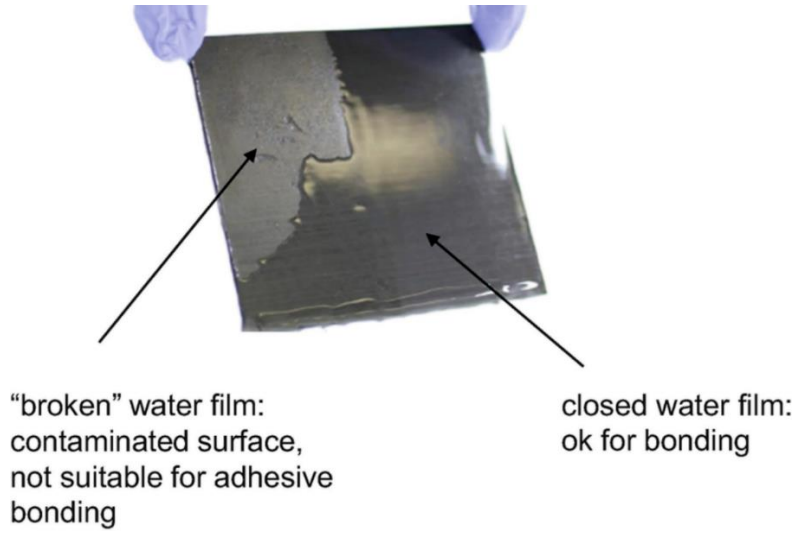

Figure 12. *Water break test principle* ***(10)***

WCA measurements can provide the possibility to test the surface before bonding to qualify for successful surface treatment and lack of contamination. The scope of this

thesis is to make such measurements and validate whether the usage of WCA measurements can be utilized in such a way or not.

2.4.3 Bonding process

Adhesive bonding on structures can be done in different ways. They can be classified into four cases, depending on the state of the materials at the start of the bonding process. These four cases are secondary bonding, co-bonding, co-curing without adhesive, and co-curing with adhesive. In Figure 13 the different cases of bonding are shown. In secondary bonding, the laminates or parts are already cured and only the adhesive film will need curing to bond. In co-bonding one of the composite laminates are cured, but the other is in the wet state. The adhesive film is used between the cured and uncured parts. Co-curing without adhesive has both laminates as uncured and does not require an adhesive film to be used, relating closely to the lay-up process of prepregs. Co-curing with adhesive has uncured laminates, but the adhesive is used between to form the bond. (3,20)

The actual curing process will depend based on material and different methods are covered in next section 2.4.4 Cure techniques. Secondary bonding is the main bonding process of interest in the scope of this work.

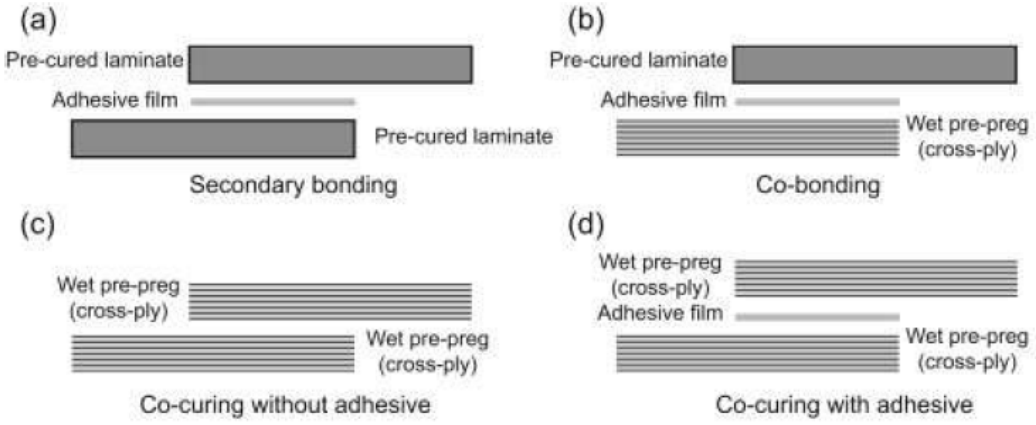

Figure 13. *Adhesive bond curing* ***(21)***

2.4.4 Cure techniques

The curing process differs based on the adhesive that is used. Curing (hardening) can be achieved in different ways. Adhesives that harden by the loss of solvent are polymer solutions in an organic solvent. Neoprene (polychloroprene) adhesives are good examples of these. Application is done on both surfaces and little time for evaporation is given

before surfaces are pressed together. The bond that forms is resistant to oils and chemicals. These types of adhesives are very common and are purchasable in form of butadiene and acrylonitrile in an organic solvent. (1,2)

Adhesives that harden by the loss of water are in higher demand due to environmental and health and safety regulations. Solvent-based are being replaced by water-based adhesives. Water-based systems have few fundamental problems. Water has a high enthalpy of vaporization which makes the evaporation slow. The water-based latex adhesives have a high absorption of water and the joints are sensitive to water presence. Starch is a good example of adhesive which hardens by the loss of water. It is used mainly for bonding paper and board. Latex adhesives are mainly used on wood since wood material absorbs the water making hardening easier. (1,2)

Adhesives that harden by cooling are hot melts. They are applied to the substrate as a hot liquid, and they quickly form an adhesive bond as they cool. They are used on non-metals, as metal tends to conduct heat too rapidly. Ethylene-vinyl acetate (EVA) hot melts contain up to 30% vinyl acetate. They also contain different fillers and additives depending on the application. Tackifiers can be added to reduce viscosity and improve wetting. Wax is used to reduce cost and viscosity. Calcium carbonate is used as a filler to lower costs and increase viscosity. Antioxidants are used to improve service life. The use of EVA includes cardboard boxes and bookbinding. Polyamide hotmelts are like EVA but have better heat resistance and higher cost. They either do not need additives. (1,2)

Adhesives, which harden by chemical reactions, are most commonly and widely used in the form of epoxies. They contain epoxy resin and different hardeners such as amines and anhydrides. The benefit of this is that no volatiles are formed during hardening and the shrinkage is low. They can cause skin diseases so safety equipment must be used. The chemical bonding occurs between the epoxy group and the amine-hydrogen bond. When aliphatic amines are used, the curing can be done at room temperature. Elevated temperatures generally make the curing process faster. Aromatic amines require an elevated temperature to cure, around 150 °C for two hours. Other adhesives, which harden by chemical reaction, include phenolic adhesives for metals, acrylic adhesives, formaldehyde condensate used for wood, anaerobic adhesives, cyanoacrylates, polyure-

thanes, silicones and polysulfides. Temperature is also limited by the process, for secondary bonding the curing temperature used for adhesive cannot exceed the temperature limit of pre-cured laminates. (1-3,5)

2.4.5 Bonded joint failure modes

Adhesive joint failures are unavoidable. When failures happen, it is important to know why. Because of this, it is necessary to differentiate failures from one another. Failure modes have been categorized in the ASTM D5573 standard. There are seven failure modes in total, which are: adhesive failure, cohesive failure, thin-layer cohesive failure, fibre-tear failure, light-fibre-tear failure, stock-break failure, and mixed failure. The illustrations of these different failures are shown in Figure 14, the mixed failure will have more than one type of failure mode. (3,20)

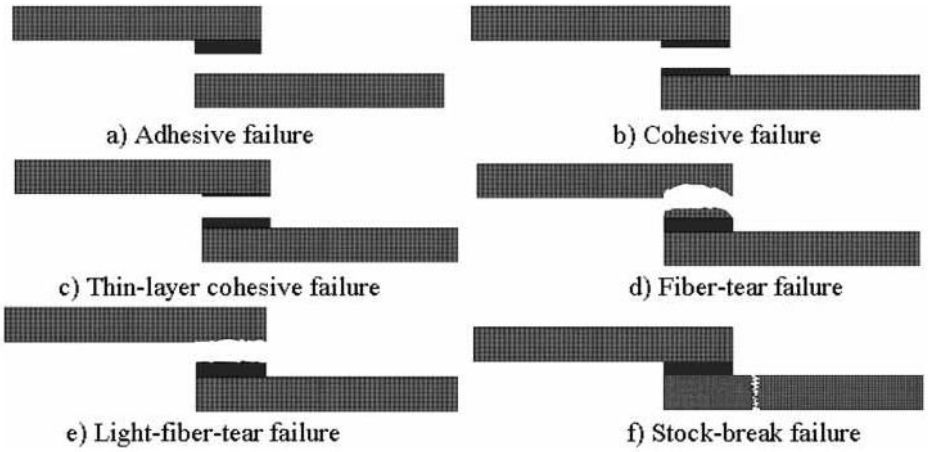

Figure 14. *FRP failure modes defined in the ASTM D5573 standard* ***(20)***

Different types of failure modes are more acceptable than others because detection and prevention are easier for certain types of failures. Cohesive failures occur within one material and can be countered in the set application by improving the components materials or design. In terms of joint strength, cohesive failures can be predicted more easily using the continuum mechanics approach for example. This model assumes that the adhesive is perfectly bonded, which means adhesive failure will not happen. (3,5,20)

Adhesive failures are common. They can be defined as the most unwanted failure. It is not possible to determine if the adhesive surface has been correctly bonded. The surface preparation and conditions at the time of bonding play a significant role. Adhesive failures can also happen because of kissing bonds. During bonding, the adhesive seems to bond well on the surface and no voids or looseness can be detected. However, under load these kissing bond areas will fail on low loads, making adhesive failure happen. Kissing

bonds are usually caused by the contamination of saltwater, which includes human sweat and breath moisture. (3,22)

When the bond between the adhesive and the adherend fails, it is called an adhesive failure. The energy required to break the bonds is called fracture energy (G_C), which is equal to the work of adhesion in adhesive failure at the interface. These bonds consist of mechanical interlocking and other forces. Work of adhesion and adhesion mechanics will be covered in Chapter 3. Failures are initiated at the crack tip, where stresses are very high. This can be an adhesive failure or within one material e.g. in the adhesive. How much energy is needed for the crack to grow, depends on the material. Toughness is a measure of the amount of energy absorbed by a material as it fractures. Fracture toughness (K_C) is the critical value of the stress intensity factor for which crack extension occurs. For adhesive joints, G_C is used instead of K_C. There is localized plasticity at the crack tip, and if there is no large-scale yielding in the bulk material, linear elastic fracture mechanics (LEFM) can be used to analyze the fracture mechanism. Two basic approaches to LEFM are the intensity factor approach and the energy release approach. Simply put, the failure occurs when applied stress intensity factor (*K)*, reaches the joints K_C. For adhesive joints, this is presented as energy release rate (G) reaching G_C. Figure 15 shows three different crack propagation modes, depending on applied forces. In the scope of this work, we will not delve deeper into these approaches. However, it is good to know how adhesives can be engineered to resist adhesive failures. An incorrectly

bonded adhesive joint is prone to the formation of these cracks, thus causing adhesive failure. (1,2,23)

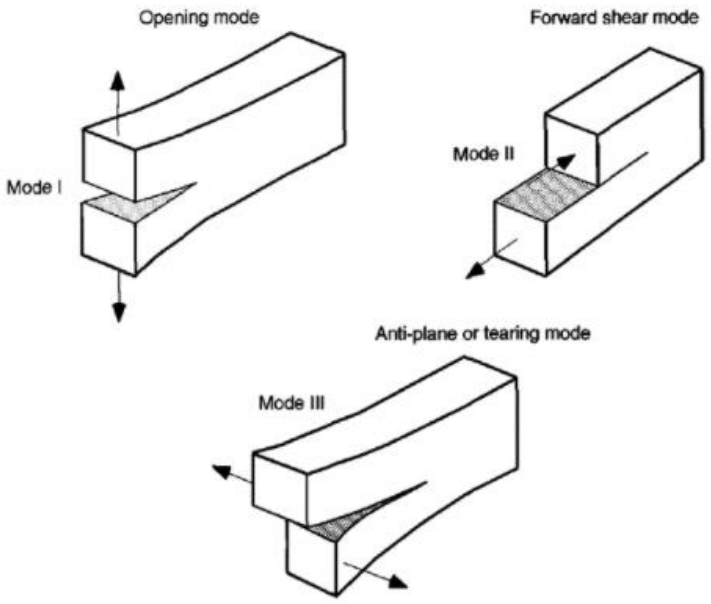

Figure 15. *Crack propagation under three different modes: opening, forward shear and anti-plane shear* ***(1)***

2.5 Quality control of composite manufacturing

There are requirements for composite manufacturing. In the USA, Federal Aviation Administration releases advisory circulars (AC), which provide information about the requirements for the manufacture of composite structures. These ACs are available from their website and affect different manufacturers and approval holders. AC No: 21-26A “Quality System for the Manufacture of Composite Structures” (24) provides information about the required procedures to verify the quality of different aspects in composite manufacturing. This includes Quality System, Material and Process Specifications, Materials and Specific Quality System Procedures, Manufacturing Controls and Final Acceptance. For the scope of this work, the Manufacturing Controls are of interest. It includes specifications for Manual lay-up and curing, but also secondary bonding.

Composite structures built from composite laminates have two types of statistically determined allowables, A-Basis and B-Basis. The Basis category is defined as a statistical strength value at which the specimen fails. For A-Basis, this strength value is at which only 1 in 100 specimens will fail with a 95% confidence level. B-Basis strength values are at which only 10 in 100 specimens will fail with a 95% confidence level. Depending on the number of specimens tested, this value may change. It is good to note that the specimen should be tested in hardware conditions and in extreme conditions, such as

hot and wet or cold and dry. This is because composites can show great strength variation based on the environment. Military handbook (MIL-HDBK-17) describes the statistical methods in more detail that should be used to determine the A-Basis and B-Basis related allowables of design.

The requirements given in AC 21-26A are for civil aircraft. Military use will have their own specifications since the conditions and purpose for military use is different. The specifications given in the military handbooks define military use.

2.6 Challenges

The verifying of correct surface conditions at the time of adhesive bonding is one of the biggest challenges. Surface roughness needs to be on the appropriate level, and it should be as uniform as possible. This is achieved by doing the surface treatment correctly. All kinds of contamination must be avoided between surface treatment and adhesive bonding. When composite structures are adhesively bonded on metals, such as in an article by Mueller (25), NDT methods can be used to detect if appropriate adhesive bonding has been achieved after curing. This is different when composite to composite adhesive bonding is used. The methods used by Mueller, such as ultrasonic resonance and pulse-echo C-scan, work poorly on pure composite adhesive joints. Even when other NDT methods can detect voids or porosities, the presence of a kissing bond remains undetectable. The only way to test them is to use them in practice, which may bring unnecessary risk. Test flights can be performed for aircraft structures, but the risk for the pilot and equipment might be too much. (12,25)

3. ADHESIVE FORCES AND ADHESION

In practice, the force needed to separate two surfaces and break their bonds is considered adhesion. It can also be defined as a state where two different surfaces are held together by interfacial contact and can transfer mechanical force. Adhesion does not have one defining theory, instead, multiple theories are explaining it, which differ by the approach. This chapter will cover the main adhesion theories and forces involved.

3.1 Adhesion theories

3.1.1 Adsorption theory

When two materials are in contact, there will be forces of attraction between them. Close contact that enables molecular and physical interactions between the materials is the basis for adsorption theory. However, interdiffusion of the surfaces is not needed for this theory. Wetting is essential for adsorption theory. Adsorption theory concentrates on secondary bonding for adhesion, which is mainly due to van der Waals and polar forces. (3,26) These are different from primary bonding forces, which fall under chemical adhesion.

Van der Waals forces consist of dipole-to-dipole, dipole-to-induced dipole, and dispersion forces. These secondary forces are caused by the asymmetry of molecules or unequal charge distribution in them. Theoretically, the bond strength of these forces is much higher than experienced in practice. When a material has hydroxyl groups, hydrogen bonds are formed. These bonds have the highest attractive force of the secondary bonds and can exhibit both dipole-to-dipole and covalent properties. (3,26)

3.1.2 Mechanical theory

Mechanical interlocking is the main mechanism for adhesion in mechanical theory. The adhesion is created by the penetration of one component into the surface irregularities of the other surface. This type of adhesion is more prone to occur in porous surfaces, such as paper, wood, or textiles. Some level of surface roughness and irregularities are required but if too much is present the wetting process might be interrupted. This would leave the contact area smaller, weakening the effect of interlocking. The level of irregularities can affect CAs. The viscosity of adherend can change depending on how quickly

the penetration happens, like when using hot melt adherends, this also changes wetting. (3,26)

3.1.3 Electrostatic theory

The basis of the electrostatic theory is an electrochemical potential difference. This potential is formed across an interface between two materials in contact. This is because there is free charge present in any condensed material. The potential difference on the two surfaces forms an electrical double layer. Two surfaces, adhesive and substrate, function as a capacitor and adhesion is an attractive force across the layer. (3,26)

The identity of the double layer is possible to be identified using a scanning electron microscope (SEM). SEM does not break the bonds. This phenomenon was reported by Fowkes to be the main adhesive force in pressure-sensitive adhesives. The force of the energy stored is small compared to van der Waals attraction, which is confirmed by several researchers. Since the force is small, the effect on adhesion is low. (3,26)

3.1.4 Diffusion theory

Diffusion theory has its roots in the self-adhesion of specific rubbers. Two interfaces of these rubbers can interdiffuse so, that the interface becomes diffuse and eventually disappears. Two dissimilar materials can also interdiffuse. The transition zone can be formed if the materials are compatible with equal solubility parameters. In these transition zones, the interdiffusion of macromolecules and molecule segments can occur. Close molecular contact by wetting is required. (3,26)

It is possible to have diffusion type adhesion in incompatible polymers. This is based more on-chain entanglements at the interface, thus making the adhesive force low. It is also possible to use copolymer compatibilizers. When a diblock copolymer is introduced

at the interface, it allows the diffusion of the copolymers ends into the respective homopolymer. (3)

3.1.5 Other theories

Chemical adhesion is a type of primary bonding between atoms. They are strong chemical bonds such as ionic, covalent, and metallic. These types of bonds may occur depending on the surface and the adherend. The work of adhesion can be 40 times larger in covalent bonds compared to van der Waals. (3,26)

Consolidation theory is a combined theory of the theories discussed before. Spreading and wetting from adsorption theory and the need for intermolecular contact with less distance than 9 Å as a necessary condition for adhesion to occur. (26)

Weak boundary layer (WBL) theory tries to explain why the calculated bond strengths differ from the actual failure strengths. In polymers, the WBL can form for several reasons such as the migration of additives, contaminants, or excessive surface treatments. Pretreatments are used to remove the WBL. These can be methods already mentioned like the use of peel ply or abrasive treatments. Corona and flame treatments are used on polymer surfaces to improve adhesion for similar reasons. (3,26)

3.2 Forces of adhesion

Surface energies are fundamental to understanding adhesion since it effects the forces of adhesion and the wetting of surfaces, which both are needed for good adhesion. When molecule moves from the bulk of the material to the surface, increasing the surface area, energy is needed. In the bulk material, the molecules are surrounded by similar molecules, making the interactions cohesive. On the surface, the top molecules are surrounded by dissimilar molecules, so the interaction energy is different. This energy is surface free energy (SFE). For liquids, SFE equals its surface tension. However, for solid materials, SFE cannot be calculated using surface tension. (2,3,26) SFE for polymers can be expressed as its polar (γ^p) and dispersive (γ^d) components giving total energy γ equation (1):

$$\gamma = \gamma^p + \gamma^d \qquad (1)$$

Figure 16 shows the interactions between polar and dispersive components. The solid surface and liquid B have the same SFE. The composition of the SFE is different. Liquid

B has a large polar component and the solid has a large dispersive component. We can see that the different components do not want to interact, meaning that the SFE value cannot solely explain if a liquid will wet a solid surface.

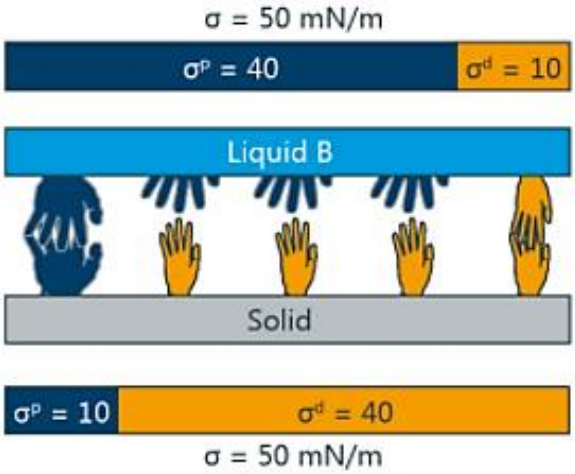

Figure 16. *Polar and dispersive components by Krüss* ***(27)***

3.2.1 van der Waals

As mentioned in Section 3.1.1, van der Waals forces include dispersion and polarization forces that arise from different dipole moments in atoms and molecules. Dispersion or London forces (London 1937) bring the most important contribution to the van der Waals forces. There, forces are always present, apart from totally neutral molecules and atoms. London established the energy of these forces by using quantum mechanical perturbation theory. The general rule for these dispersion forces is that they can be effective from a large distance of 10nm to the atomic level. They may be repulsive or attractive and they align atoms and molecules in a weak manner. Dispersive interaction between two

bodies is affected by the presence of other bodies. (2,3) London theory was modified by Spruch (1986) since it did not allow molecules bigger than 0.5nm.

The polar forces, such as dipole-dipole and dipole-induced dipole, do not require simultaneous excitation of both molecules as dispersive forces need. Keesom (1922) and Debye (1921) calculated the energies for these polarization forces. The total van der Waals free energy of interaction can be found combining each of these forces.

3.2.2 Lewis Acid-Base interaction

Lewis acid-base interactions are the widely used definition of the electron pair bond in chemistry. It was first introduced by Lewis in 1923. The basic definition is that a basic substance with a lone pair of electrons can be used to complete a valence shell of another atom, which is called the acid. The acid substance can employ a lone pair of electrons from another atom, which is the base, and complete its own valence shell. (3)

These interactions are used as adhesion components in some theories which will be explained in Chapter 4. In the scope of the experiments, the Acid-Base forces are not in focus. This is because the SFE calculation method we use utilizes polar and dispersive forces.

3.3 Work of adhesion

Work of adhesion is the work required to separate reversibly the interface between two bulk phases. The work from their equilibrium distance to infinite distance was defined by Dupre (1869) and is now termed as the work of adhesion. (3,28) This work studies the solid-liquid interface, so the Dupre equation (2) is as follows:

$$W_a = \gamma_L + \gamma_S - \gamma_{SL} \qquad (2)$$

Where W_a is the work of adhesion, (γ_L) the energy of liquid, (γ_S) the energy of solid and γ_{SL} the energy of the solid-liquid interface. This equation 2 can be used further to combine with CA measurements which we will cover in chapter 4. The work of adhesion is the force that is overcome when the adhesive joint fails at its interface. In practice, this G is usually greater than the surface energy term. (3)

4. CONTACT ANGLE MEASUREMENTS

CA measurements are widely used to characterize surfaces and study wetting. They are rather simple methods and have a lot of versatility. Most of the measurements are done using major measurement techniques. These include techniques such as static CAs, sliding angles, advancing angles and receding angles.

4.1 Theory

The basic theory for CAs starts at the solid-liquid interface, where vapour is saturated. It is a static system and measured at mechanical equilibrium (28). Young's ideal system is shown in Figure 17. The surface is ideally homogeneous, planar, rigid and smooth. For this equilibrium point, Young described an equation, the Young's equation (3) which can be expressed as:

$$\gamma_{LV} * cos\theta = \gamma_{SV}^{o} - \gamma_{SL} \quad (3)$$

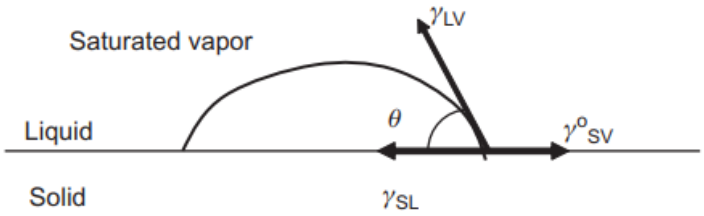

Figure 17. *Equilibrium CA on an ideal surface* ***(2)***

It is possible to combine equations (2) and (3). This can be done using Harkins and Livingston correction, which is known as the spreading coefficient. This brings us to Young-Dupre's equation (4), which shows that the work of adhesion can be calculated using the CA of the droplet on the ideal surface.

$$W_a = \gamma_{LV}(1 + cos\theta) \quad (4)$$

Wetting and spreading are processes that need to be considered when measuring CAs. As shown in Figure 18, the static CA measurement involves both processes. When

measuring a smooth surface the wetting is even in all directions, but on a rough surface, the droplet can stick on the surface. This can distort the drop shape, making it possible to have different CAs based on the direction. This behaviour should be taken into account when taking measurements. (28)

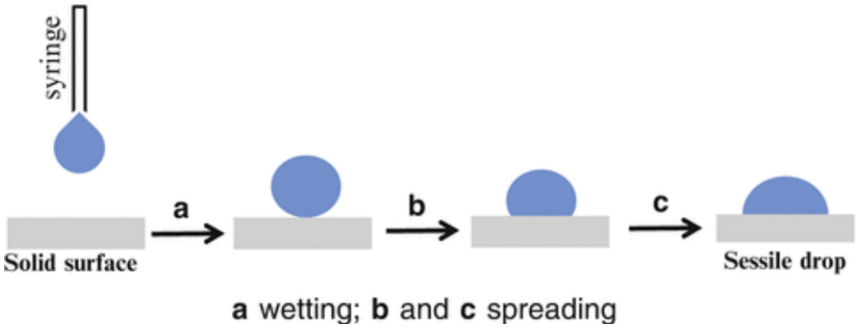

Figure 18. *Sessile drop method* ***(28)***

4.1.1 Wetting and surface treatments

Wetting determines how liquid behaves on a solid surface, surrounded by saturated vapour or other liquid if the liquids have the miscibility cap. When a liquid is poured on a surface, it can behave in different ways. For example, water usually wets the surface well, spreading across. If used on a Teflon pan, water forms small droplets. Cooking oils for example spread on Teflon surfaces. Mercury is in a liquid state at room temperature. It has extremely high surface tension and does not wet or spread on most surfaces, but instead forms droplets on them Wetting can be described as good or bad. Good wetting is when the CA between the solid and the liquid is under 90°. Bad is considered when the CA is over 90°. When wetting is so good that the CA goes to 0°, the term used is spreading. The CA can be measured when liquid wets a surface. (3,28)

Thermodynamics is used to model the wetting process. For a smooth surface, the concept is quite simple. From the molecular kinetic and hydrodynamic theories point of view, the contact line of the droplet will cease to move as soon as the kinetic energy has been dissipated by friction. The kinetic energy in our case comes from the droplets placement on the surface. For the static CA, the measurement is taken when the kinetic energy is used, and the equilibrium point is reached. The different measurable CAs and their relation to Gibbs free energy are shown in Figure 19, θ_A and θ_R for advancing and receding angles. The static CA (θ) at mechanical equilibrium and θ_{eq} is the equilibrium in terms of thermodynamics.

Wetting is a time, temperature, and humidity dependent process. Changes in CA based on these conditions are shown in Figure 20 and Figure 21. Behaviour depends highly on the material tested and probe liquid used. Figure 20 shows the dependency of WCA on

the temperature. The measurements done in this work are done at the low-temperature area. There is a difference between the measured and theoretical values. The general trend for water is that measured angles decrease as the temperature is increased. In Figure 21, WCA relation to time is shown with different relative humidity levels. An increase in relative humidity makes WCA decline slower and evaporation of droplets take longer. The temperature in the laboratory environment is usually set to 22 °C and relative humidity is around 50%. (28)

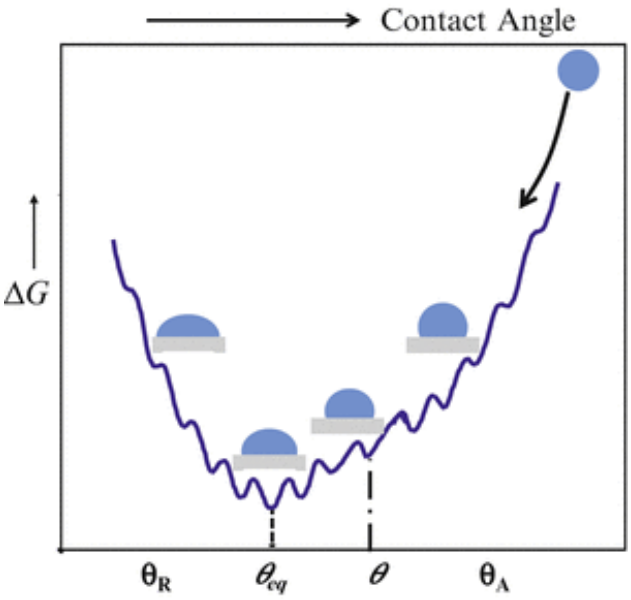

Figure 19. *A schematic showing the wetting process and the Gibbs free energy relationship among the four measurable CAs* ***(28)***

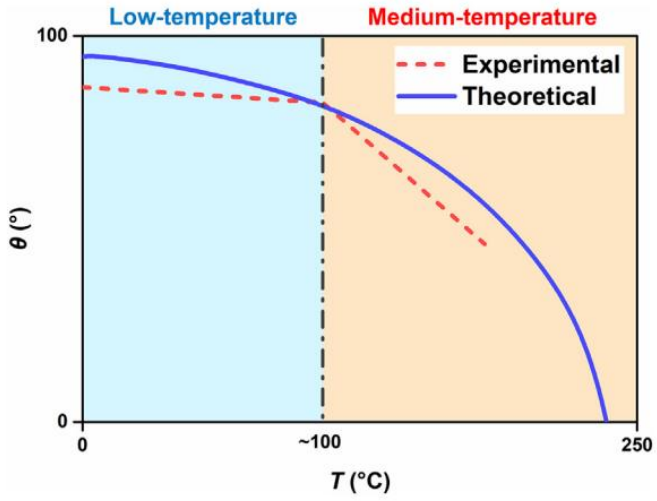

Figure 20. *Measured and predicted trends of the temperature dependence of WCA on a polymeric surface* ***(29)***

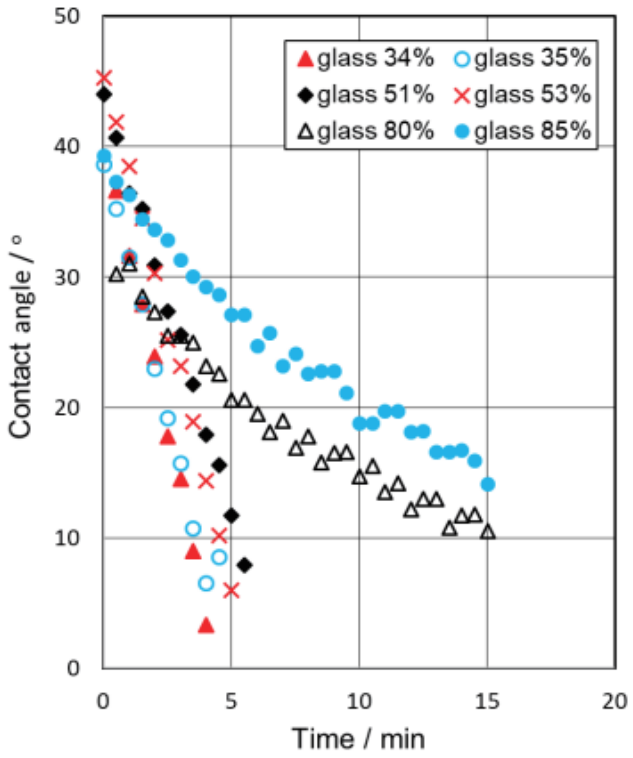

Figure 21. *The WCA vs. time for various relative humidity levels on a glass substrate* ***(30)***

For rough surfaces, there are two classic models explaining wetting, which are Wenzel and Cassie-Baxter states. Wenzel was the first to describe wetting on a rough surface using a thermodynamic argument. Wenzel stated that, if a liquid wets a solid surface, the roughness of the surface will increase the wetting. If the liquid resists wetting on a solid surface, the roughness will increase its resistance. When the rough surface is also porous such as most textiles or natural materials, Cassie and Baxter extended the statement. When a liquid wets a porous surface, air pockets are formed, where liquid-solid-air interfaces are formed. The CA of liquid-air interface is 180°. The illustration of these models is shown in Figure 22. There have been arguments against both models and combined models are also used. (28)

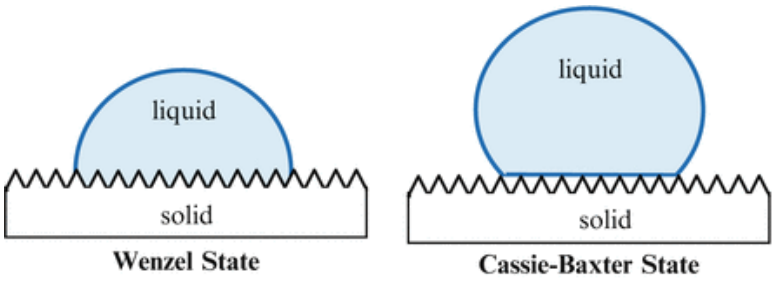

Figure 22. *Schematic of the two possible wetting states on rough surfaces* ***(28)***

4.1.2 Surface free energy of solids

Different methods have been developed to determine the surface tensions of solids using CAs. The first of these models was the so-called Zisman model. It was created by Fox and Zisman, using a plot of cosθ against surface tension for a series of n-alkanes on polytetrafluoroethylene (PTFE) surface. The plots have linear areas where the model operates, which makes it limited to low surface energy materials and alkane solvents, where the van der Waals forces are the main interaction force. (28)

The original Fowkes method was published in 1962. (28,31) In the Fowkes model, the dispersion component caused by London dispersion forces was the only surface tension component considered. When only the dispersion component is present, the Young-Dupre equation modified by Fowkes, (28,31) can be expressed as equation (5):

$$\gamma_{SV} = \gamma_{SV}^{d} = \frac{\gamma_{LV}^{2}}{4\gamma_{LV}^{d}} \cdot (1 + \cos\Theta)^{2} \qquad (5)$$

From equation (5), it is possible to calculate the surface tension (γ_{sv}) by measuring the CA θ of a liquid whose γ_{LV} is known (28). Newer methods using surface tension components have emerged. This work will focus on these later methods, which we will use to determine the surface energy of solid in the experimental section. Owens and Wendt modified the Fowkes model by assuming that the surface tensions are composed of two components. The dispersion component and hydrogen-bonding component. At the same time, Rabel and Kaelble published a similarly modified version using two components for surface tension, polar and dispersive components. (28) From these published studies a method called Owens–Wendt–Rabel–Kaelble (OWRK) was made. This method is used to calculate surface energies in this work. Similarly, to the Fowkes original method, the OWRK method can be combined with the Young-Dupre equation. The OWRK methods equation has two unknowns, dispersive component of the solid-vapour interface (γ_{SV}^{d}) and polar component of the solid-vapour interface (γ_{SV}^{p}). It is possible to calculate the

SFE if CAs of two different known liquids are measured. The OWRK methods equation combined with Young-Dupre's equation can be expressed as equation (6): (28)

$$\gamma_{LV}(1+\cos\Theta) = 2\sqrt{\gamma_{SV}^{d}\cdot\gamma_{LV}^{d}} + 2\sqrt{\gamma_{SV}^{p}\cdot\gamma_{LV}^{p}} \quad (6)$$

The extended Fowkes method is further refined from the OWRK. It was done by splitting the dipole-dipole interaction into polar and H-bonding, by Kitazaki et al. (28) Three components are dispersion (d), polar (p), and H-bond (h). Similarly, as before, the method can be combined with Young-Dupre's equation resulting in the equation (7). This method requires three different liquids to be usable. (28)

$$\gamma_{LV}(1+\cos\Theta) = 2\sqrt{\gamma_{SV}^{d}\cdot\gamma_{LV}^{d}} + 2\sqrt{\gamma_{SV}^{p}\cdot\gamma_{LV}^{p}} + 2\sqrt{\gamma_{SV}^{h}\cdot\gamma_{LV}^{h}} \quad (7)$$

A different approach was presented by Van Oss, Chaudhury, and Good's (vOCG) and it is similar to the extended Fowkes method. It also consists of three components, which are: Lifshitz-van der Waals (LW) including all dispersion and all dipole forces, and short-range hydrogen interaction in form of Lewis acid and Lewis base (electron acceptor and donor). (28) Equation (8) shows the relation of the vOCG model and Young-Dupre equation.

$$\gamma_{LV}(1+\cos\Theta) = 2\sqrt{\gamma_{SV}^{LW}\cdot\gamma_{LV}^{LW}} + 2\sqrt{\gamma_{SV}^{+}\cdot\gamma_{LV}^{-}} + 2\sqrt{\gamma_{SV}^{-}\cdot\gamma_{LV}^{+}} \quad (8)$$

4.2 Measuring devices

For the static CA measurement, the basic method is the sessile drop method. Using a normal laboratory atmosphere, a sessile drop is placed onto a horizontal solid surface using a motor-controlled microsyringe unit. The surface and other equipment must be clean and the test liquid should be the best solvent grade. Test machinery should be vibration dampened so that outside vibration cannot affect the wetting and spreading of the liquid. After the sessile drop is formed, it is captured by camera equipment. It is pos-

sible to calculate the CA from the picture. Advanced machines have software that calculates the CA automatically and almost instantly. The sessile drop method was shown in Figure 18. (28)

Another method that uses the Young's equation (3) is called the captive bubble method. In this method, the liquid is in a container and the solid surface is placed on it. A gas (air) bubble is injected into the liquid and it floats against the solid surface and gets trapped. This creates similar interfaces as in the sessile drop method shown in Figure 23. This method is less popular since it requires a lot of the liquid and for the solid surface to be partly submerged in the liquid. (28)

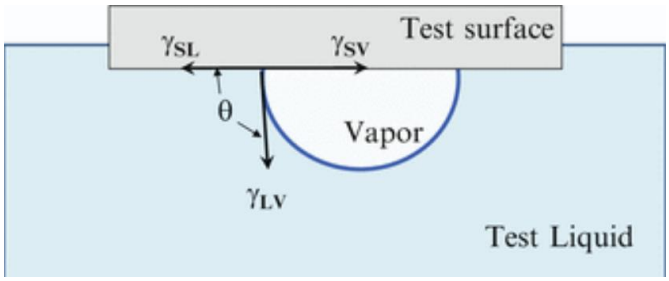

Figure 23. *Captive bubble method* ***(28)***

Some methods use tilting of the surface to determine the surface energy. The sliding angle uses the retention force of friction to determine the surface energy. The droplet is distorted as the plane is tilted since gravity starts to pull the droplet. The CAs and tilt angles are recorded as the droplet starts to move, making it possible to determine the surface energy.

Similarly, advancing and receding CAs are used by a few methods. First, it uses a microsyringe to expand the drop and then contract it, making the CAs advancing when the droplet is expanded and receding then contracted. The tilting plate method uses a similar principle.

Wilhelmy plate technique uses a solid plate dropped into a liquid. Figure 24 shows the variables measured in the Wilhelmy plate method. The basic principle is that the force

on tension is equal to force on wetting minus buoyance plus the force of gravity. It is possible to calculate the advancing and receding angles using this method.

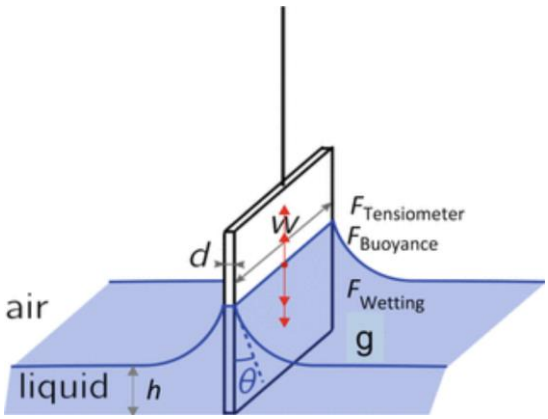

Figure 24. *Wilhelmy plate method* ***(28)***

4.3 Probe liquids

The CA measurements are done with pure liquids. This is due to mixtures having preferential adsorption, which would make the measurements inaccurate. The liquid cannot have a physical or chemical reaction with the solid surface. To form measurable drops, the liquid should have higher surface tension than the solid. (28,32)

Water is the most used liquid in CA measurements since it is generally available and in contact with surfaces naturally. Another common probe liquid is diiodomethane, which surface tension consists of the dispersive component only. There are terms used for surfaces based on the CAs with liquids. A good example of this is are hydrophobic and hydrophilic surfaces, where the hydrophobic surface has a CA over 90° and hydrophilic surfaces under 90°. (28) Similar definitions are used with oils, i.e., oleophobic and oleophilic.

4.4 Challenges in measurements

The conditions for accurate measurements differ depending on the liquid and the solid surface being measured. Even when the measurements are done in a laboratory with temperature and humidity control, some liquids tend to evaporate. This means that the CA is not static, rather receding, which increases the variance in results. Water and hexadecane for example can be used in a laboratory environment without high concerns. If evaporation is a problem, test machinery with a closed chamber can be used. This way

the equilibrium can be ensured by removing the evaporation. Temperature can be controlled by advanced machines, which allows CA measurements in elevated or low temperatures. (28,32)

Challenges relating to the droplet itself are its size and wetting behaviour. Although the Young's equation does not consider the size of the droplet, gravity will inevitably distort its edges if the size of the droplet is too big. When using a liquid that has lower surface tension, the distortion by gravity affects the shape easier. Too small droplet size makes it hard to determine its boundaries. Small size can result in optical errors due to light scattering, diffraction, evaporation, and uncertainty of its baseline. The wetting is a time-related process that is also affected by temperature and surface roughness, and it can be challenging to know when its complete so that the correct CA can be measured. (28,32,33)

The actual angle of contact can be measured from the picture by hand. It is a slow and operator dependent process. Nowadays it is usually done automatically by a computer algorithm. The detection of the CA from the picture is done by using an algorithm. There are different algorithms used such as circle- and ellipse-fitting and ADSA-P algorithm. The CA each method provides differs from one another by a little. This should be accounted for when the results are compared to one another. Sometimes even when using an algorithm to measure the angles, the detection of the droplet may fail. It is possible to manually adjust so that the algorithm finds the droplets boundaries. This makes the operator a variable to the measurements, as it is possible to adjust the measured angles this way. (28,33)

5. EXPERIMENTS

The experiments are done using static CAs with water and are done on unidirectional carbon fibre reinforced epoxy composite. The main goal of the experiments is to qualify the different surface treatments using the WCA. In addition to the WCA, SFE measurements will be performed using four different liquids and the OWRK method. The composite surface will have different treatments. The time between the surface treatment and measurements will be recorded. The environment for testing is a basic laboratory environment and the temperature and humidity will be recorded for each measurement. Surface roughness will be measured to verify its effect. Figure 25 shows the block diagram of the experimental process and thesis objectives.

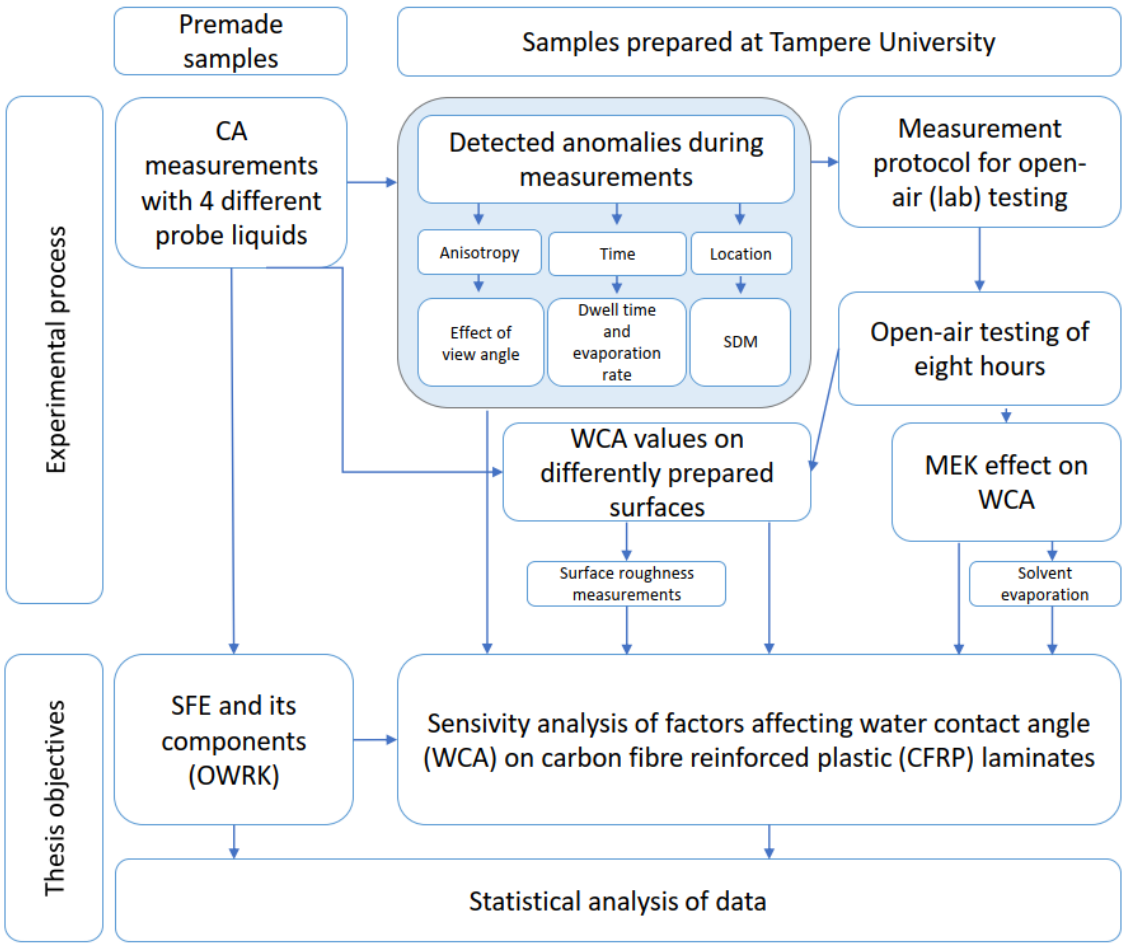

Figure 25. *Block diagram of experimental process and thesis objectives*

5.1 Target

The target of the measurements is to determine how CAs depend on surface treatment and time. To achieve this, the first step is to test the samples using water and other liquids to determine their CA values on different surfaces. From these CA measurements, it is possible to calculate the SFE and its components. This is to determine the changes in both polar and dispersive components as well as the total SFE. Surface treatments should increase the SFE making measured angles smaller.

The WCA is the focus after the first measurements. Different challenges, which occurred during the first measurements, will be tested. These are 1) the effect of the view angle since the droplet may not be ideal and 2) the time dependency over one minute of WCA. These are to observe what needs to be accounted for later measurements.

Surface contamination and changes after surface treatments are observed with open-air contamination tests. This is done in two different trial runs testing two different sanding paper brands. The WCA is measured over a period of up to eight hours.

As the surface treatments modify surface roughness, the surface roughness will be measured on the selected sample to approximate its effect on WCA. This is done using optical profilometry (by using a device from Alicona).

5.2 Materials and methods

The CFRP laminates used for testing are based on prepreg AS4/3501-6 UD. A water jet cutter was used to cut the provided laminates into suitable testing samples. Two different sizes are used, 150mm x 150mm for determining SFE and 100mm x 100mm for the rest. Figure 26 shows the laminates used for testing, left one being laminate with peel ply intact, the middle one with only peel ply removed and the right one has medium sanding. Surface treatments are done after samples are cut, to ensure no contamination will be caused by the cutting process. Because the samples are small, a 15mm area from the

edges of the sample will not be used for measurements. This is to ensure the measured area has even surface treatment applied.

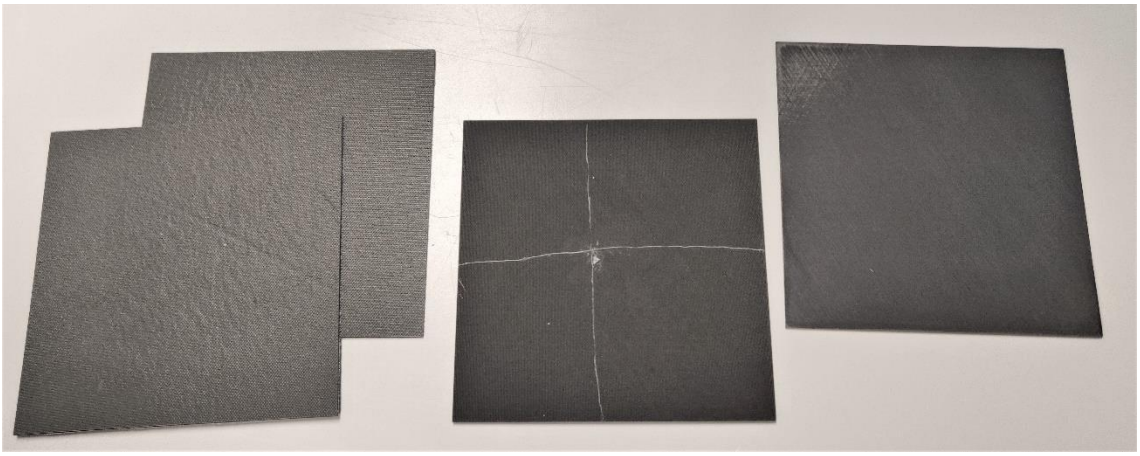

Figure 26. *100mm x 100mm size samples used for testing, left one being laminate with peel ply intact, the middle one with only peel ply removed and the right one has medium sanding*

The surface treatments are listed in Table 2. Sanding is done by hand using two different papers, which are Ecowet P180 (Mirka) and 300D Stikit disc (3M). Both papers have the same grit size of 78 microns. The main difference between the sanding papers is the grain material. 300D has aluminium oxide (Al_2O_3) grain and Ecowet has silicon carbide (SiC) and Al_2O_3 mix. The grain type and adhesive affect the colour of the sanding papers, which is shown in Figure 27. Grit blasting is done using an industrial-grade blast cabined and 50µm white Al_2O_3 grit. After sanding, samples are cleaned using dry and solvent wiping. Solvent wiping is done using methyl ethyl ketone (MEK) and special cheesecloth is used for wiping. Samples are stored in plastic boxes during and after the measurements to avoid contamination. Some samples will be used for surface roughness measurements after CA measurements, so keeping the surface clean is needed.

Table 2. *Surface treatments that are used in the experiments by name with an explanation of the procedure used in each surface treatment.*

Treatment	Step 1	Step 2	Step 3
PPR0	Peel ply removal	Drywipe	(Baseline sample)
A Light	Peel ply removal	Soft sanding	Drywipe
A Med	Peel ply removal	Medium sanding	Drywipe
A Hard	Peel ply removal	Hard sanding	Drywipe
B Med	Peel ply removal	Medium sanding	MEK-wipe
B Wa	Peel ply removal	Medium sanding	MEK-wipe + water and Scotch-Brite flush
Grit Blast	Peel ply removal	Al_2O_3 (50µm) grit blast	

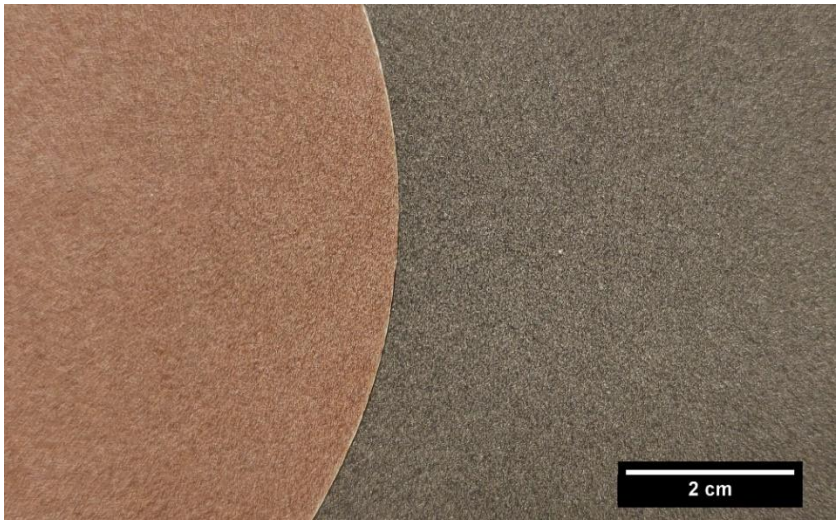

Figure 27. *Sanding papers that were used. 300D (3M) on the left with orange colour, and Ecowet (Mirka) on the right with a darkish colour*

The CA measurements will be conducted using the Krüss DSA100 Drop shape analyser, shown in Figure 28. Krüss ADVANCE software is used to operate the analyser, setting up the measurement protocols, correction images and data extraction. The fitting method used to measure the CA from the droplets will be Ellipse(tangent-1), which allows us to record the right CA(r) and CA(l) left side of the droplet separately. CA(m) is the average of right and left sides. Recording right and left separately allows us to see if the surface is tilted or if the droplets have stuck on one side when wetting. The time dependency is measured using pre-determined drop locations per time series. This also ensures that if some abnormalities are detected, it is possible to evaluate the surface on the drop location afterwards. For the untreated sample and B Med surface treatments, the location dependency is tested using a CA mapping. Pre-determined drop locations are measured and the samples are sealed for surface analysis. The dwell time is the time the droplet remains on the surface before measurements are taken. The dwell time used will differ from three (3) seconds onwards. This is because most droplets are very unstable right after placement, which results in a large deviation in the results. The algorithm that is

used is prone to select incorrect baseline when dwell times under three seconds are used.

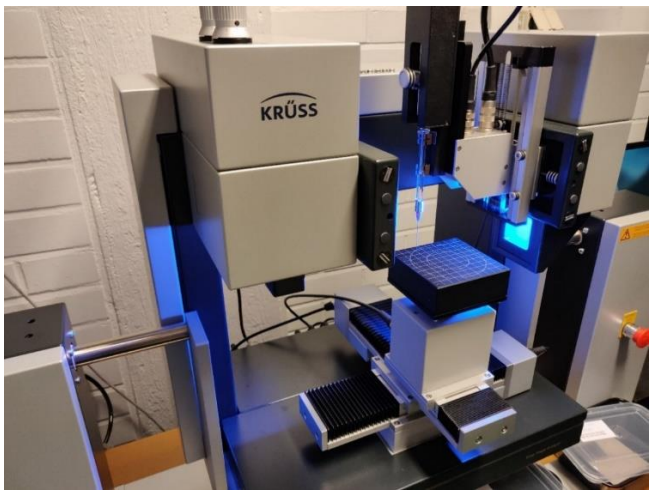

Figure 28. *DSA100 (Krüss) with a water syringe setup*

Surface roughness might affect the CA values. Profilometry is used to determine the surface roughness of the different samples. It is possible to focus on the areas where the CA measurements have been taken. The apparatus used is Infinite Focus (Alicona) white light profilometry (WLP), shown in Figure 29.

Figure 29. *Infinite Focus (Alicona) measurement device*

5.3 Test campaign

5.3.1 Calculation of SFE

The OWRK method that is provided in the DSA100 software Krüss ADVANCE is used to calculate the SFE of the samples. The surface treatments tested are listed in Table 2. Surface treatment techniques remain the same through different experiments. These

surface treatments include hand sanding with 180 grit paper with different intensities, solvent wiping with MEK, dry wiping with a cloth, wiping with water and Scotch-Brite, and Al_2O_3 grit blasting. The samples for the first test were surface treated two months before testing and their size is 150mm x 150mm. Samples are flushed with acetone and dried for 20 minutes in a fume hood. This is to remove possible contamination during storage. Acetone used for flushing is gathered into a beaker and dried in a fume hood to gather any particles that might have been removed. The liquids used for SFE measurements are MilliQ water, Glycerol (98%), Ethylene Glycol, and Diiodomethane. The surface tension components of these liquids are listed in Table 3. These are the values defined by the measurement software. Slightly different values for each component can be found in the literature (34,35).

Table 3. *Probe liquid surface tension and its components used in the measurements and calculations by Krüss ADVANCE software* ***(36)***

Probe liquid	Surface tension total (mN/m)	Dispersive component (mN/m)	Polar component (mN/m)
MilliQ Water	72.8	21.8	51.0
Glycerol	64.0	34.0	30.0
Ethylene Glycol	48.0	29.0	19.0
Diiodomethane	50.8	50.8	0.0

Six droplets of each liquid are measured on the sample. Dwell time used is five (5) seconds, monitoring time is five seconds for the first four samples and 10s for the rest. This is due to changes during the measuring. The droplet sizes are four (4) microliters for water and glycerol and two (2) microliters for ethylene glycol and diiodomethane.

5.3.2 Time dependency and droplet anisotropy

Water droplets will vaporize over time when left on the surface. This behaviour was tested using two (2) microliter water droplets, three (3) second dwell time and one minute monitoring time. CA was measured once a second. This testing was performed on the B Med, B Wa and the glass surface. Glass surface used is VWR Microscope Slides 631-1552. They were prepped using household vinegar wiping and acetone wiping before measuring.

Droplet anisotropy was tested using B Med and B Wa surface treatments. The CA was measured from different angles on multiple droplets. These angles were: laminates 0-fibre orientation and the lens principal axis being parallel, surface fibres of laminates being parallel with the lens principal axis, and surface fibres of laminates being perpendicular with the lens principal axis. The water droplet size of four (4) microliters were

used with a three (3) second dwell time, 20s monitoring period and one measurement per second.

5.3.3 Location sampling for uniform surface

As the surface treatments are done by hand, it is necessary to test if different locations on the sample will have different CAs. It was decided that the edges of the laminates would not be measured as the surface treatment might be uneven. This means that a 15mm area from the edges of the laminates were not measured. The measured area for 100mm x 100m size samples was 70mm x 70mm for this reason. Location sampling was done using the sessile drop mapping (SDM) program available in Krüss ADVANCE. This allows fast measurements of multiple drop locations. An illustration of the route is shown in Figure 30. A total of 121 water droplets of two (2) microliters in volume are measured using a five (5) second dwell time.

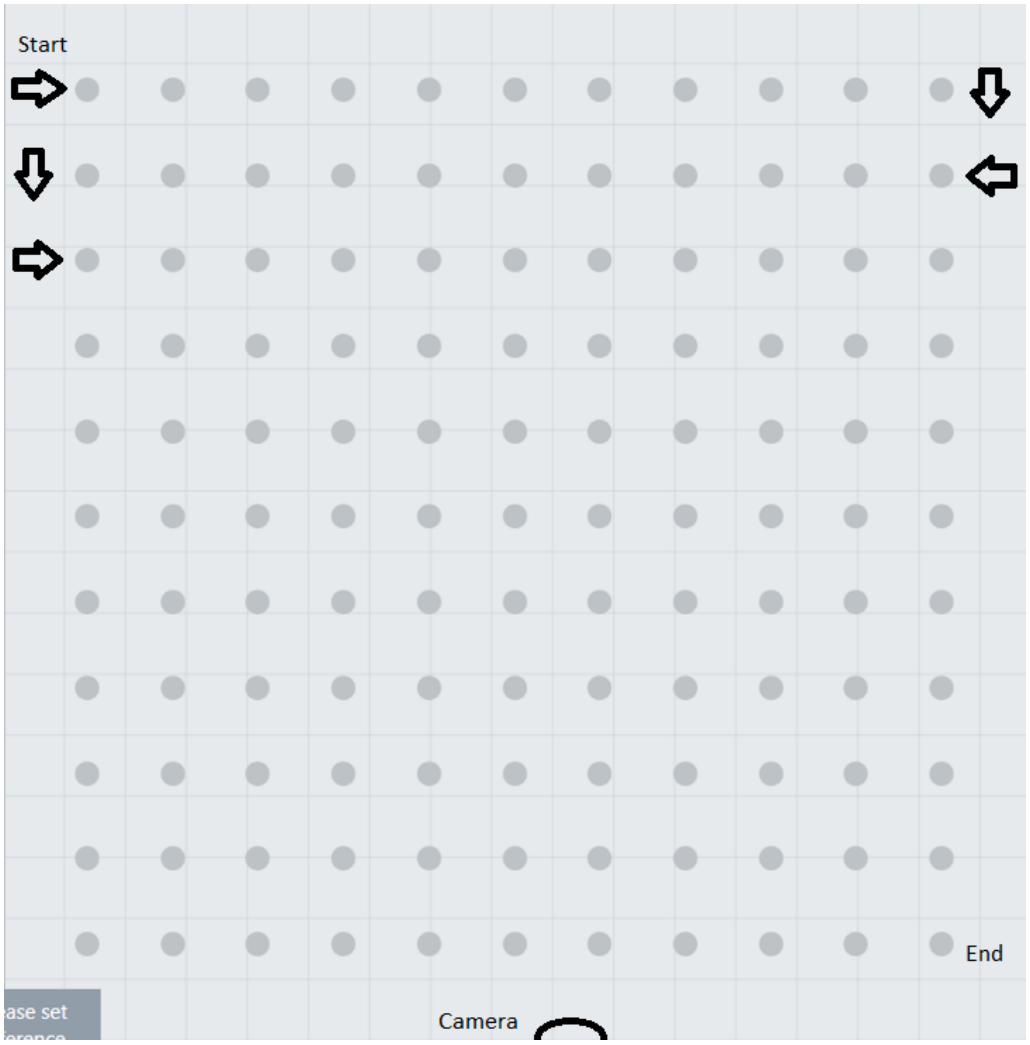

Figure 30. *Sessile drop mapping route*

5.3.4 WCA and open-air contamination

Open-air contamination was done using 100mm x100mm laminates. Surface treatments shown in Table 2 were used. Two separate sets of samples were prepared, using different sanding paper. The first set of samples was sanded with Ecowet (Mirka) and the second set using 300D (3M) sanding paper. Measurements were done at different times. Starting at 30 minutes after the surface treatments were completed and up to eight hours after. The set of five droplets of two (2) microliters in volume per time series were placed and measured after three (3) seconds dwell time for five (5) seconds. Left and right CA were measured with standard deviation (StDev). Droplet locations are shown in Figure 31 for each time series. It also shows how the samples are placed and how to fibres align. Samples are sealed after CA measurements to avoid contamination and preserve them if additional tests will be performed after some time.

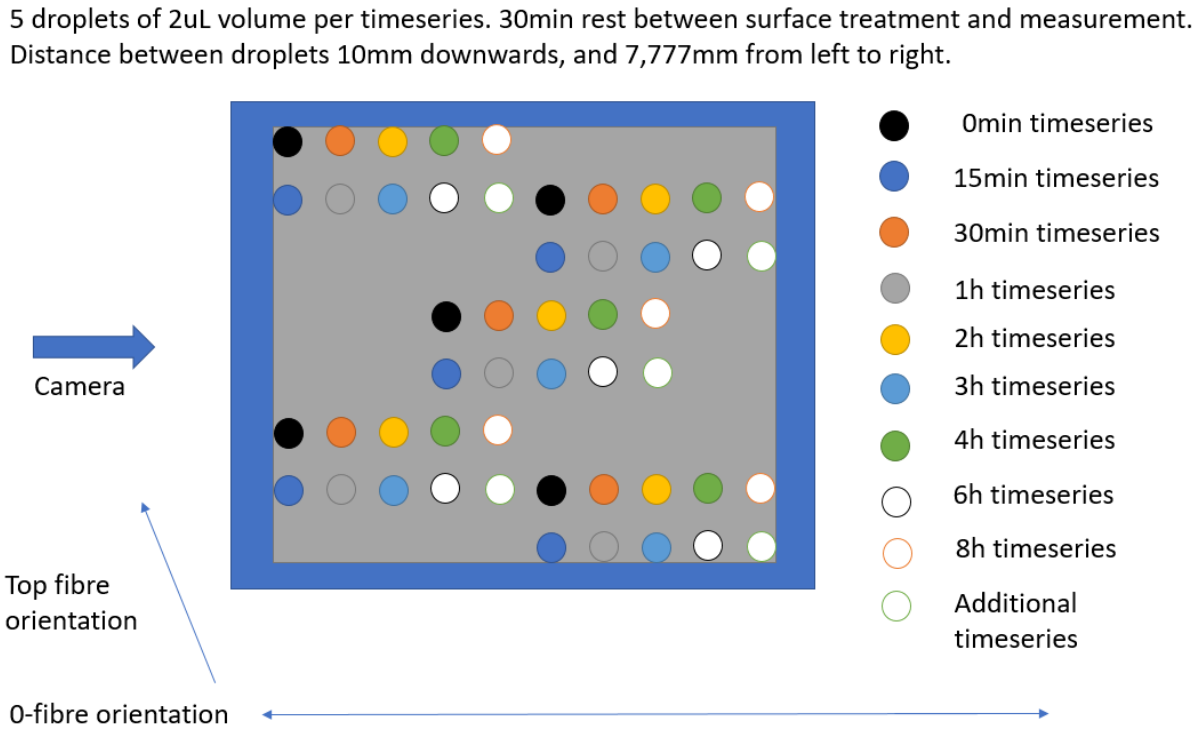

Figure 31. *Droplet locations for open-air contamination*

5.3.5 Solvent evaporation testing

Between the SFE and open-air contamination samples, WCA values on solvent wiped samples had a significant difference. The solvent seemed to have stick to the surface increasing the WCA values on the open-air contamination samples. For SFE samples this was not notable. The main difference of the samples was the storing time between surface treatments and measurements, as the SFE samples were prepared two months

ahead. To test the effect of storing, two similarly sanded samples were prepared. One was wiped with MEK and the other with Acetone, which was used for SFE samples for flushing purposes. WCA was measured multiple times over a two month period, similar to what SFE samples were stored to see if storing time is the reason for a change in WCA values for those samples. The droplet placement and protocol used will be the same as in open-air contamination testing.

5.3.6 Surface roughness and WCA

The surface roughness was measured from the open-air contamination samples. This will bring insight into the difference the sanding paper has on the treated surface. It is also possible to measure the surface roughness on the exact spot where the droplet was placed and WCA measured as these locations were recorded individually. Measurement locations will be from the 0-time series. Profile average roughness (R_a) values will be used to define surface roughness as it is used in other studies. These R_a values will be measured according to the ISO 4287 and ISO 4288. We can scan the surface for topographic images. This can be done for the SDM samples, to see if the topography map correlates to the WCA map from the SDM measurements.

5.3.7 Comparison of measurement devices

During the project, we had the possibility to measure WCAs on glass samples, which had been prepared and measured by the Zurich University of Applied Sciences (ZHAW) in Switzerland. Similar WCA measurements were conducted by both sides on the same slides. Measurements were done using DSA100 (Krüss), using two (2) microliter droplet volume and five (5) second dwell time. The microscope slides used as control surfaces were manufactured by Thermo Scientific.

5.3.8 Statistical analysis

Statistical analyses are performed using Microsoft 365 Excel. The main analysis tool is Student's t-test, which function in Excel is =TTEST(array1;array2;tails;type). The null hypothesis used for all of the T-Tests is that there is no statistically significant difference between arrays (sample data) 1 and 2. A two-tailed test is used for all the tests in this thesis. The type will depend on the data. Type 1 (paired data) is used when the selected data is measured from the same sample. Type 2 and 3 are used when comparing data from different samples. Type 2 is a two-sample test of equal variance and Type 3 is a two-sample test of unequal variance. The significance of variance is analysed using an f-test, which yields confidence similar to the t-test. Confidence of 95% is used to select

Type 3 over Type 2 for the t-test. T-test will yield p-values, which represents the probability of chance. For scientific data, the p-value needs to be 0.05 (5%) or below for the rejection of the null hypothesis. When the null hypothesis is rejected, an alternative hypothesis will be considered valid. For t-tests in this thesis, the alternative hypothesis states that there is a statistically significant difference. In other words, there is at least a 95% confidence that the difference is statistically significant. All of the t-test results are presented as this confidence percentage. The results which have a confidence of 95% or over in this thesis have statistically significant differences in terms of scientific accuracy. Results in this thesis are presented even when this confidence is lower. This is because the size of data used for testing is small and to present the magnitude of difference between samples. Such as having a confidence of 90% compared to 10%.

6. RESULTS AND ANALYSIS

This chapter will cover the results and analysis of the experimental data. More detailed information from the different open-air contamination screenings can be found in Appendix A and B. Appendix C will have pictures of the screening samples, since the hand sanding process relies on visual observation to achieve the correct level of sanding for the set surface treatment. Appendix D includes the main t-test analysis confidence for the SFE and open-air contamination screening (Screening 1 and Screening 2) samples.

6.1 SFE results

The objective was to measure CA with different liquids and determine the SFE and its components based on surface treatment. The results are given as average values with StDev. If the StDev is larger than the difference of the SFE values between the samples, it will be hard to differentiate the different surface treatments from one another. SFE results can be seen in Figure 32. The SFE increases based on the level of sanding. Samples A Med and Hard have larger SFE values than the A Light. This is also true for both the B samples and the Grit Blasting sample. This is due to the removal of the weak epoxy layer and the revealing of the CF. The values of the PPR0 and A Light treatments,

which had low or no sanding, have SFE values that match with the ones found in other studies (37-39).

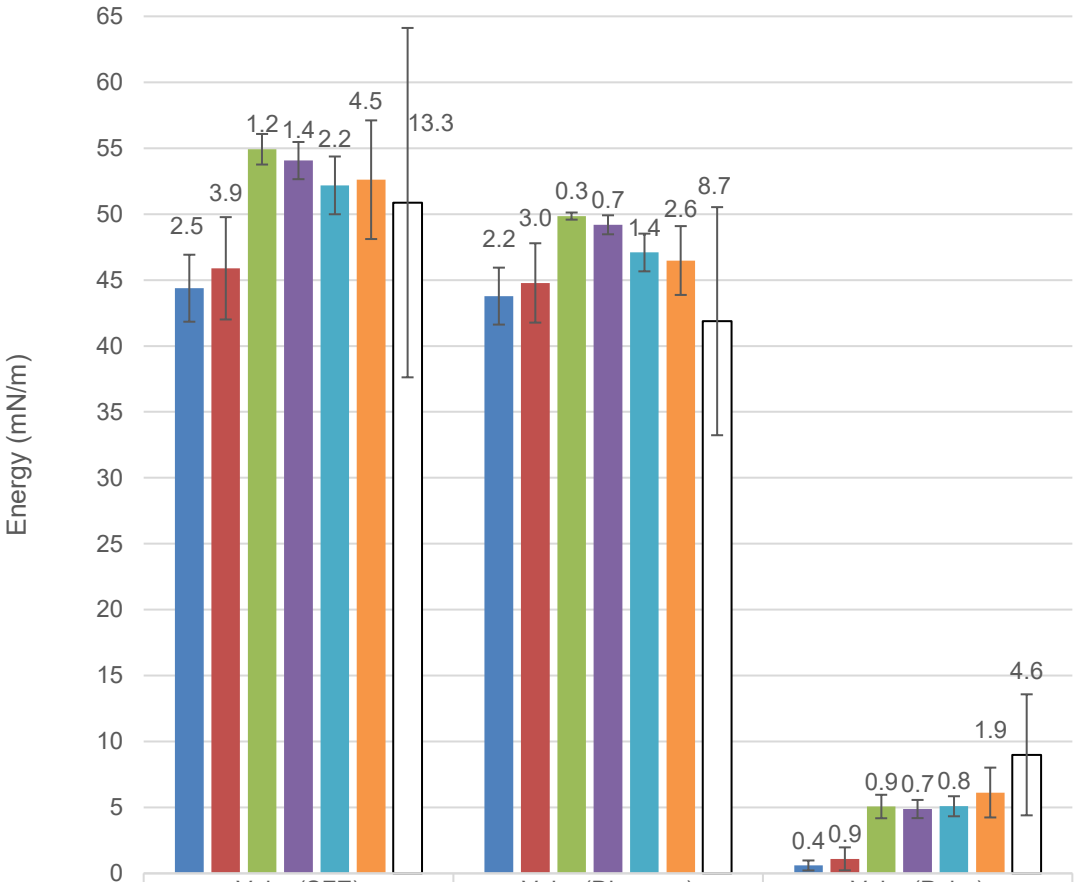

	Value(SFE)	Value(Disperse)	Value(Polar)
PPR0	44.4	43.8	0.6
A Light	45.9	44.8	1.1
A Med	54.9	49.9	5.1
A Hard	54.1	49.2	4.9
B Med	52.2	47.1	5.1
B Wa	52.6	46.5	6.1
Grit Blast	50.9	41.9	9.0

Figure 32. *SFE and StDev of samples*

SFE values for the A Med, A Hard, B Med, B Wa and Grit Blast treatments are in a similar range to each other, between 50-55 mN/m. Both of the SFE components increase, the dispersive component varying between the samples and the polar component being quite similar for samples that have medium sanding. For the Grit Blast sample, the polar component has the highest value, but the StDev is also much greater. After acetone flushing, the Grit Blast sample had runoff marks, which indicated that the Al_2O_3 was removed unevenly. Al_2O_3 might have been left on the surface, which could affect the polar

component’s high values. The flushing removed black dust from all the sanded specimens even from the ones that were wiped with solvent. The acetone used for flushing was collected into a beaker. Then it was left for evaporation and the black dust was left at the bottom of the beaker. This shows that it is difficult to remove all the sanding dust from the surface.

Wetting can be predicted, by constructing a wettability envelope using the SFE data. In Figure 33, the wettability envelopes for 40° CA for the SFE samples have been constructed. The envelope gives the SFE component values for a liquid to have a CA of 40°. When liquids SFE values are smaller than on the envelope, the predicted CA values of the liquids will be less than 40° on the surface. If the SFE is greater, the CA will be higher than 40°. The PPR0 and A Light surfaces have quite similar wetting profiles with smaller SFE values. The other surface treatments have similar envelopes to one another, which was indicated by the results of the SFE. The probe liquids are also shown in the envelope plot and their CA can be approximated on the surfaces. Based on the envelopes, diiodomethane should have CA values under 40° and ethylene glycol CA values should be over 40° for the PPR0 and A Light surfaces and under 40° for the rest. Glycerol and water should have CA values over 40° on all surfaces. These values are predictions and are heavily influenced by the deviation in the theoretical SFE values. The wettability envelope can be used to predict a liquids CA that was not used in the experiments. This makes it possible to scout if other liquids would have SFE values in the areas where the

different surfaces could be differentiated with better precision. The usage is not limited to liquids, adhesives could be compared based on their predicted wetting.

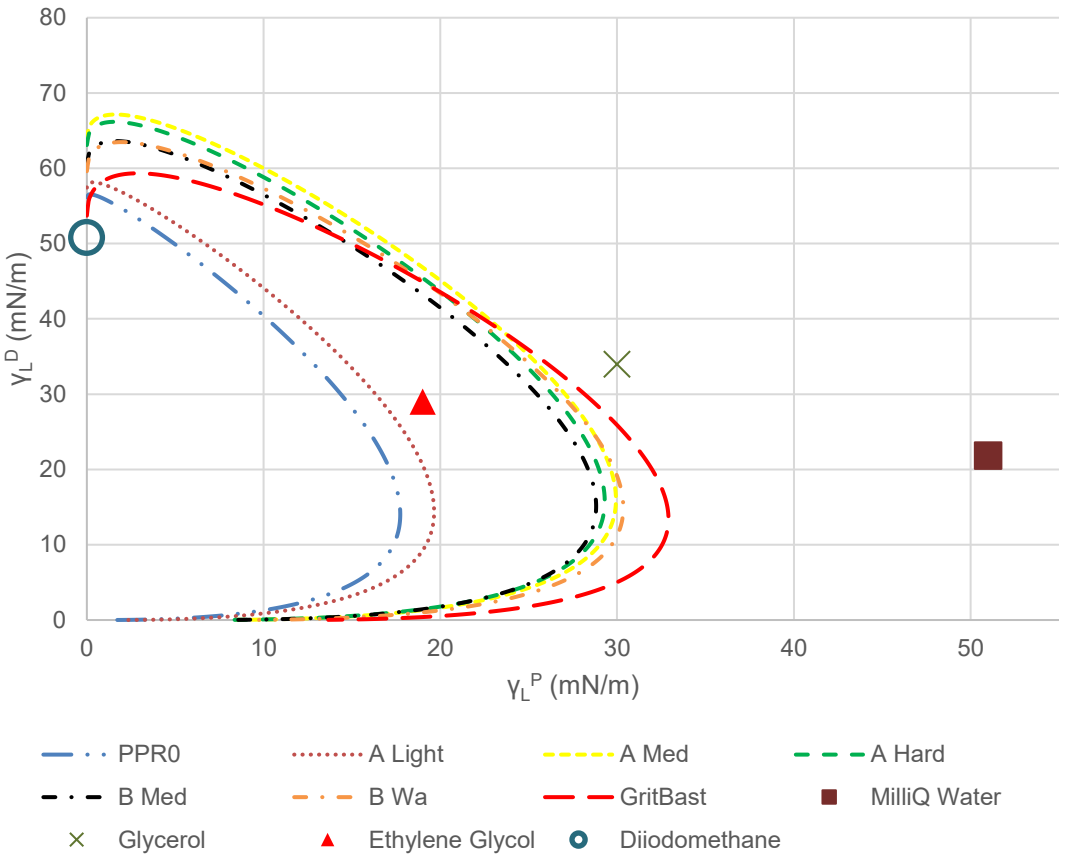

Figure 33. *Wettability envelopes based on the 40° CA for CFRP surfaces from the SFE data and the SFE of the probe liquids used*

In terms of qualifying the surface treatments using WCA, the StDev is important. If the StDev is too high, the accuracy of the method is not enough to properly qualify the state of surface treatment that would lead to good adhesive bonding. The WCA values are shown in Figure 34. Lower WCA values relate to better wetting, higher surface energy and better quality of adhesive bonding. For the PPR0 and A light samples the WCA is high, which was noted before as low SFE. Grit Blast samples StDev is very high compared to other samples, which was also true for SFE values. The WCA value is the lowest, which was indicated by the high polar component value in SFE.

Based on the StDev and the WCA values, it will be difficult to differentiate the sanded surface treatments from one another. The B Med sample has the highest WCA value, which is related to the MEK wiping. Figure 34 also includes the average WCA of the left and right angles. The ellipse(tangent-1) fitting method gives insight into the surface flatness, as the sanding process seems to curve the samples. This seems not to be an issue if the peel plies are removed from both sides before surface treatments are done, which

should be a normal procedure before adhesive bonding. Student's t-test can be used to determine if the difference between the samples is statistically significant. For scientific data, a confidence level of 95% or higher is typically used for the data to be statistically significantly different. Appendix D contains the results of these tests. Table D 1, Table D 2, Table D 3 and Table D 4 are shown the t-tests for the SFE measurements for each probe liquid. Most of the surface treatments have a statistically significant difference with two liquids at least. This is shown in the tables by set comparison having over 95% confidence. The A Med and A Hard samples are different since the only probe liquid that can differentiate them is diiodomethane. However, the diiodomethane did not work well with the Grit Blast sample. The measurements overall with diiodomethane were tricky since the CA values with it are very low. The difference between the A Med and A Hard samples is in our interest since their difference is the damage to the top fibres by sanding. Since the A Med surface treatment is stopped when CF is released, it should have less

damage on the top fibres than when the A Hard treatment is applied. However, based on our data this is hard to prove.

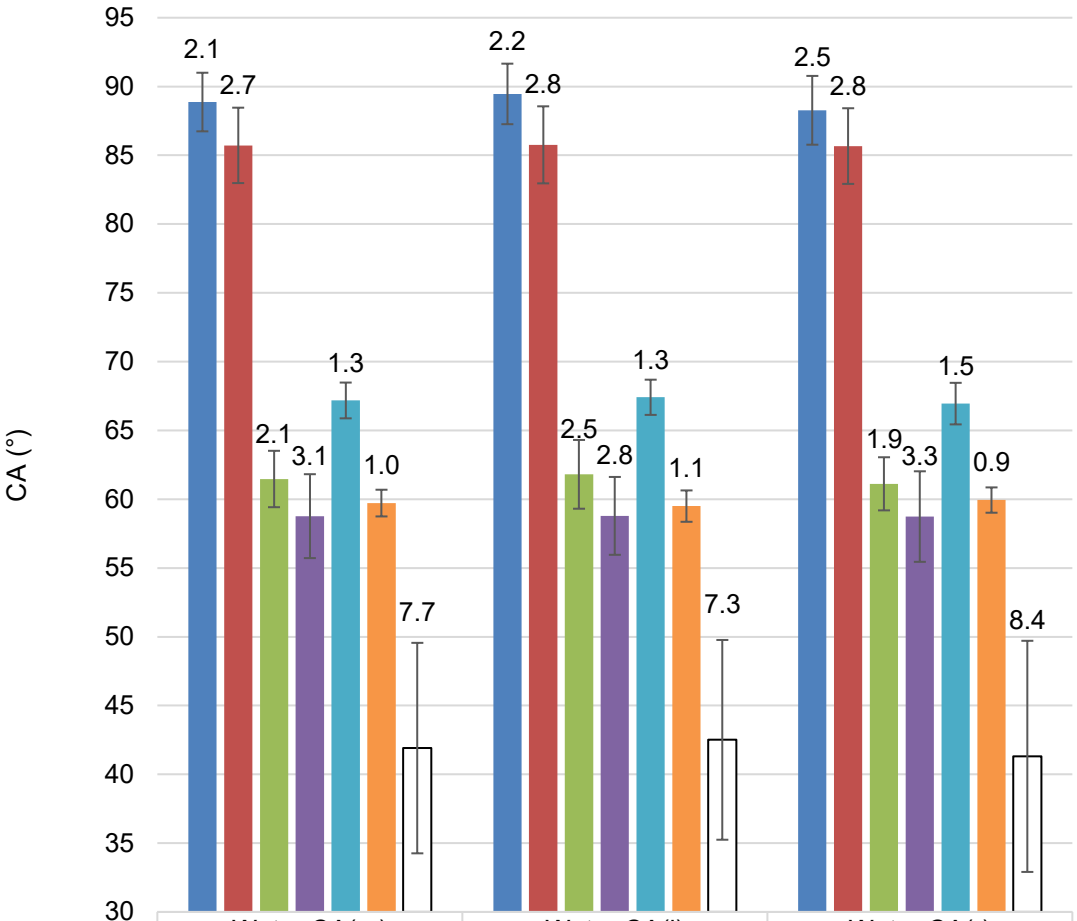

	Water CA(m)	Water CA(l)	Water CA(r)
PPR0	88.9	89.5	88.3
A Light	85.7	85.8	85.7
A Med	61.5	61.8	61.1
A Hard	58.8	58.8	58.7
B Med	67.2	67.4	67.0
B Wa	59.7	59.5	59.9
Grit Blast	41.9	42.5	41.3

Figure 34. *Water CA(m), CA(l) and CA(r) values from SFE sample*

In a study by A.D. Gilpin et al. (40) on plasma-treated polyethylene (PE) surfaces, the relation of plasma treatment to WCA has been analysed. For the system they used, a strong linear correlation between WCA and polar component was found (40). This appears when the SFE is compared to the cos(WCA(m)). This type of linear correlation can be seen in the Young-Dupre equation, where the surface tension and CA are linked. In Figure 35, the SFE and WCA relation is shown including the relation from the ISO 15989 (41). Using a linear trendline, we can see that our values follow it. Pearson's correlation coefficient was used to statistically measure the strength of the linear relationship. For

the polar component, the correlation is very strong, over 99% confidence. For the dispersive component, the strength of the correlation is very low, around 5% confidence. Total SFE reaches 89% confidence in correlation, which is mostly lowered by the dispersive component. This is similar to the relation found in the work by Gilpin et al. (40). WCAs could be used to predict the SFE and the polar component of the measured surface. In the ISO 15989, a conversion chart is used to predict the SFE from measured WCAs. The ISO 15989 can be used for corona treated plastic films. We can see that the ISO 15989 conversion slope is steeper than our measurements. Meaning that from its data, the change in WCA will have a higher effect on the SFE of the plastic film. This is reasonable since the purpose of corona treatment is to introduce functional groups on the surface, which affect SFE greatly.

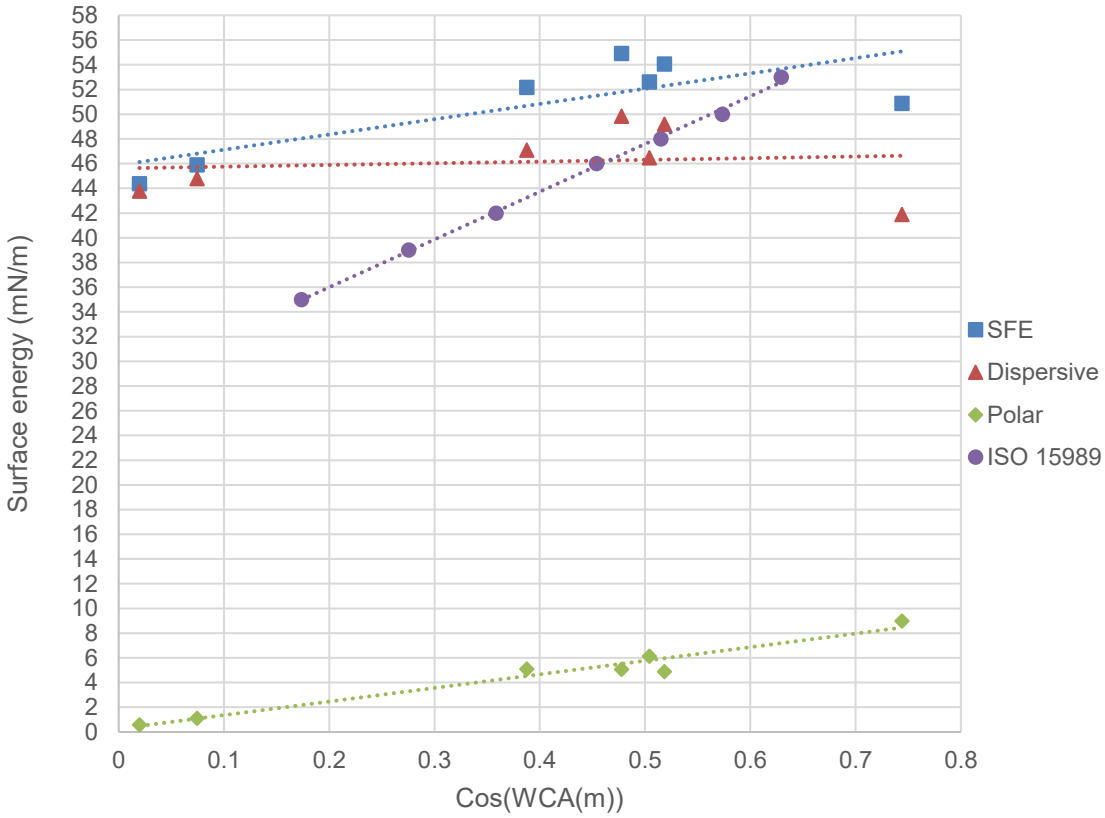

Figure 35. *SFE and its components to Cos(WCA(m)) from SFE measurements and surface energy correlation from the ISO 15989*

The droplets on highly sanded samples showed larger anisotropy than on samples that had lighter sanding applied. It seems to be related to fibre orientation, but it needs further testing. In Figure 36 a water droplet on the A Hard surface is shown. The droplet is longer in the direction of the fibres. Figure 37 presents droplet shapes on chemically stripe-

patterned surfaces that shows similar behaviour as our droplets. It is unknown what sizing is used on the CF in the laminates, which might affect the CA measurements.

Figure 36. *Water droplet on A Hard treated surface, droplet length 3mm*

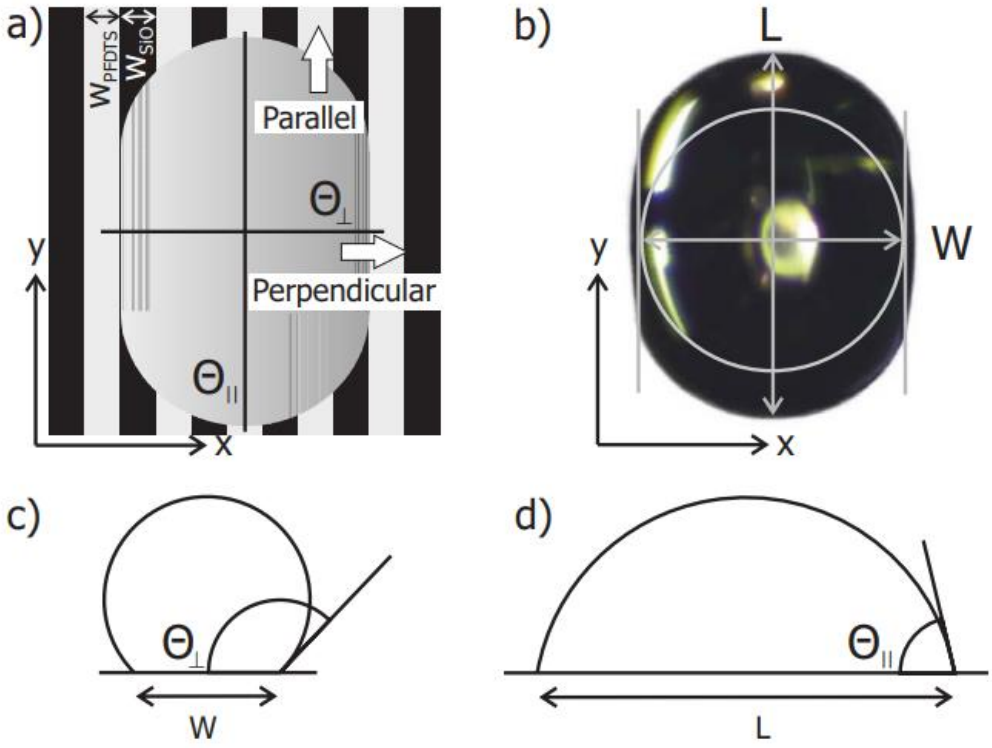

Figure 37. *Anisotropic drops a) top view, b) glycerol droplet c) perpendicular view d) parallel view* ***(42)***

6.2 Time dependency and droplet anisotropy

The purpose was to observe if CA stabilizes over time. Results over one minute of observation can be seen in Figure 38. The CA decreases linearly over time. Decrease for the first five seconds is faster because the droplet is still stabilizing. The surface does not have an effect on the decreased speed. Over one minute the CA on the CFRP surface decreased around six degrees and for glass around seven degrees. Water behaves similarly on glass and CFRP. The decrease is similar to in surfaces that do not absorb water, as shown in the work of L. Muszynski et al. (43). The total CA change thus relies solely on evaporation, which makes it important to record the humidity and temperature of the measurements. It was also observed that the droplets completely disappear between five to ten minutes of the deposition, which was slightly faster for the glass surface than CFRP. This might be because water wets the glass surface better than the CFRP resulting in a larger area covered, making evaporation faster. Using linear regression analysis, it can be said that the observation times of zero (0) seconds and one (1) seconds can be considered outliers. This is because their standard residuals are over three, verifying that very short dwell times should be avoided.

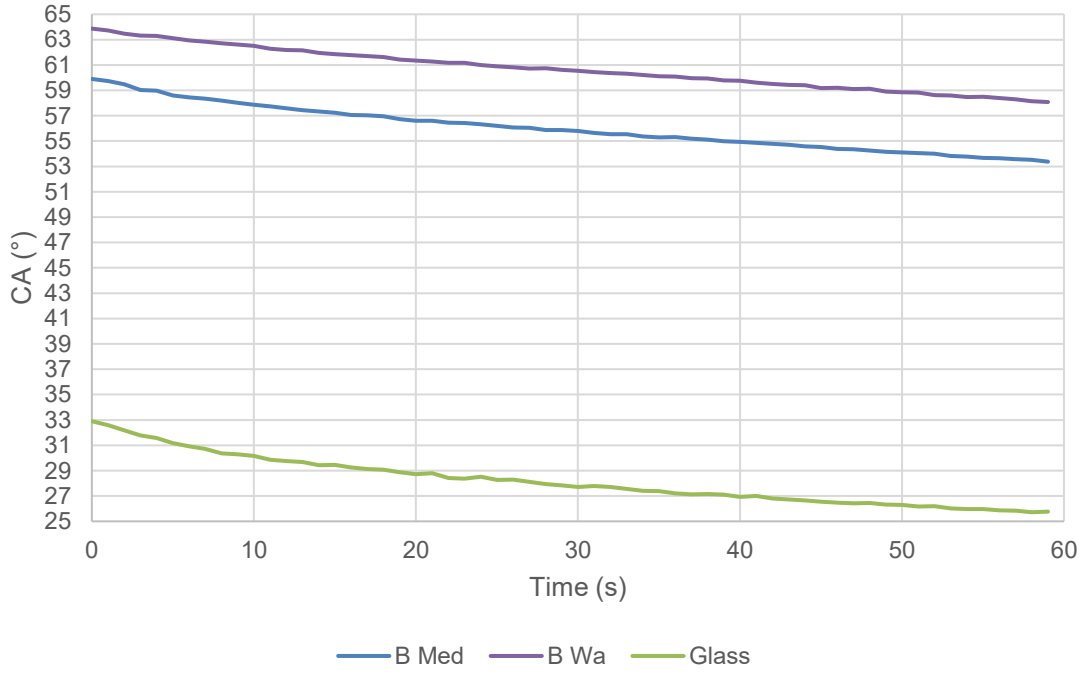

Figure 38. *Average CA(m) of multiple water droplets over 1 minute on selected surfaces*

Anisotropy of the droplet was measured on the B Med and B Wa samples. Three different view angles were used. The basic view angle is that the lens is parallel to the laminate

0-fibre orientation. In Figure 41 the two other view angles are shown. The parallel view angle measures the CA of the droplets wetting in the direction of the top fibres. The perpendicular view angle measures the CA of droplets wetting against the top fibres. The results are presented in Figure 39. Based on this, the measurement angle affects the measured CA. Change in CA is greater than the StDev between the parallel and perpendicular angles. The basic view angle is 30° from the parallel view angle and 60° from the perpendicular view angle. The behaviour seems similar to droplets on chemically stripe-patterned surfaces by Bliznyuk et al. (26) and David and Neumann (42,44). In Figure 40 the view angles relation to CA from Bliznyuk et al. is shown. View angles for our measurements and those used by Bliznyuk are the same. We can see that the measured CA values are close to each other when using a parallel view angle. Similar behaviour is seen in our results since the parallel view angles and the basic view angles results are close to each other. To analyse if the differences in the CA are significant enough, a t-test was performed. For B Med, the parallel fibre orientation can be differentiated from the two other orientations with a confidence of 99%. The other two do not have a significant difference. T-test results for B Wa are similar, parallel fibre orientation can be said to be different from the other two orientations with 99% confidence.

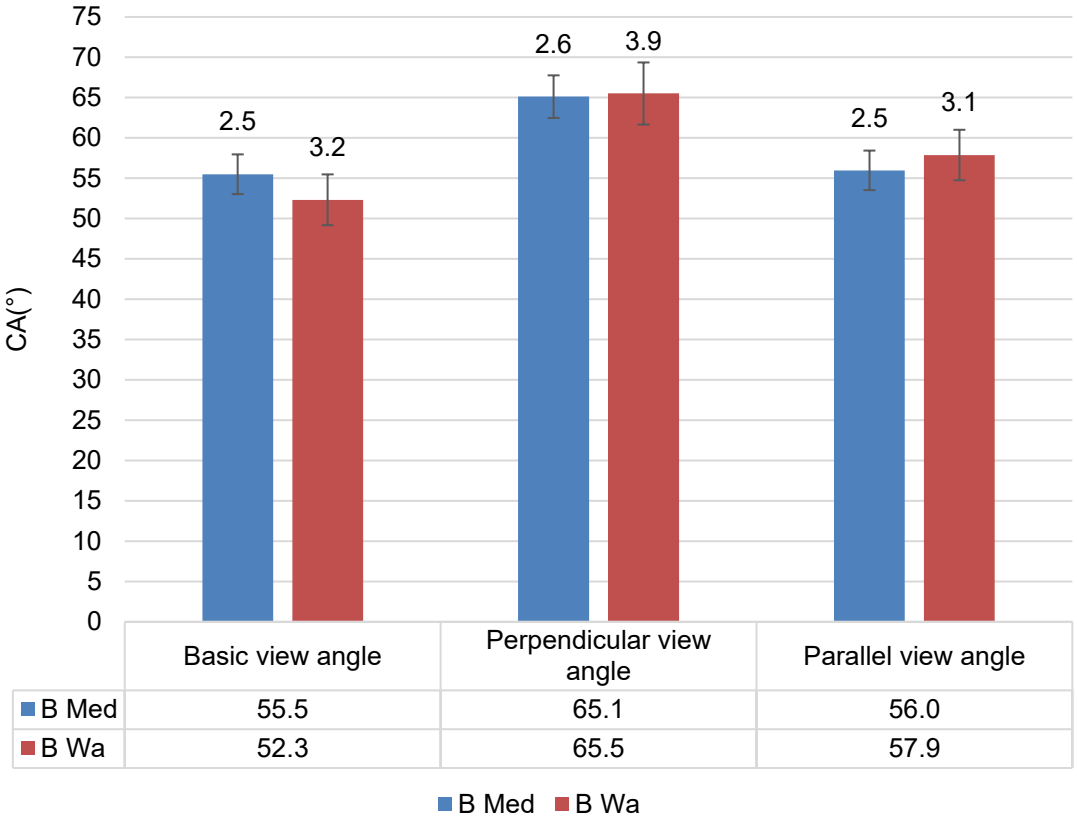

Figure 39. *Droplet anisotropy, CA values with different view angles*

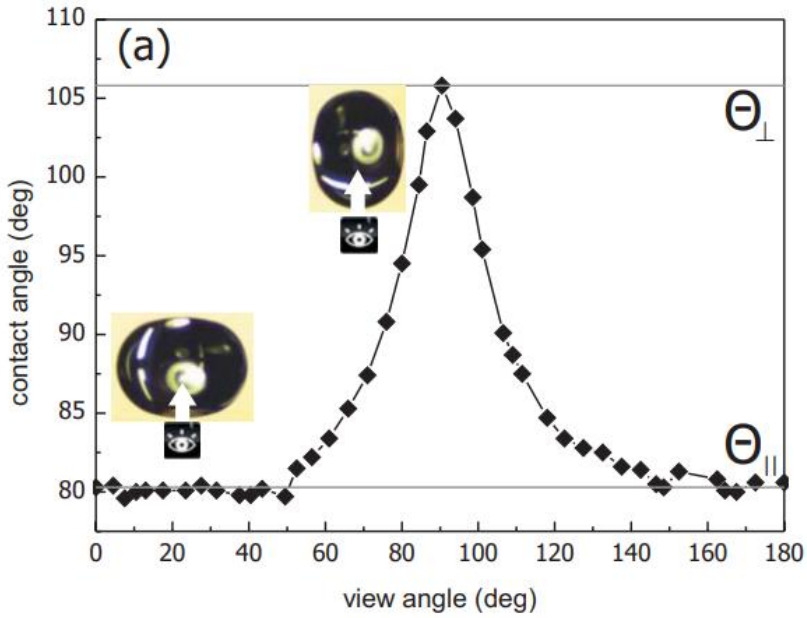

Figure 40. *CA measurements along the contour of a sessile droplet on different view angles* ***(42)***

6.3 Location sampling for uniform surface

Location sampling was done on the untreated CFRP surface, which had peel ply removed. The other surface tested was the B Med surface treatment, which results are affected by the MEK wiping. The measurement of 121 droplets takes about 25 minutes meaning the last drop location have been exposed for longer than the first ones. Average WCA(m), WCA(l) and WCA(r) of the SDM are shown in Figure 41. The B Med samples WCAs are very high compared to values in other measurements, which were around 67°. The use of MEK increases WCA values making the surface hydrophobic. The StDev for the untreated sample is similar to in earlier measurements for the PPR0 surface. The

deviation of the B Med compared to the prior test seems to be a bit higher. This is probably partly caused by uneven sanding or the wiping process.

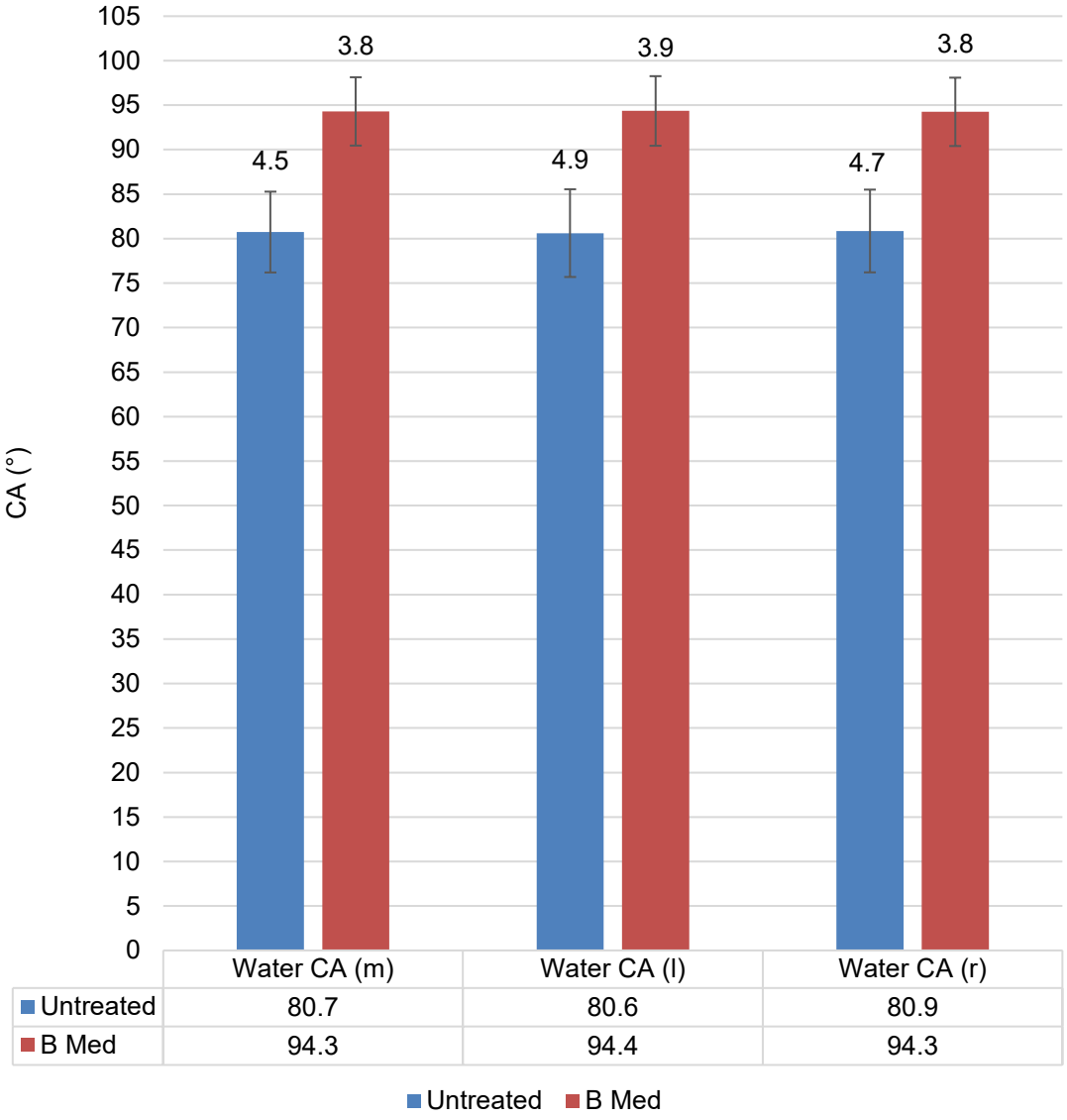

Figure 41. *Average WCA(m), WCA(l) and WCA(r) of the SDM samples*

SDM tool includes a plotting map. These maps are shown in Figure 42 for the untreated sample and Figure 43 for the B Med sample. The red colour indicated high WCA and blue low WCA values. For the untreated sample, the mapping is rather even, few locations stand out as red and orange. Removal of peel ply can be the reason. A knife must be used for the start of the removal, which leaves marks on the surface. When pulling the peel ply off, it usually sticks on some locations more than others. On the B Med sample, it is noticeable that the bottom area has high WCA values compared to the top. This can be due to sanding or that the MEK is influencing some areas more than others.

The MEK wiping sometimes leaves greasy looking spots that are hard to get rid of. A total of 12ml of MEK was used to clean this sample.

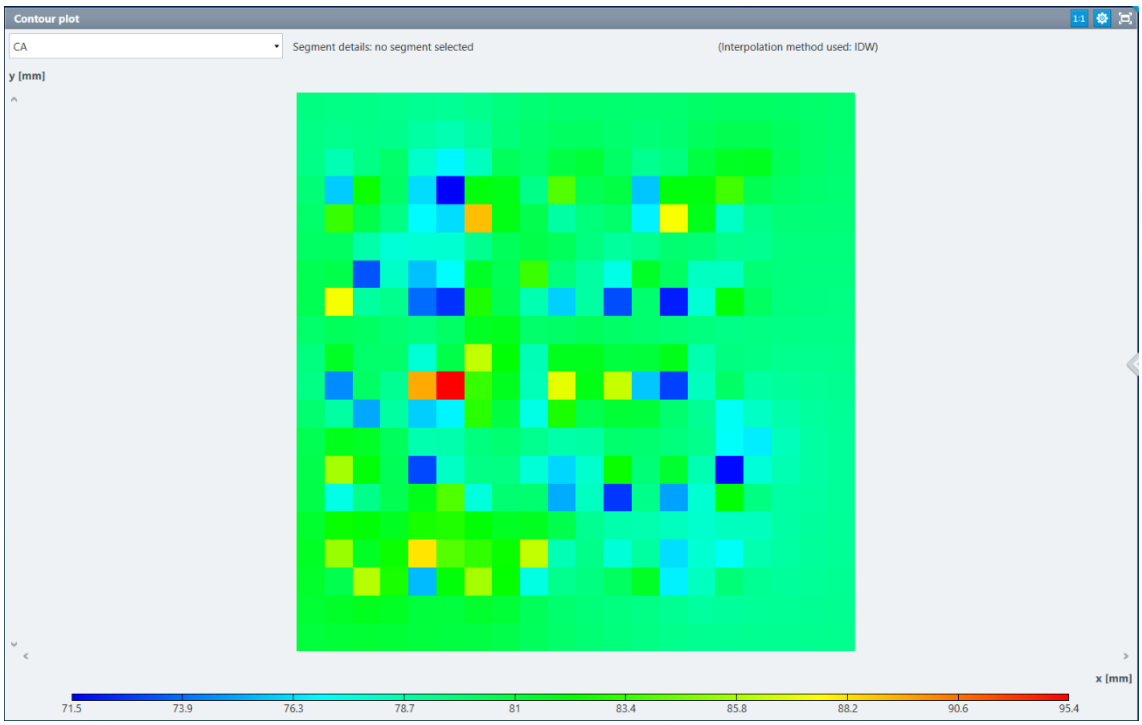

Figure 42. *Untreated SDM contour plot, min(blue) 71.5° and max(red) 95.4°*

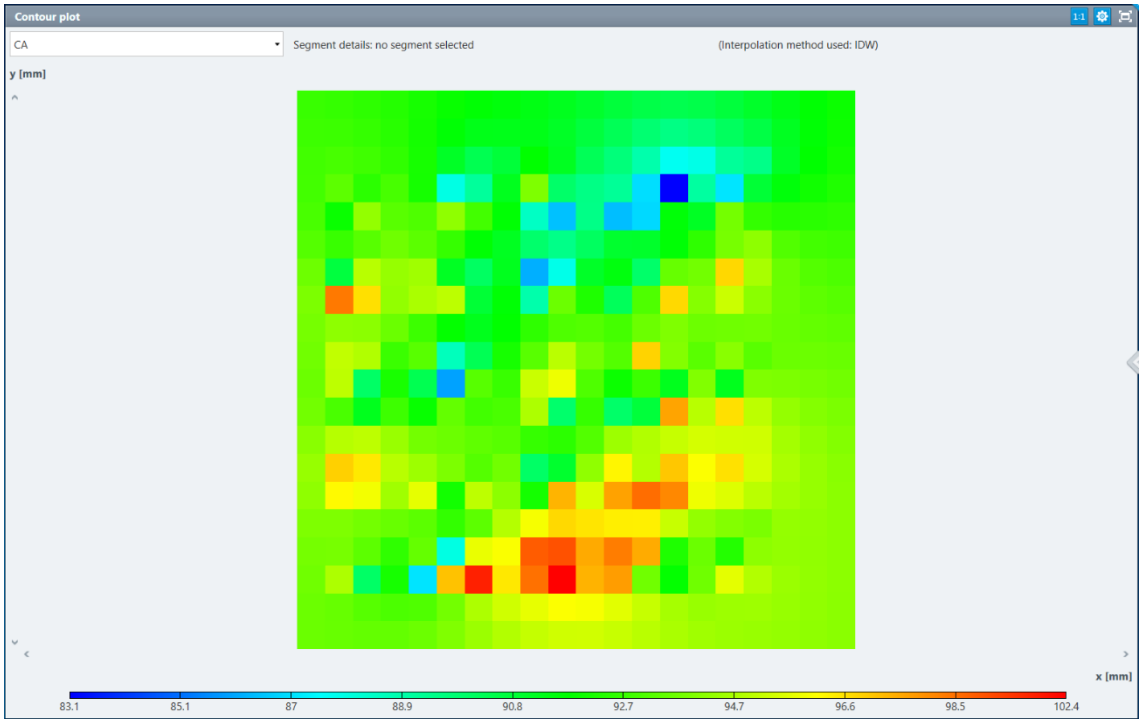

Figure 43. *B Med SDM contour plot, min(blue) 83.1° and max(red) 102.4°*

The number of droplets for SDM samples was greater than for the screening samples. This makes it possible to analyse if the WCA values follow a normal distribution, which

was a requirement for the use of the Student's t-test. This can be done using a quantile-quantile(Q-Q) plot, which makes it possible to compare two probability distributions. In Figure 44 and Figure 45 the data quantiles from the SDM measurements are compared against normal theoretical quantiles. The linearity of the data points suggests that WCA values are normally distributed. We can also use the t-test to see if WCA(l) and WCA(r) have significant differences for the SDM samples (a hypothesis). Using t-test we get the result that for both samples there is no statistically significant difference between WCA(l) and WCA(r) values.

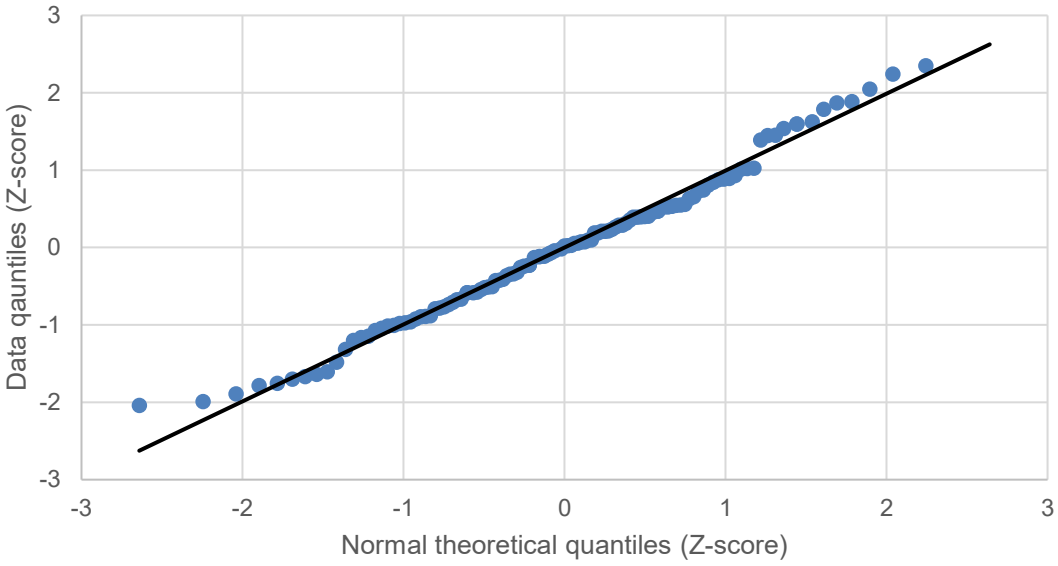

Figure 44. *Q-Q plot for the data of untreated SDM sample*

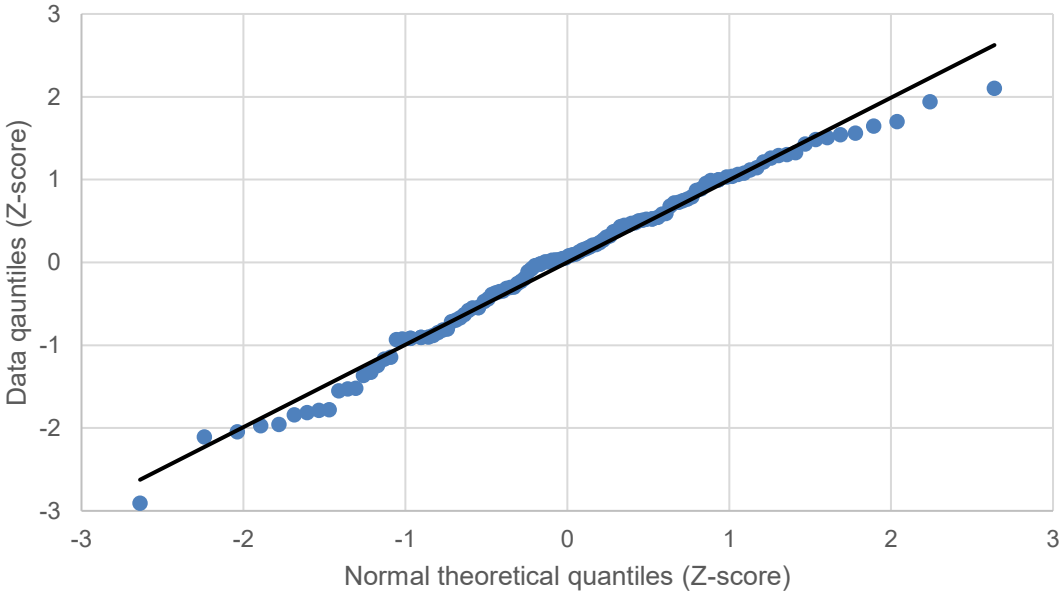

Figure 45. *Q-Q plot for the data of B Med SDM sample*

6.4 WCA and open-air contamination

The results of the open-air contamination screening can be found in Appendix A: Open-air screening results and Appendix B: Open-air screening 2 results. They include the WCA(m), WCA(l) and WCA(r) for each time series and surface treatment with an average of the StDev for each complete time series. The samples in Appendix A were sanded using Ecowet P180 and the samples in Appendix B using 300D Stikit disc. The observation period was lowered on second testing for practical reasons. The roughness differences of these samples will be discussed in section 6.6. This section includes the simplified figures of the results. Appendix C: Sample pictures, including pictures of the samples. The analysis also includes notable factors from Appendix C. T-test results are found in Appendix D, which will be discussed at the end of this section.

The PPR0 is the baseline sample, which included peel ply removal and the two-wipe method. Figure 46 shows WCA(m) results for the PPR0, A Light and A Light2 samples. Number 2 is used to distinguish the results of the second screening from the results of the first screening. StDev is marked as an average from the StDev from each timeseries for each sample. These are used in figures throughout this section. The StDevs for PPR0 are fairly high, but when compared to the untreated SDM sample they are lower. The PPR0 sample in SFE measurements had an even lower StDev. The 0min WCA values are close to those of the untreated SDM sample and the higher WCA values match the PPR0 surface from before. The trend seems to be a slight peak at the start and higher WCA values after four hours of open-air. Figure A 1 shows that there is a difference in WCA(l) and WCA(r). Based on the analysis of SDM samples, there should not be a difference in WCA(l) and WCA(r) for these samples since they are made on a flat surface. From Appendix C: Figure C 1, we see that the knife marks from the removal of the peel ply are visible. They did not affect measurements as droplets were not placed on them.

The A Light treatment included peel ply removal and light sanding with the 2-wipe method to remove sanding dust. The WCA values are constant, but when compared to the A Light from the SFE measurements, the WCAs are around 20° lower. The level of sanding might be different since the sanding was done by a different operator. Storing might also affect the WCA value since the SFE samples were surface treated long before testing. The StDev is lower than in the PPR0 sample, which relates to a more even sample because of sanding. The general trend here is that the WCA values remain constant at the beginning and are reduced as time goes on. A larger dropping in the WCA can be seen at the end of the observations, which happens for other samples as well. The left and right WCA are close to each other, which are shown in Figure A 2 and Figure B 1. The results of the second screening have more linear WCA values, which are close to 65°,

and the StDev is slightly lower. The pictures of the A Light and A Light2 samples in Figure C 2 shows that visual sanding marks are present, and the orientation of the fibres can be seen slightly. The marks from the peel ply removal are slightly visible.

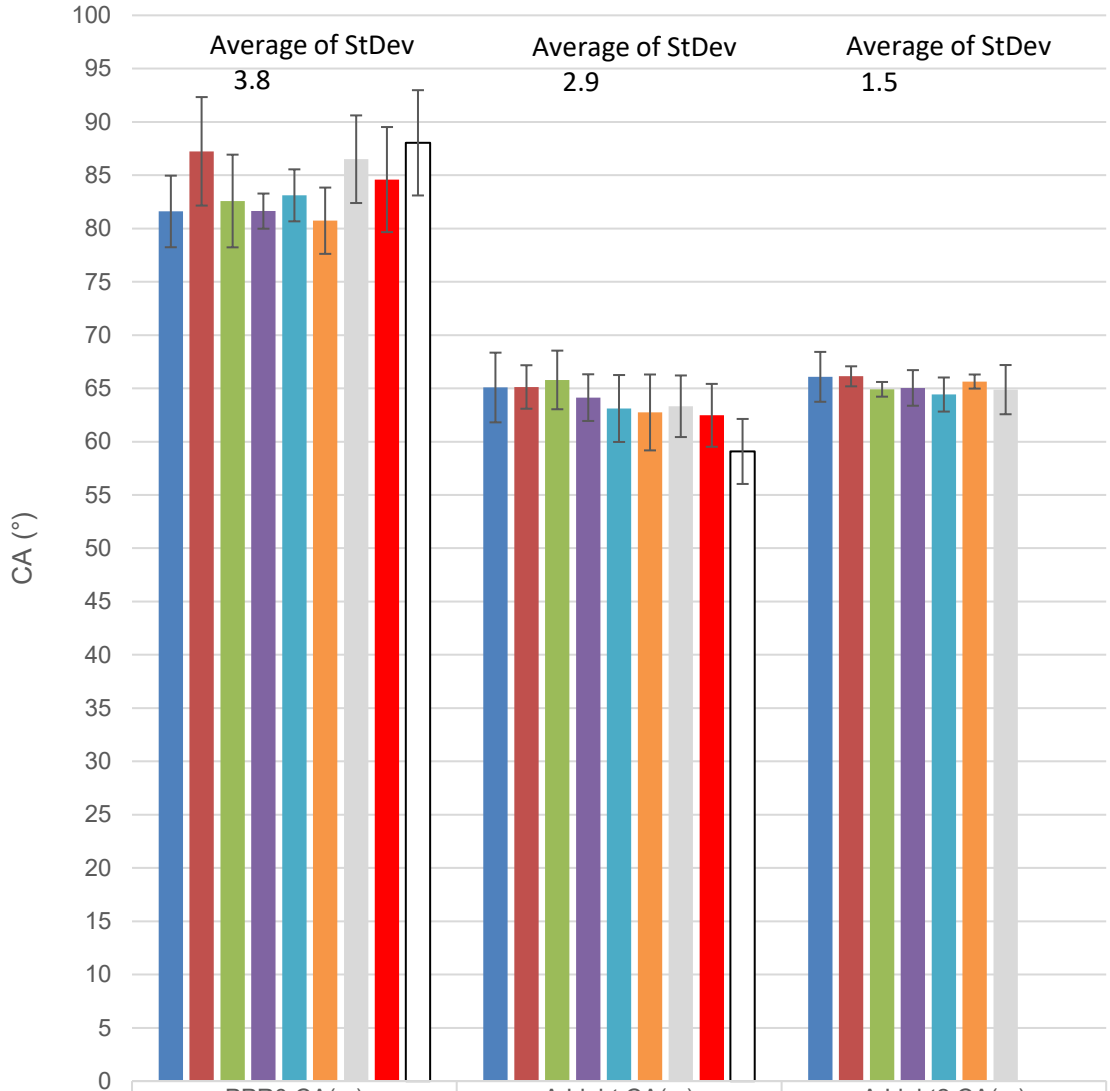

	PPR0 CA(m)	A Light CA(m)	A Light2 CA(m)
0min	81.6	65.1	66.1
15min	87.2	65.1	66.1
30min	82.6	65.8	64.9
1h	81.6	64.1	65.0
2h	83.1	63.1	64.4
3h	80.7	62.7	65.6
4h	86.5	63.3	64.9
6h	84.6	62.5	
8h	88.0	59.1	

Figure 46. *CA(m) values for PPR0, A Light and A Light2 samples*

The A Hard surface treatment was the most intensely sanded. The WCA(m) values for the A Med, A Med2, A Hard and A Hard2 samples are shown in Figure 47. The surface

of both A Hard samples was evenly glossy and reflected light well, which made the measurements more difficult. Compared to the A Hard surface from SFE measurements, the WCA values are around 12° lower for the first screening and eight degrees lower for the second. The series itself is rather similar for both screenings, but again at the end of the observation, the WCA values seem to dip at the eight hour mark. Appendix C: Figure C 3 shows the pictures of the A Hard samples. The surfaces reflect light and the fibre orientation is visible. The fibre orientation of the second layer is visible.

The A Med surface had slightly lighter sanding than in the A Hard. The surface was not as glossy as the A Hard. Darker spots can be seen in the laminate because of lighter sanding. Similarly, when comparing the WCA of SFE samples to the A Med, the difference is around 12° for the first screening. The WCA values of the second screening seem to be almost the same as for the A Hard. The sanding was done differently but the results are almost the same. The use of different sanding paper or the surface having different roughness might be the reason. The time series WCA values are not as even as for the A Hard, but the StDev is almost the same. The dipping at the end of the observation time is similar. Appendix C: Figure C 4 shows that the A Med samples have more dark areas and are not as glossy if compared to the A Hard samples. With the right angle, the fibres of the second layer are visible. The surface, which was prepared with

300D (3M) sanding paper, seem to reflect more light than the other one. Another possibility is that the samples between the screenings originate from different large laminates from which they were cut, although the material specifications should be the same.

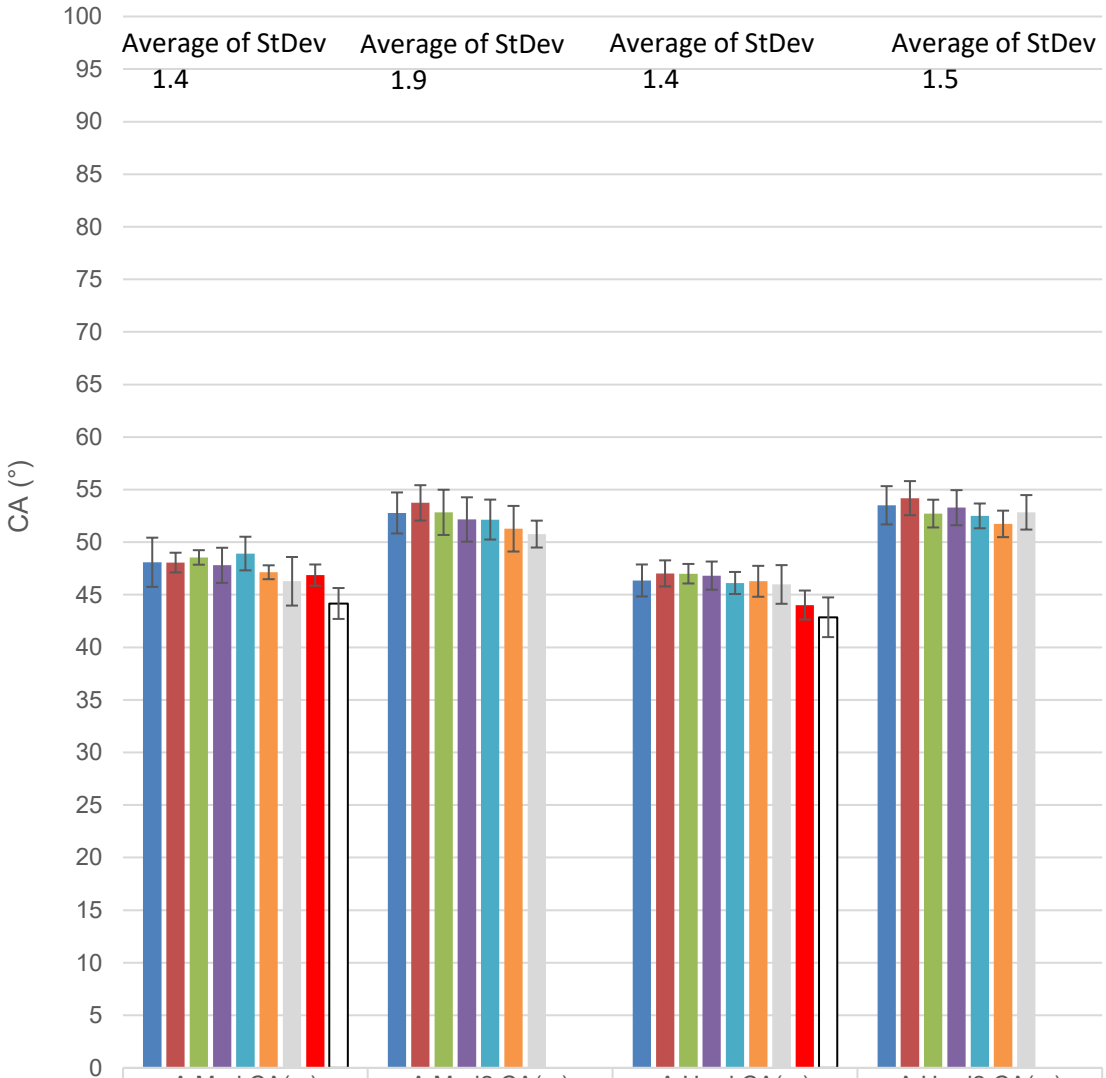

	A Med CA(m)	A Med2 CA(m)	A Hard CA(m)	A Hard2 CA(m)
0min	48.1	52.8	46.4	53.5
15min	48.1	53.7	47.0	54.2
30min	48.6	52.8	47.0	52.7
1h	47.8	52.2	46.8	53.3
2h	48.9	52.2	46.1	52.5
3h	47.1	51.3	46.3	51.7
4h	46.3	50.8	46.0	52.8
6h	46.9		44.0	
8h	44.2		42.9	

Figure 47. *WCA(m) values for A Med, A Med2, A Hard and A Hard2 samples*

The WCA(m) values for the B Med, B Med2, B Wa and B Wa2 samples are shown in Figure 48. The difference between the B Med to the A Med is the MEK wiping. MEK's

effect on WCA is similar as seen before in the SDM sample, the CA being close to 90°. It is more than the B Med sample had on the SFE measurements. The high WCA is probably due to MEK sticking onto the surface, making it almost hydrophobic. The StDev is larger than before on the SFE B Med sample. However, there is no difference in StDev between the screenings. On second screening the starting measurements have over 90° angles, but they lower down towards the three hour mark, to the same level as in the first screening. Appendix C: Figure C 5 shows a picture of the B Med samples. They look similar to the A Med samples, where the sanding level should be the same. MEK wiping has a slight effect on the surface reflection. In general, it was harder to get good measurements from MEK wiped surfaces. From the right sample, a dark line can be seen, this is probably due to fibre placement during lay-up, or fibre missing. These dark lines were more prominent on the laminates used for the second screening.

The B Wa surfaces had Scotch-Brite application and rinsing with water. The B Wa WCA values are lower than in the B Med, but the StDev is higher. Compared to the B Wa in SFE measurements StDev is considerably larger. This can be due to the uneven sanding or removal of the MEK by the flushing. Between the screenings, the results are close to one another, which suggests that the difference is with the MEK flushing rather than sanding. The water flushing might leave water molecules on the surface that do not evaporate before measurements. Appendix C: Figure C 6 shows the surface of the B WA samples. They are similar to the others with the same level of sanding, such as the B Med. Surface reflections differ slightly due to Scotch-Brite wiping. Other than that, there

are no visual indicators to differentiate the A Med, B Med and B Wa samples from one another which all have medium sanding applied.

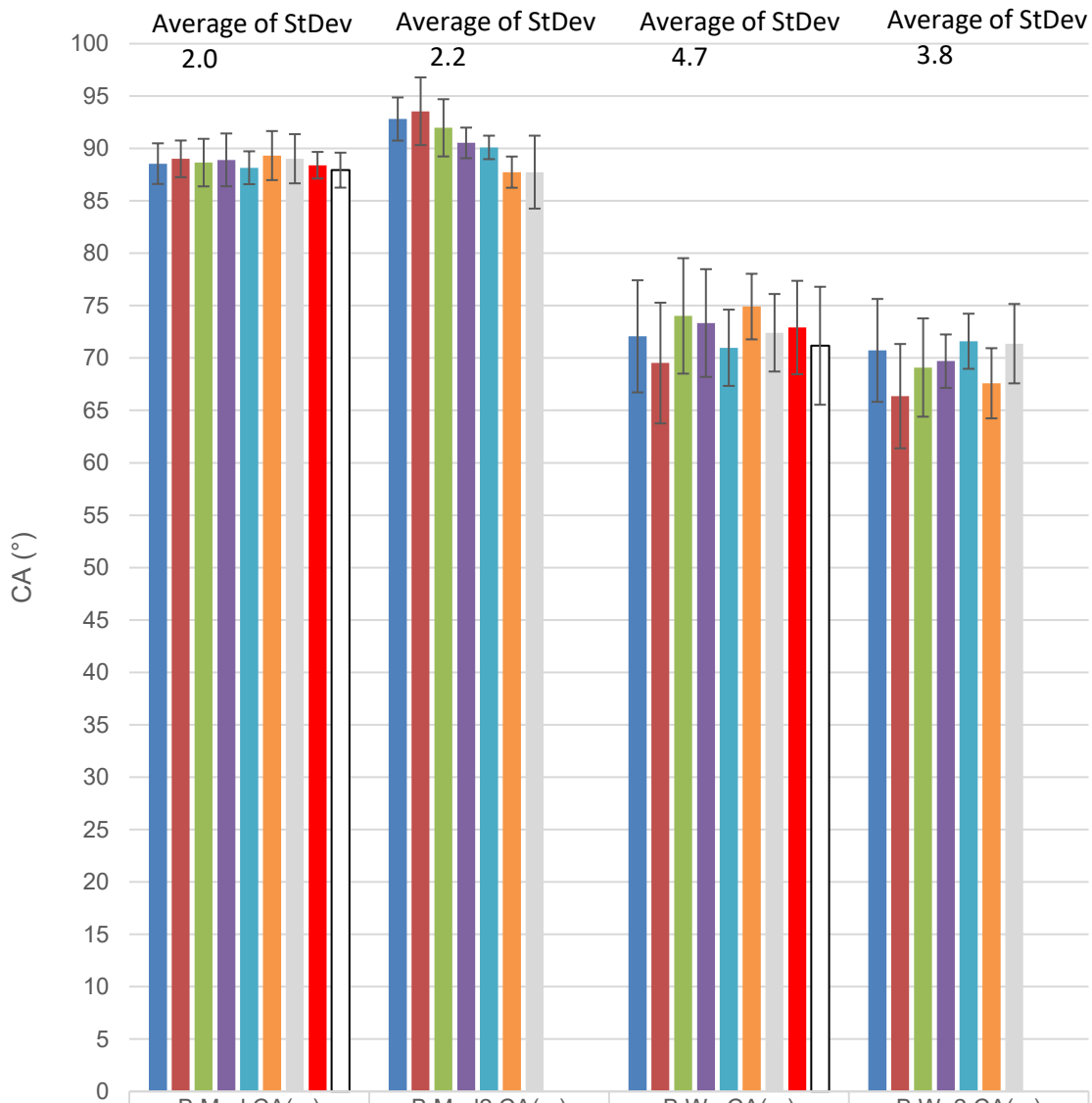

	B Med CA(m)	B Med2 CA(m)	B Wa CA(m)	B Wa2 CA(m)
0min	88.6	92.8	72.1	70.7
15min	89.0	93.6	69.5	66.4
30min	88.7	92.0	74.0	69.1
1h	88.9	90.5	73.3	69.7
2h	88.2	90.1	71.0	71.6
3h	89.3	87.7	74.9	67.6
4h	89.0	87.7	72.4	71.4
6h	88.4		72.9	
8h	87.9		71.2	

Figure 48. *WCA(m) values for B Med, B Med2, B Wa and B Wa2 samples*

The WCA(m) values for the GritBlast and GritBlast2 samples are shown in Figure 49. Grit blasting was done with different equipment between the screenings. The deviation

is still high even with no acetone flushing was used unlike in the SFE measurements. The industrial-grade grit blaster seems to give better results. The general trend is that WCA increases for the first screening and then decrease and for the second screening the fluctuation of the WCA value over time is low. The WCA values are around 5-10° higher than in the SFE grit blasted sample. The SFE sample and the first screening sample look similar, the second screening sample has more material removed, which was the point of using the industrial-grade grit blast cabinet. Appendix C: Figure C 7 shows pictures of the GritBlast samples. They look apart from one another, which is due to the usage of different equipment. In the first screening, the surface material removal was artificial. The peel ply removal markings are still visible, because of this. The Al_2O_3 is stuck on the surface leaving slight marking where the droplets were placed. The second screening looks completely different. Material has been removed a lot more compared to the first screening. In the right bottom corner, the top fibres are missing. From

the technical point of view, it is hard to sand small samples like these in a way to get a visually even look.

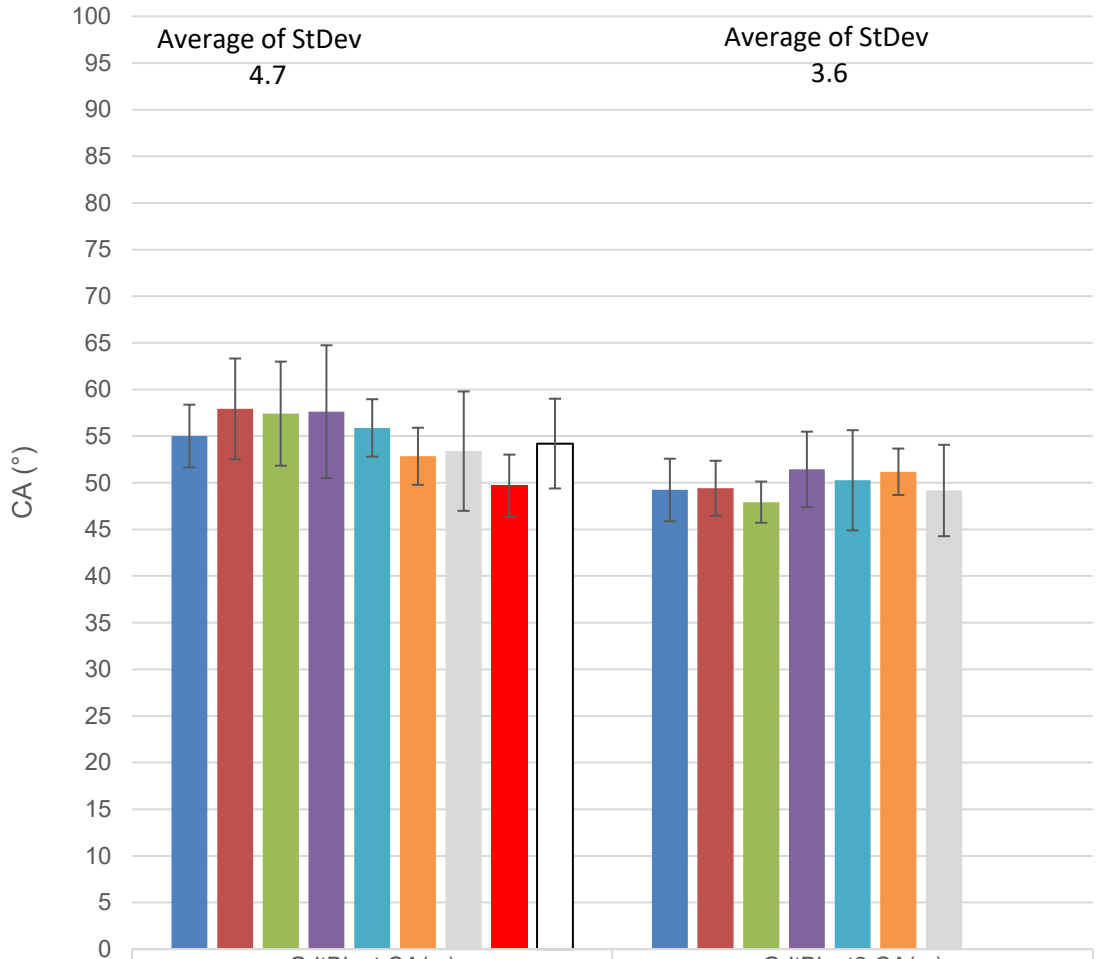

	GritBlast CA(m)	GritBlast2 CA(m)
0min	55.0	49.2
15min	57.9	49.4
30min	57.4	47.9
1h	57.6	51.4
2h	55.9	50.3
3h	52.8	51.2
4h	53.4	49.2
6h	49.7	
8h	54.2	

Figure 49. *WCA(m) values for Grit Blast and Grit Blast2 samples*

The effect of WCA measurements getting higher and lower angles at different times might be the effect on vapour adsorption or evaporation. The relative humidity fluctuated

between 49% and 59% during the measurement, which affects evaporation. After sanding the fresh surface was not been in contact with air. Generally, it is thought that the adsorption of vapour of liquids on a solid surface raises the CA. Schrader in his work (45) concludes that in principle this might not be the case, and it might also lower it, or have no effect at all. There might be other particles like dust, forming on the surface during long measurements, but nothing was detected visually. The change in WCA is relatively small and within the range of StDev of measurements.

Appendix D contains the confidence of the t-test results for Screenings 1 and 2. They show how confidently a statistically significant difference is between the results of the different surface treatments. The confidence for Screening 1 is shown in Table D 5. The surface treatments from one another in Screening 1 can be differentiated with a confidence of 95% or higher, except the A Med and A Hard from one another. The confidence for the A Med and A Hard is 75%. For Screening 2, there are more samples that cannot be differentiated. They are shown in Table D 6. The A Light and B Wa samples have 88% confidence, and the A Med and Grit Blast samples have 90%. Between the A Med and A Hard, the confidence is 43%, which is very low compared to the Screening 1. The t-testing can be used to analyse if there is a significant difference between different observation times. The confidence that there is a difference between 0min and 15min compared to 3h and 4h values are shown in Table D 7. For Screening 1, the only sample that has a significant difference is the B Wa. The Screening 2 has more samples that have over 95% confidence. Those are the A Med, A Hard and B Med samples. Because there is a significant difference found, the observation time should be recorded and kept within a certain length, such as from zero minutes to two hours.

6.5 Solvent evaporation testing

The solvent evaporation was tested using MEK and acetone and the samples were prepared with medium sanding. Measurements were taken from both surfaces at recorded times throughout two months. The results are shown in Figure 50. The starting WCA values are similar to the ones measured in the open-air contamination testing section. At one day measurement, the WCA values drop by seven degrees. This happens with both samples. With only one sample it could be the measurement locations effect, but here both samples have similar behaviour. After around a week the measured values have risen by 10° but are around the same level when compared to each other. After 18 days, the WCA values drop again and it seems that the MEK samples WCA values are a bit lower than in the Acetone sample. The final measurement at two months give values that are similar to the values at the start of the measurements. Storing the samples in plastic

boxes does not have a clear effect on the WCA values. When comparing zero minutes values to the two month values using the t-test, the confidence that there is a significant difference falls under 22% for both samples.

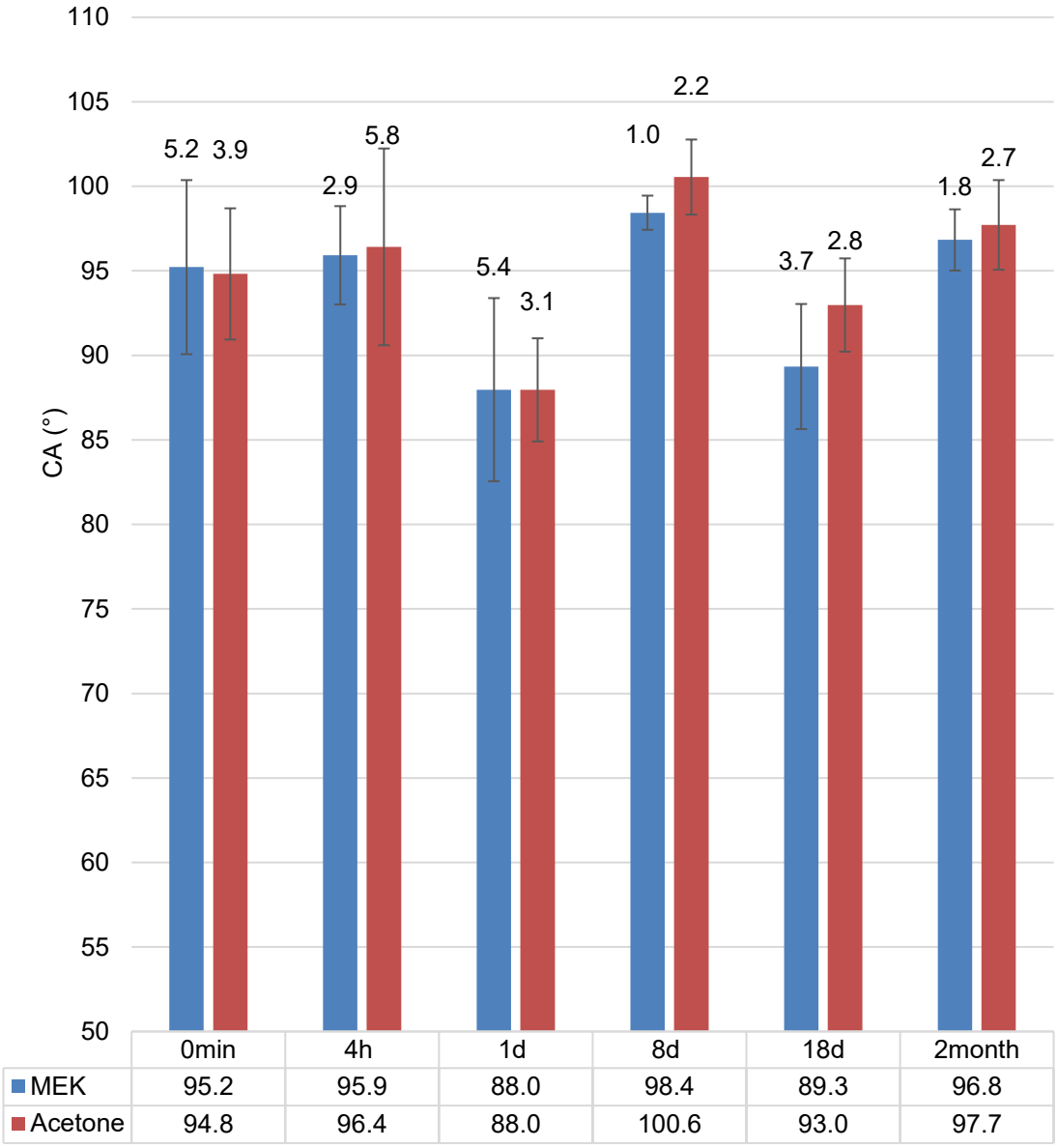

	0min	4h	1d	8d	18d	2month
MEK	95.2	95.9	88.0	98.4	89.3	96.8
Acetone	94.8	96.4	88.0	100.6	93.0	97.7

Figure 50. *Solvent evaporation testing over 2months, average WCA(m) values for each time on MEK wiped and acetone wiped surfaces*

6.6 Surface roughness and WCA

The surface roughness was measured on the drop locations of 0 time-series on the open-air contamination samples. Figure 51 shows average CA values over average surface roughness for the tested samples. The PPR0 has the highest surface roughness. The

surface left from the removal of peel ply is very rough. The pattern of the peel ply cloth is visible. Surface roughness for the Grit Blast samples is rather high compared to the sanded specimen. They are still rather close to each other in surface roughness and WCA, although the visual look on the samples was quite different. The A Light samples have almost the same WCA values, but their surface roughness values are a bit apart from one another. They also had slight traces of the peel ply pattern on their surface, which is understandable since the sanding was superficial. The rest of the samples have almost the same surface roughness values. The medium and hard sanding does not seem to affect the surface roughness. This is also true for solvent and Scotch-Brite wiping. The A Med and A Hard treatments are close in WCA values, but the B types have higher WCA since the MEK increased the WCA values. It seems that there is no clear correlation between surface roughness and WCA. The chemical composition of the surface affects WCA values, which is notable in the solvent wiped samples. Because the surface roughness values are very close for the sanded samples, a more precise analysis can be done using a t-test. Table 5 shows the confidence of difference between the R_a of the samples. The A Hard and A Med samples have over 95% confidence, which they did not have when the WCA values were compared. This is true for the A Hard and A Hard2 samples. Few samples have very similar data, like the B Med and B Wa have only the confidence of 11%. The confidence that there is a difference between the two screenings is 99%. This means that is quite probable that the sanding paper affects the surface finish.

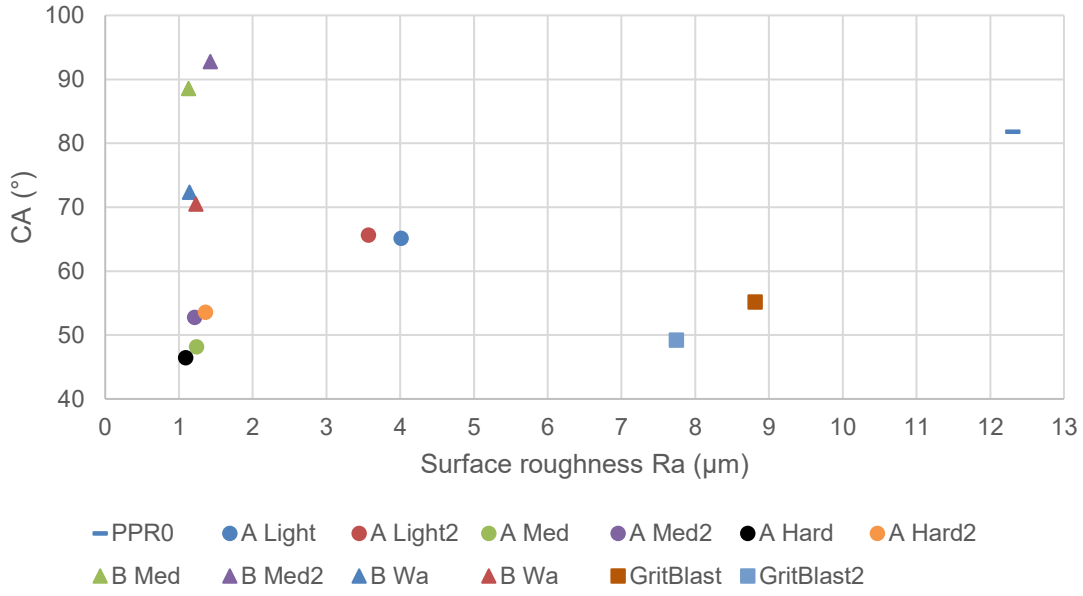

Figure 51. *WCA and surface roughness averages*

Table 4. *Confidence that there is a statistically significant difference between surface average roughness (R_a) between different samples*

T-TEST	B Wa 2	B Wa	B Med 2	B Med	A Hard 2	A Hard	A Med 2
A Med	24 %	82 %	66 %	92 %	99 %	100 %	41 %
A Med2	26 %	58 %	72 %	70 %	97 %	94 %	
A Hard	100 %	53 %	90 %	51 %	100 %		
A Hard2	99 %	99 %	27 %	100 %			
B Med	88 %	11 %	85 %				
B Med2	69 %	82 %					
B Wa	76 %						

Figure 52 shows a collection of magnified images of different samples from the surface roughness measurements. From the PPR0 sample, the intensive pattern the peel ply has left on the epoxy surface can be seen. This pattern diminishes as the level of sanding is increased from light to hard. For the A Light sample, the deep peel ply pattern is visible. In the A Med and A Hard samples, the colour difference of the remaining epoxy location

and CF is notable. The A Med sample still has the peel ply imprint present on some areas, while the A Hard sample is smooth.

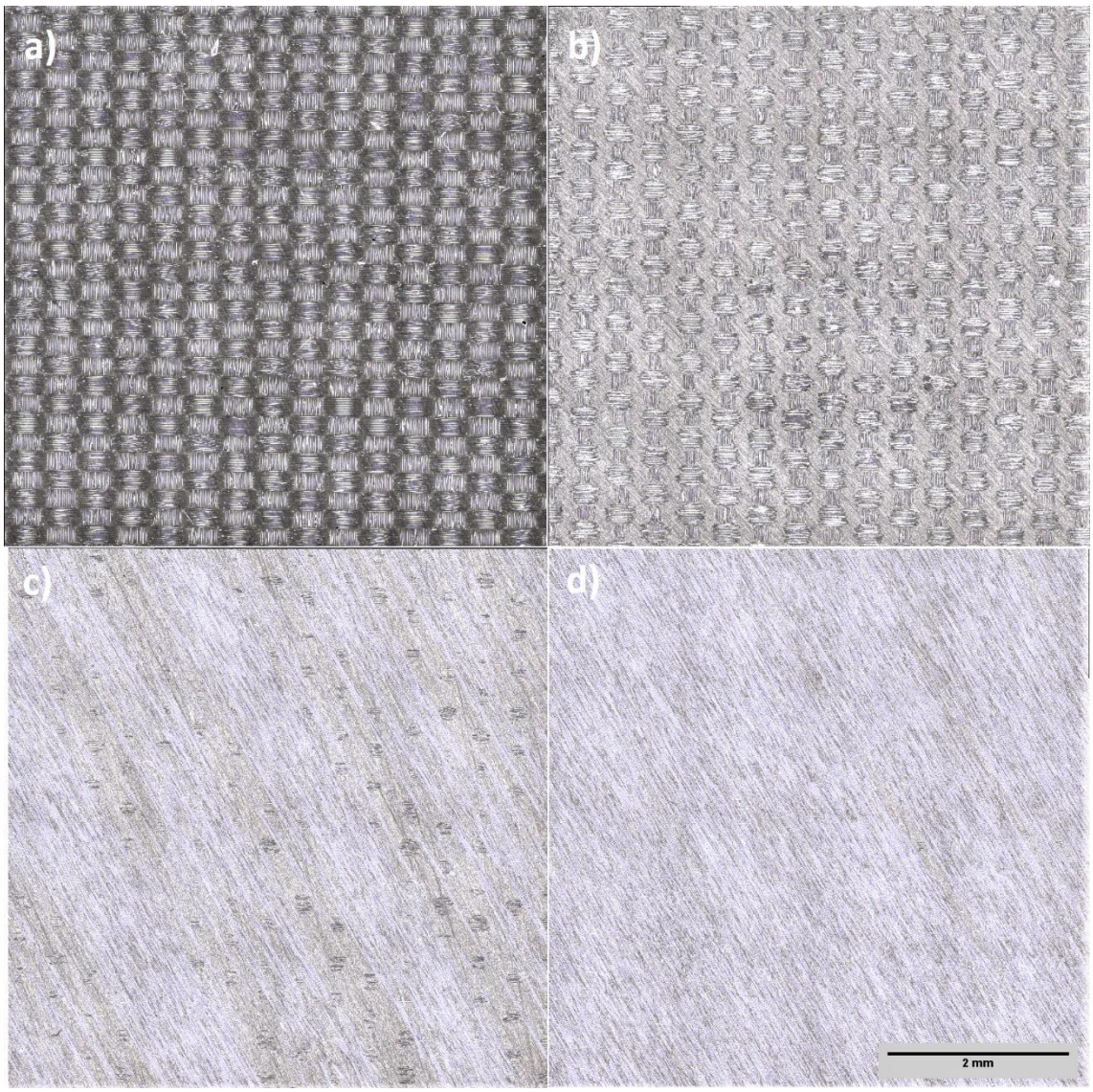

Figure 52. *10x magnified surface images of different samples. a) PPR0 b) A Light c) A Med d) A Hard, scale bar on the right lower corner is 2mm and represent the length scale for all the images (a-d)*

With the surface roughness measurements, it was possible to scan the surface for a topographical image. This was done on the SDM samples. The biggest problem was the size of the samples since scanning from large areas results in a large data file. This caused the resolution to be lower since the size of the images was capped by the software. Figure 53 and Figure 54 show the topographical primary and roughness maps of the SDM samples. The primary profile includes roughness (high-frequency wavelength) and waviness (low-frequency wavelength). The PPR0 surface has those knife marks which were mentioned before. When comparing the primary and roughness profiles, it is

clear that the surfaces had waviness. The roughness is even across the surface for both samples. No clear correlation to the SDM results can be seen. The B Med surface has similar features. The primary profile is lower on the sides and the middle section is higher. This is mainly due to sanding removing material more from the edges, which contributed to the waviness. The roughness profile is quite even, but the edges are the only where lower areas are present. This is probably due to the sanding process. The B Med topography does not correlate to the SDM. Both topography images show smaller squares, which is caused by the process of creating the larger image from the smaller ones.

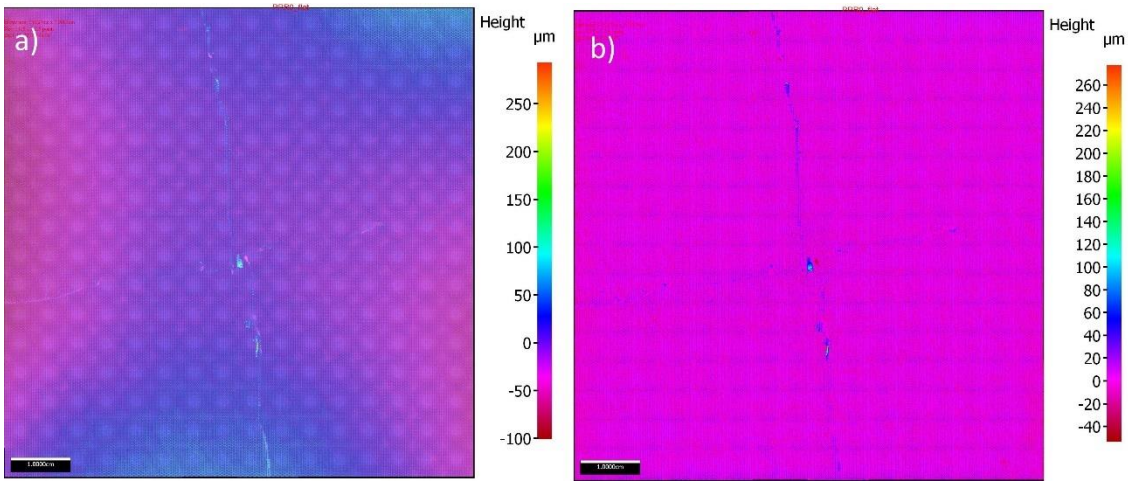

Figure 53. *Topography of the PPR0 surface from SDM measurements a) primary profile b) roughness profile, scale bar is 1cm*

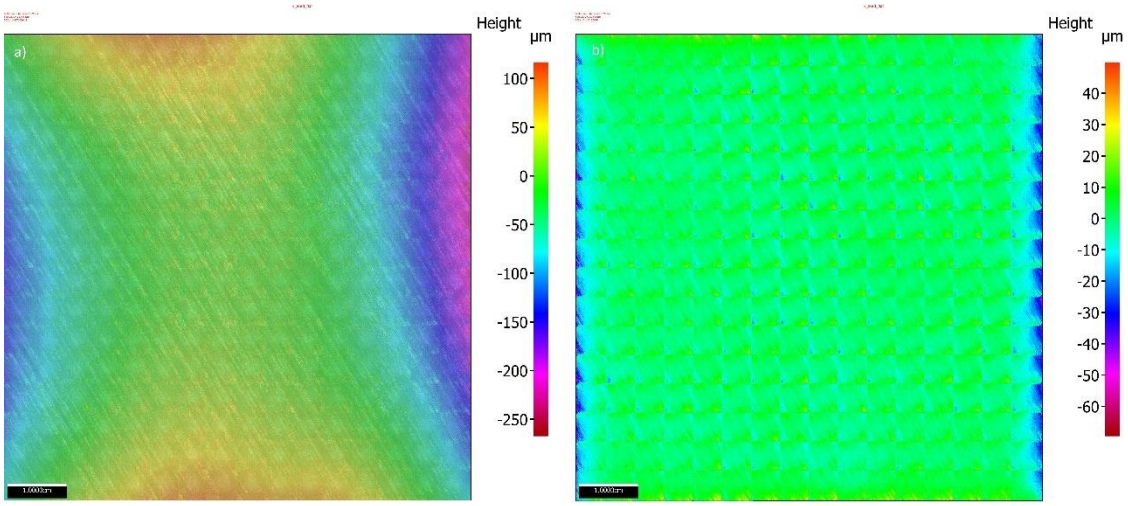

Figure 54. *Topography of the B Med surface from SDM measurements a) primary profile b) roughness profile, scale bar is 1cm*

6.7 Comparison of measurement devices

A total of five glass samples were measured by both sides. Figure 55 shows the results from both sides, red columns are ZHAW measurements and blue columns are TAU measurements. Values for each sample are averages. Measured values are within a few degrees between different samples. StDev is quite good for most samples. In general, the TAU measurements have slightly lower WCA values, which might be due to transportation and storage affecting the samples. When a t-test is used to analyse if the difference is significant, over 95% confidence is found for three samples. Table 5 shows the confidence of a significant difference between measurements on the same sample. Samples 101 and 103 do not show over 95% of confidence against the hypothesis but the rest do. When comparing the results from each operator as one data group, there is a statistically significant difference with a confidence of 99%.

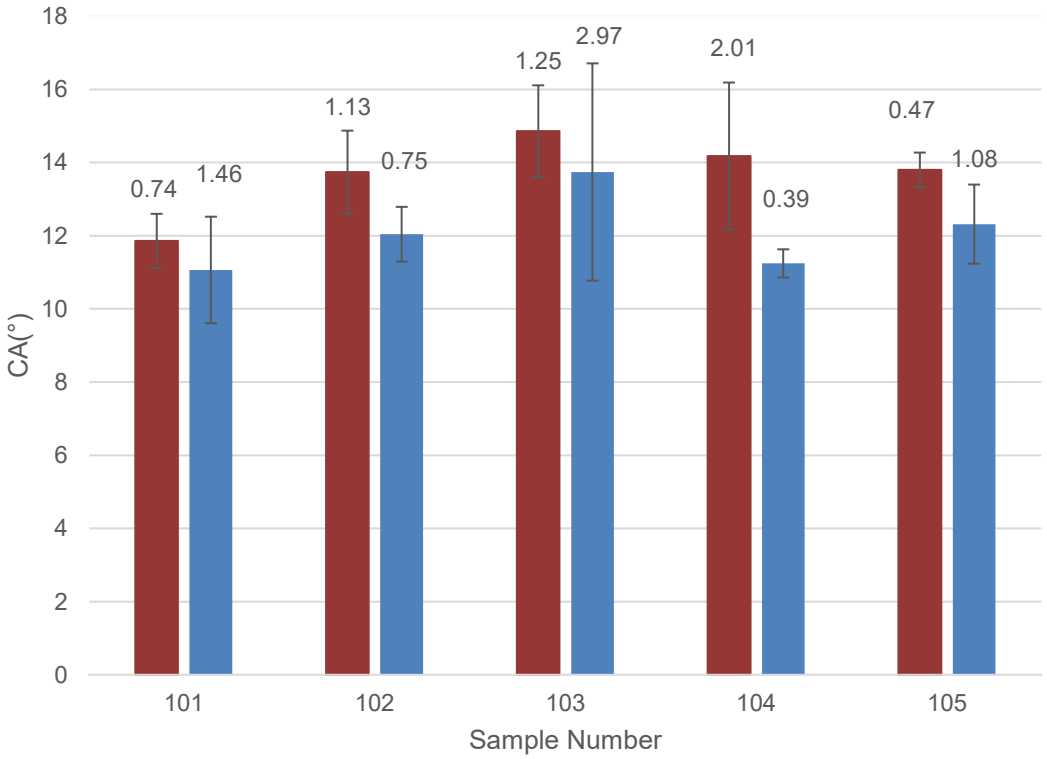

Figure 55. *WCA on glass samples, ZHAW measurements (Red), TAU measurements (Blue)*

Table 5. *Confidence that there is a statistically significant difference between measurements made by ZHAW and TAU on the same glass sample*

T-test for sample	101	102	103	104	105
Glass	69%	97 %	46 %	95 %	96 %

7. DISCUSSION

CA measurements were performed on multiple different CFRP samples with different surface treatments. The main focus was WCA, but measurements were also performed using other liquids to gain information on SFE and its components of the samples. This provided information on different factors that may affect CA measurements. Further CA measurements were used to determine the factors affecting the measured angles and sensitivity of CA measurements. The effect of those factors and the sensitivity will be discussed here.

The first measurements were done on samples that were surface treated two months prior. They were sealed in plastic bags and kept in an office environment. This meant that the temperature was quite constant, but no records are available. The SFE of the samples were determined using four different probe liquids and the OWRK method was used in the actual calculation. SFE of the samples were similar as in the studies of current scientific literature (37-39), which for us was around 45-55mN/m. It should be noted that the exact material composition of the laminate used in this work was unknown, meaning that the correspondence of these values is not exact. The type of release agents used could affect these results as well. SFE measurements should be redone on freshly surface treated samples for better accuracy. Conditioning should also be mentioned. In the ISO 19403 (46), conditioning is stated to be a minimum of 16 hours before testing in 23 °C (± 2 °C) and 50% (± 5%) relative humidity. In the ISO 15989, it is stated that conditioning is not generally needed for routine quality assurance or process control. This is because after conditioning the measured values no longer represent the actual conditions. The actual use for these laminates does not include conditioning, which has been mentioned in the standards. The experiments should be conducted in similar conditions as is used for the surface preparation and bonding process. Another note relating especially to these samples is the black dust, which separated from the surface. This was extensive for the ones that had not been solvent wiped, but all samples had the same behaviour.

From the SFE results, it was possible to construct a correlation between the WCA and SFE. A similar correlation was done as by Gilpin (40) and found in the ISO 15989 as a conversion chart. Our results show a rather low increase in SFE based on the change in WCA. For this, it is advisable to conduct the SFE measurements again, if more accurate results are wanted. It should be noted that neither the SFE nor WCA does not tell much about the actual state of the surface and how it relates to the actual adhesive bond. The

data for this will come from mechanical testing. This type of study has been done by Bechikh et al. (47). The correlation for our samples should focus on the polar component since based on the Pearson test, the correlation strength between the WCA and polar component was very strong.

The next experiments were about the factors that were known to affect CA and on anomalies, which were detected during SFE measurements. How the measurement time affects the measured CA was experimented on first. From the theory point of view, the CA should be measured after the kinetic energy has been depleted. In the ISO 19403, it is said that measurement should be conducted immediately after dosing. The ISO 15989 states that instrument manufacturer's instructions should be followed if specified. If not, the measurement should be taken within one (1) minute ± 10s of the droplet transfer. For our experiments, three (3) second dwell time was commonly used with five (5) second observation time. The observation period was increased to one minute for the evaporation testing. This was conducted on CFRP surfaces and glass surfaces. Glass surface was used as a reference. This was to determine if evaporation was the main cause for the decrease in CA, rather than liquid penetrating the surface. Liquid penetrating the surface happens with natural surfaces, which was studied by Muszynski et al. (43). Using linear regression analysis, it is advised to use a dwell time of five (5) seconds. Then the droplet has settled on all surfaces before measurement. On Grit Blast surfaces, the droplet was still visibly unstable at three (3) seconds.

It was observed that the droplets were anisotropic. For highly sanded surfaces, the anisotropy was greater. Droplets were wetting the surface more in the direction of the fibres. This was similar behaviour as on chemically striped surfaces, which were studied by Neumann et al. and Bliznyuk et al. (42,44). A chemical analysis would be needed for the samples used in this work to confirm similar behaviour. Three different view angles were experimented on and the results were similar as in the studies mentioned before. The most stable area is when the top fibre of the laminate is normal to the camera, which is the view angle that should be used. This way the measured CA is from the direction of wetting, resulting in lower angles. Using a t-test, a statistically significant difference between the view angles was found. The view angle should be studied with a piece of more precise equipment, to determine the limits where the CA results are not affected by it. It should be noted that this is only applicable to UD laminate. If a different type of fibre orientation or weave is used, the view angle should be studied for that specific setup.

Surface roughness measurements were done three months after the CA measurements. The samples which were medium or hard sanded had similar surface roughness values. Profile roughness average (R_a) was the surface roughness used. The R_a was different

based on its relation to top fibres. Normal to top fibre was used since it gave higher values than parallel. T-test showed no clear correlation between R_a and the sample. Because of this, the surface roughness seems to have a trivial effect on the CFRP samples used in this work. However, there is a significant difference between the surfaces treated with different sanding paper. Another reason for the difference in roughness could be the laminate material. The use of different grit sanding papers could be tested to see if there is a roughness difference with medium sanding based on the grit size. This way the surface composition between samples would be closest to the same, similarly as in the study by Wei et al. (48), where a correlation between WCA and surface roughness was found.

The precision and reliability of the measurements should be discussed. The ISO 19403 and ISO 15989 use repeatability limit (r) and reproducibility limit (R). The repeatability limit is stated as, “the value below which the absolute difference between two single test results, each the mean of valid duplicates, can be expected to lie with a probability of 95% when this method is used under repeatability conditions” (46). Reproducibility limit is stated as, “the value below in which the absolute difference between two single test results, each the mean of valid duplicates, can be expected to lie with a probability of 95% when this method is used under reproducibility conditions” (46). In the ISO 19403, r is 2.4°and R is 6.7°. Screening tests had too small a sample size to calculate these limits. Usually, a minimum of 30 tests per series should be conducted, which would mean that 30 measurements from each sample are prepared the same way. T-tests were used to find out with how high confidence the WCA could differentiate the surfaces from one another. In t-test confidence of 95% and more is considered to be statistically significant. We found out that for WCA it is quite hard to differentiate the medium and hard sanding from one another. This was true for all the measurements. For other samples, confidence over 95% was found in most cases. Some samples have a high StDev which affects the accuracy. Uneven sanding and solvent remnants are the most probable cause for the high StDev in these samples. Surface treatment process could be improved by the technician having more experience or by using some type of machinery for the surface treatment.

8. CONCLUSIONS

CA measurements were utilized to study CFRP surface and the effect of different surface treatments. The first objective of the thesis was to calculate SFE and its components using the OWRK method and CA measurements with four different probe liquids. These liquids were MilliQ water, Ethylene Glycol, Glycerol and Diiodomethane, which are common probe liquids. The SFE increased with the sanding and the increase in polar component value was significant. Similar values for SFE were found in the literature for CFRP surfaces, which gave the results reliability. The SFE measurements had anomalies, which were experimented on later.

The second objective of this thesis was to conduct an experimental sensitivity analysis of factors affecting WCA on CFRP laminates. This was done in multiple separate experiments. It was found that the view angle of the measurement affects the measured values. This means that a standard view angle should be selected. The CA was also affected by dwell time. This was experimented using a one minute observation time and one second measurement interval. A dwell time of five (5) seconds seems to yield optimal results. The kinetic energy of the droplet has been consumed, but the effect of evaporation is still small. The sample surfaces did not show absorption behaviour. The level of sanding reduced the measured WCA values. Higher WCA values for light sanding and lower values for medium and high sanding. This means that the wetting was increased by surface treatments, which benefits the adhesive bond. The StDev for medium and highly sanded samples was quite small, making it possible to different surface treatments from one another based on WCA value. The time between the surface treatment and WCA measurement seemed to matter little when it was under eight hours. Experiments verified that CA measurements are sensitive and measured values depend on many different aspects.

For further measurements, some key factors should be considered. A standardized measurement protocol should be selected for further measurements. This protocol should include the type of probe liquids used, droplet size, view angle, dwell time, the time between the surface treatment and measurement, equipment and procedure of the surface treatment, and possible storing procedure. This way the results made in separate locations by different operators and devices could be compared with better accuracy. Table 6 combines the most important results and findings of this thesis. Detailed explanations can be found in earlier chapters. Figure 56 shows a collection of different droplet shapes and how measured WCA values are affected. These shapes and effects are

based on the experiments and results of this thesis. The effect that different phenomena have should not be combined e.g. low sanding and solvent combined resulting in high CA, as it was not studied in this thesis. The droplet shapes show why surfaces yielding similar WCA values were hard to differentiate from one another. For surfaces that can be differentiated from one another with a confidence of 95%, it is possible to visually confirm the shape difference between droplets. Surfaces with medium and hard sanding have almost identical droplets, making it impossible to see any visual difference. This was also shown in the t-test results for these surfaces.

Table 6. *Most important results and findings from the experiments and analyses*

SFE calculations and results
Surface treatments increase SFE. Depending on probe liquid, the possibility to differentiate differently treated surfaces changes. A strong linear correlation between the polar component and cos(WCA(m)) was found
Time dependency and droplet anisotropy
Measured CAs decrease over time as the droplet evaporates. View angle has a significant effect on the measured CAs on UD-laminate
SDM results
Measurement location affects the measured CA. Measured CA values follow a normal distribution. There is no significant difference between right and left angles.
Open-air contamination testing (screening)
Exposure to air lowers the measured CAs over 8h observation period. Measurements should be taken within a set time from the surface treatment
Solvent evaporation testing
MEK and Acetone remain on the surface for over 2months. They increase WCA values to close to hydrophobic (over 90°)
Surface roughness measurements and results
Peel ply imprint on the surface is visible even after medium sanding. Sanding lowers the profile roughness average (R_a). No clear correlation between surface treatment and R_a
Measurements with different devices
CA on the same glass surfaces taken with different devices in different locations are within a few degrees of each other. The significance between the devices depends on the sample resulting in mixed results
T-test results
It is possible to differentiate differently treated surfaces with a confidence of 95% based on the CA data by using a t-test. This depends on surface treatment e.g. between surfaces of medium and hard sanding, 95% confidence is not reached

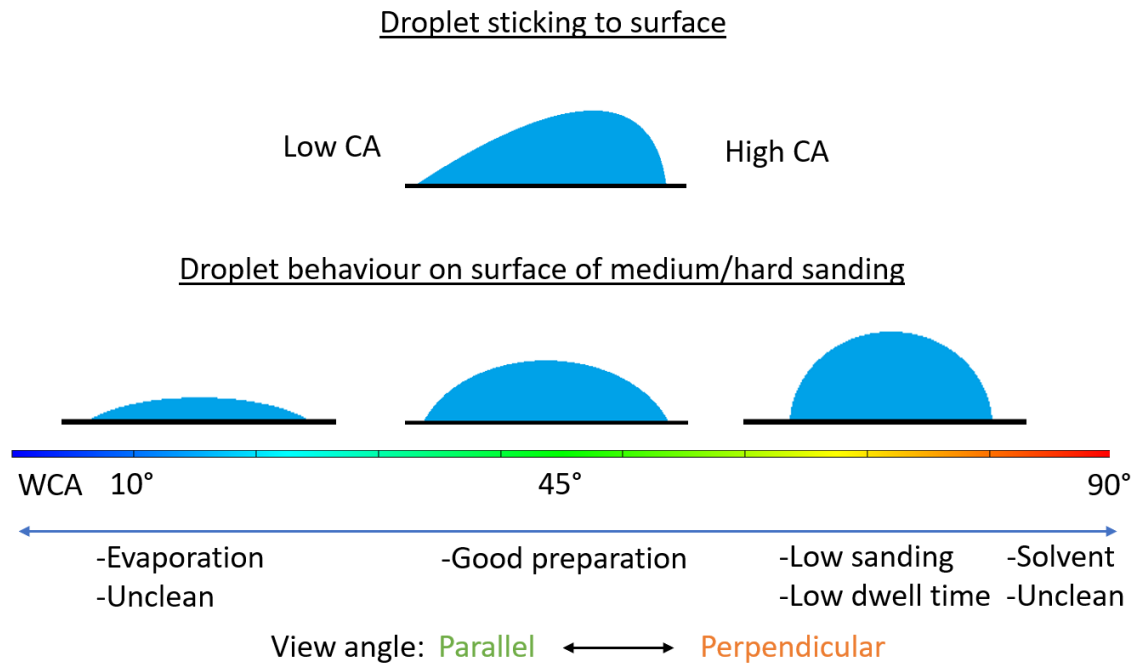

Figure 56. *Droplet shapes and how different phenomena affect WCA based on the experiments and results. WCA values on surfaces with medium or hard sanding should be in the green area, around 45°*

REFERENCES

(1) Adams RD. Adhesive bonding Science, technology and applications. Cambridge: Woodhead Publishing Limited; 2005.

(2) Ebnesajjad S, Landrock A. Adhesives technology handbook. 3rd ed. London, England: Elsevier; 2015.

(3) da Silva LFM, Öchsner A, Adams RD. Handbook of Adhesion Technology. Cham: Springer International Publishing AG; 2018.

(4) Campbell FC. Structural composite materials. Materials Park, Ohio: ASM International; 2010.

(5) Campbell FC. Manfacturing processes for advanced composites. New York: Elsevier; 2004.

(6) Beaumont PWR, Soutis C, Hodzic A. The Structural Integrity of Carbon Fiber Composites Fifty Years of Progress and Achievement of the Science, Development, and Applications. 1st ed. Cham: Springer International Publishing; 2017.

(7) Wenbin Y, Johnathan G, Byron PR. Effect of Sizing on the Interfacial Properties of Carbon Fiber Composites. 2017:1.

(8) Campbell Jr F C. Manufacturing Technology for Aerospace Structural Materials. 1st ed. Oxford: Elsevier Science & Technology; 2006.

(9) VN-composites. 10.1.2021; Available at: http://www.vn-composites.fr/en/Know-how/Manufacturing-methods.

(10) Breuer UP. Manufacturing Technology. 2016:73-132.

(11) Schweizer M, Meinhard D, Ruck S, Riegel H, Knoblauch V. Adhesive bonding of CFRP: a comparison of different surface pre-treatment strategies and their effect on the bonding shear strength. J Adhes Sci Technol 2017;31(23):2581-2591.

(12) Encinas N, Oakley BR, Belcher MA, Blohowiak KY, Dillingham RG, Abenojar J, et al. Surface modification of aircraft used composites for adhesive bonding. Int J Adhes 2014;50:157-163.

(13) Gude MR, Prolongo SG, Ureña A. Adhesive bonding of carbon fibre/epoxy laminates: Correlation between surface and mechanical properties. Surf Coat Tech 2012;207:602-607.

(14) Wu GM, Shyng YT, Kung SF, Wu CF. Oxygen plasma processing and improved interfacial adhesion in PBO fiber reinforced epoxy composites. Vacuum 2009;83(1):S271-S274.

(15) Wetzel M, Holtmannspötter J, Gudladt H, Czarnecki JV. Sensitivity of double cantilever beam test to surface contamination and surface pretreatment. Int J Adhes 2013;46:114-121.

(16) Sun C, Min J, Lin J, Wan H, Yang S, Wang S. The effect of laser ablation treatment on the chemistry, morphology and bonding strength of CFRP joints. Int J Adhes 2018;84:325-334.

(17) Ebnesajjad S, Landrock A. Adhesives technology handbook. 3rd ed. London, England: Elsevier; 2015.

(18) Chesterfield L. "Water-break-free" test. . *Products Finishing*, vol. 77, no. 8, Gardner Publications, Inc, 2013.

(19) Joining of Organic-Matrix Composites: The Water-Break Test. In: ASM Handbook, Volume 6: Welding, Brazing, and Soldering Vol 6. ASM International; 1993.

(20) Banea MD, da Silva LFM. Adhesively bonded joints in composite materials: An overview. P I Mech Eng L-J Mat 2009;223(1):1-18.

(21) Renart J, Costa J, Sarrado C, Budhe S, Turon A, Rodríguez-Bellido A. Mode I fatigue behaviour and fracture of adhesively-bonded fibre-reinforced polymer (FRP) composite joints for structural repairs. 2015:121-147.

(22) Morimoto T, Fujimoto A, Katoh H, Kumazawa H. Mechanism of weak bond formation in CFRP epoxy adhesion joints. Advanced composite materials. 2021;30(4):396–408.

(23) Callister WD, Rethwisch DG. Materials science and engineering : an introduction. 9th ed. Hoboken, NJ: John Wiley and Sons; 2014.

(24) AC 21-26A - Quality Control for the Manufacture of Composite Structures. 2010.

(25) Mueller EM, Starnes S, Strickland N, Kenny P, Williams C. The detection, inspection, and failure analysis of a composite wing skin defect on a tactical aircraft. Composite structures. 2016;145:186–93.

(26) Kuusipalo J. Papermaking science and technology. Book 12, Paper and paperboard converting. 2nd ed. Helsinki: Finnish Paper Engineers' Association; 2008.

(27) Kruss Scientific, SFE. Available at: https://www.kruss-scientific.com/en/know-how/glossary/surface-free-energy.

(28) Law K, Zhao H. Surface Wetting Characterization, Contact Angle, and Fundamentals. 1st ed. Cham: Springer International Publishing; 2016.

(29) Song J-W, Fan L-W. Temperature dependence of the contact angle of water: A review of research progress, theoretical understanding, and implications for boiling heat transfer. Advances in colloid and interface science. 2021;288:102339–102339.

(30) Ikuma Y, Suzuki H, Hokari D, Maruyama T, Niwa K. Effect of relative humidity on water contact angle on TiO2 single crystals: behavior of photoinduced hydrophilicity after turning off UV irradiation. Transactions of the Materials Research Society of Japan 2019;44(6):211-215.

(31) Fowkes FM. Determination of interfacial tensions, contact angles, and dispersion forces in surfaces by assuming additivity of intermolecular interactions in surfaces. J Phys Chem 1962;66(2):382.

(32) Kwok D, Neumann A. Contact angle measurement and contact angle interpretation. Advances in colloid and interface science. 1999;81(3):167–249.

(33) Xu ZN. An algorithm for selecting the most accurate protocol for contact angle measurement by drop shape analysis. Rev Sci Instrum 2014;85(12):125107.

(34) Boerio FJ, Roby B, Dillingham RG, Bossi RH, Crane RL. Effect of Grit-Blasting on the Surface Energy of Graphite/Epoxy Composites. J Adhesion 2006;82(1):19-37.

(35) Ström G, Fredriksson M, Stenius P. Contact angles, work of adhesion, and interfacial tensions at a dissolving Hydrocarbon surface. J Colloid Interface Sci 1987;119(2):352-361.

(36) Krüss Scientific. ADVANCE. 2019.

(37) Gallant D. Synergetic Effect of Grit-Blasting and Atmospheric Cold Plasma Pretreatments on the Surface Free Energy of a Fibreglass/Epoxy Vinyl Ester Composite. J Adhesion 2010;86(2):165-191.

(38) Park S, Lee S. Studies on Surface Free Energy of an Anhydride–Epoxy Cured System: Effect of Side Alkenyl Chain Length of Hardener on Tensile and Impact Properties. J Colloid Interface Sci 2000;228(1):90-94.

(39) Danchenko Y, Andronov V, Teslenko M, Permiakov V, Rybka E, Meleshchenko R, et al. Study of the free surface energy of epoxy composites using an automated measurement system. Eastern-European journal of enterprise technologies 2018;1(12-91):9-17.

(40) Gilpin AD, Oakley BR, Dillingham RG. Water contact angle as a quantitative measure of total polyethylene surface energy. J Adhes Sci Technol 2015;29(9):890-895.

(41) ISO 15989:2004 Measurement of water-contact angle of corona-treated films.

(42) Bliznyuk O, Vereshchagina E, Kooij ES, Poelsema B. Scaling of anisotropic droplet shapes on chemically stripe-patterned surfaces. Phys Rev E 2009;79(4):041601.

(43) Mittal KL. Application of Droplet Dynamics Analysis for Assessment of Water Penetration Resistance of Coatings. In: Contact Angle, Wettability and Adhesion, Volume 3. VSP - An imprint of BRILL; 2003. p. 1–1.

(44) David R, Neumann AW. Anisotropic drop shapes on chemically striped surfaces. Colloid Surface A 2012;393:32-36.

(45) Mittal KL. Effect of Adsorbed Vapor on Liquid-Solid Adhesion. 2003:1.

(46) ISO 19403:2020 Determination of the surface free energy of solid surfaces by measuring the contact angle.

(47) Bechikh A, Klinkova O, Maalej Y, Tawfiq I, Nasri R. Effect of dry abrasion treatments on composite surface quality and bonded joints shear strength. Int J Adhes Adhes 2021:103058.

(48) Wei XT, Shi WL, Xu J, Li ZY, Wu XL, Wang ZG. The Influences of Surface Roughness on the Water Contact Angle for Coated Substrate with F-DLC. Key Eng Mat 2018;764:68-77.

APPENDIX A: SCREENING 1

CWP – FIN – 13.8.2021

Material: laminate based on prepreg 3501-6/AS4 UD (Mirka Ecowet P180)

Sample PPR0 with time intervals, a new droplet in each value

Measurement in practice: according to Protocol FIN-SW

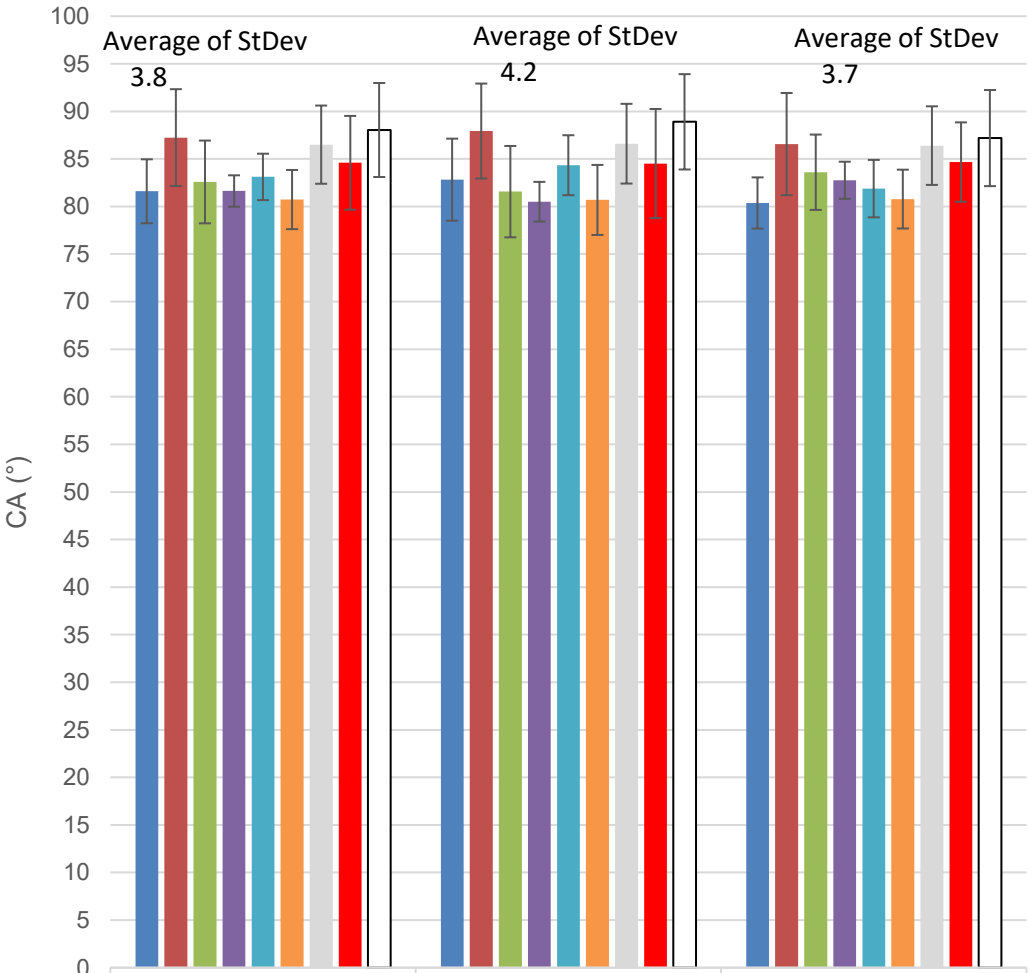

	Water CA(m)	Water CA(l)	Water CA(r)
0min	81.6	82.8	80.4
15min	87.2	87.9	86.6
30min	82.6	81.6	83.6
1h	81.6	80.5	82.8
2h	83.1	84.3	81.9
3h	80.7	80.7	80.8
4h	86.5	86.6	86.4
6h	84.6	84.5	84.7
8h	88.0	88.9	87.2

Figure A 1. *Screening 1, WCA, Open air, PPR0, T =23 C, RH% = 55*

Sample A Light with time intervals, a new droplet in each value

Measurement in practice: according to Protocol FIN-SW

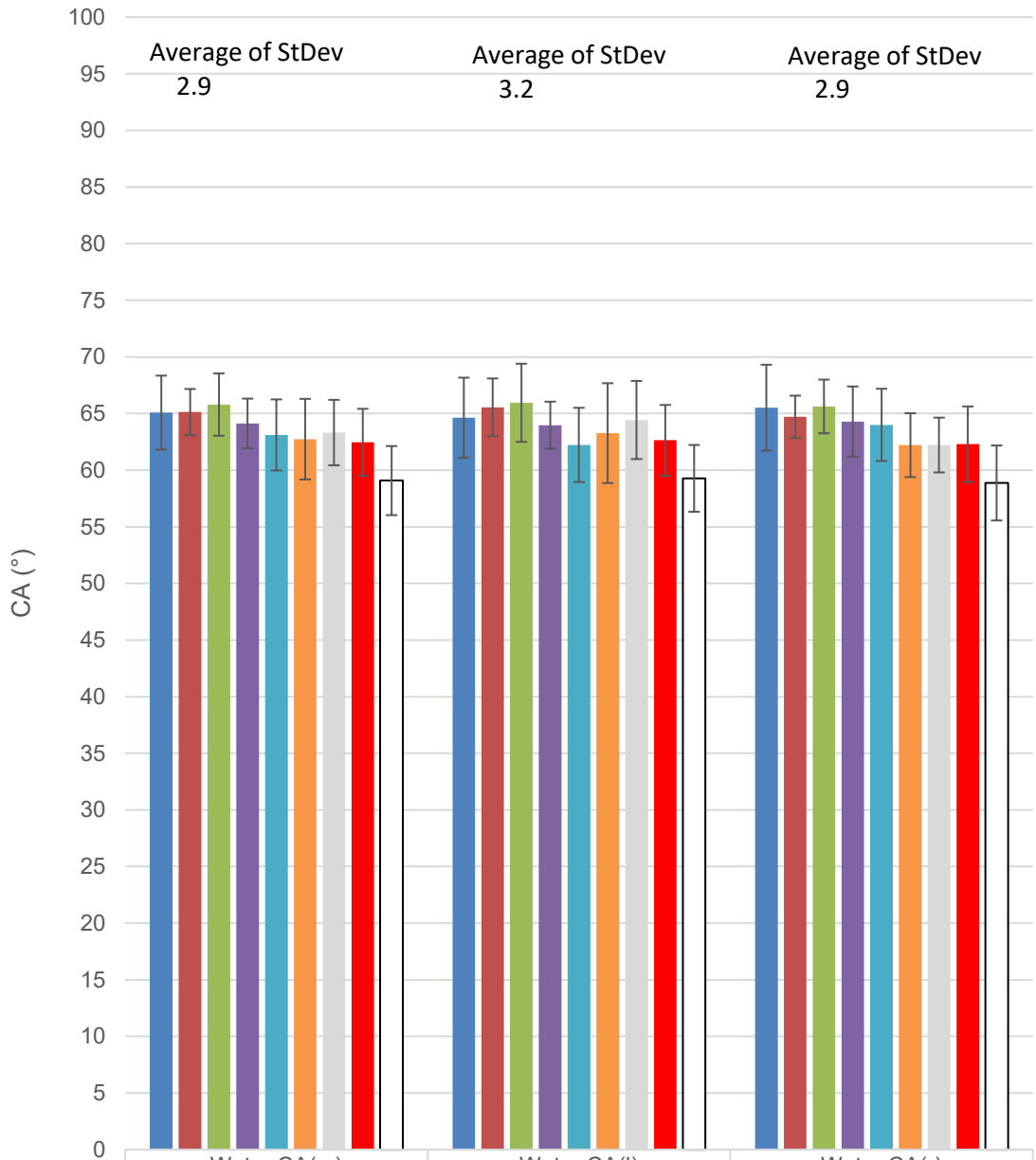

	Water CA(m)	Water CA(l)	Water CA(r)
0min	65.1	64.6	65.5
15min	65.1	65.6	64.7
30min	65.8	66.0	65.6
1h	64.1	64.0	64.3
2h	63.1	62.2	64.0
3h	62.7	63.3	62.2
4h	63.3	64.4	62.2
6h	62.5	62.6	62.3
8h	59.1	59.3	58.9

Figure A 2. *Screening 1, WCA, Open air, A Light, T = 24 C, RH% = 58*

Sample A Hard with time intervals, a new droplet in each value

Measurement in practice: according to Protocol FIN-SW

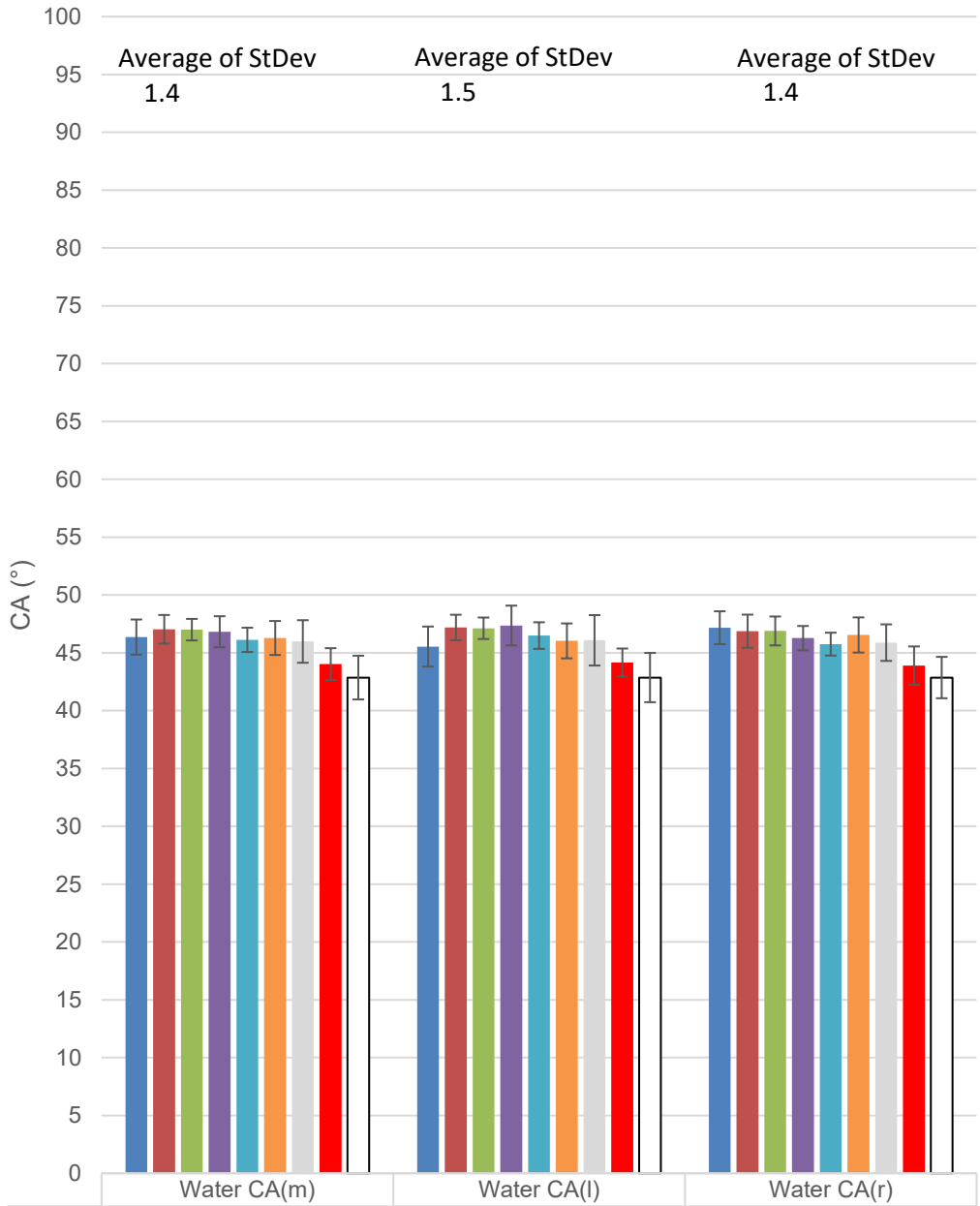

	Water CA(m)	Water CA(l)	Water CA(r)
0min	46.4	45.5	47.2
15min	47.0	47.2	46.9
30min	47.0	47.1	46.9
1h	46.8	47.4	46.3
2h	46.1	46.5	45.8
3h	46.3	46.0	46.5
4h	46.0	46.1	45.9
6h	44.0	44.2	43.9
8h	42.9	42.9	42.9

Figure A 3. *Screening 1, WCA, Open-air, A Hard, T = 24 C, RH% = 58*

Sample A Med with time intervals, a new droplet in each value

Measurement in practice: according to Protocol FIN-SW

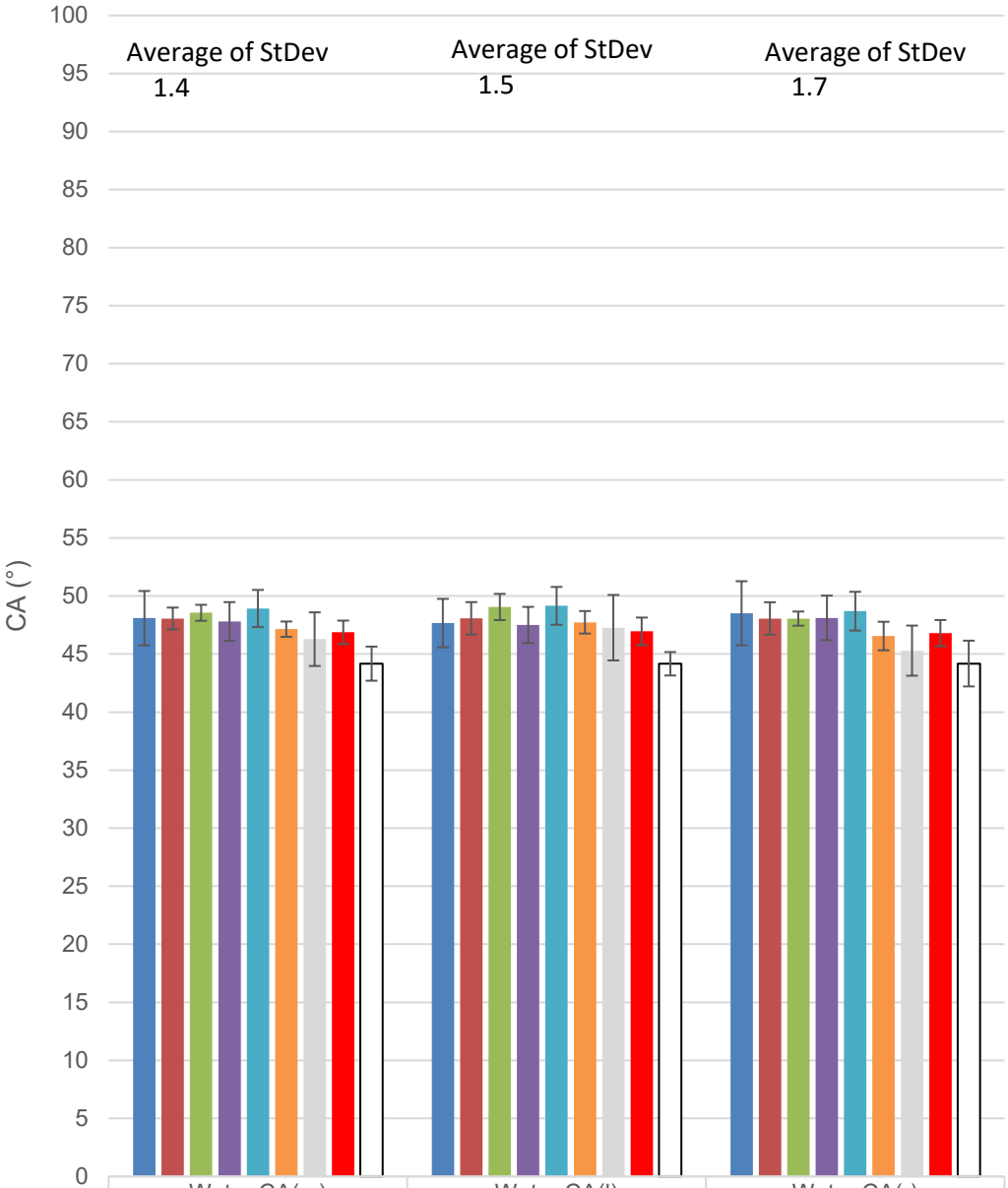

	Water CA(m)	Water CA(l)	Water CA(r)
0min	48.1	47.7	48.5
15min	48.1	48.1	48.1
30min	48.6	49.1	48.1
1h	47.8	47.5	48.1
2h	48.9	49.2	48.7
3h	47.1	47.7	46.6
4h	46.3	47.3	45.3
6h	46.9	47.0	46.8
8h	44.2	44.2	44.2

Figure A 4. *Screening 1, WCA, Open-air, A Med, T = 24 C, RH% = 57*

Sample B Med with time intervals, a new droplet in each value

Measurement in practice: according to Protocol FIN-SW

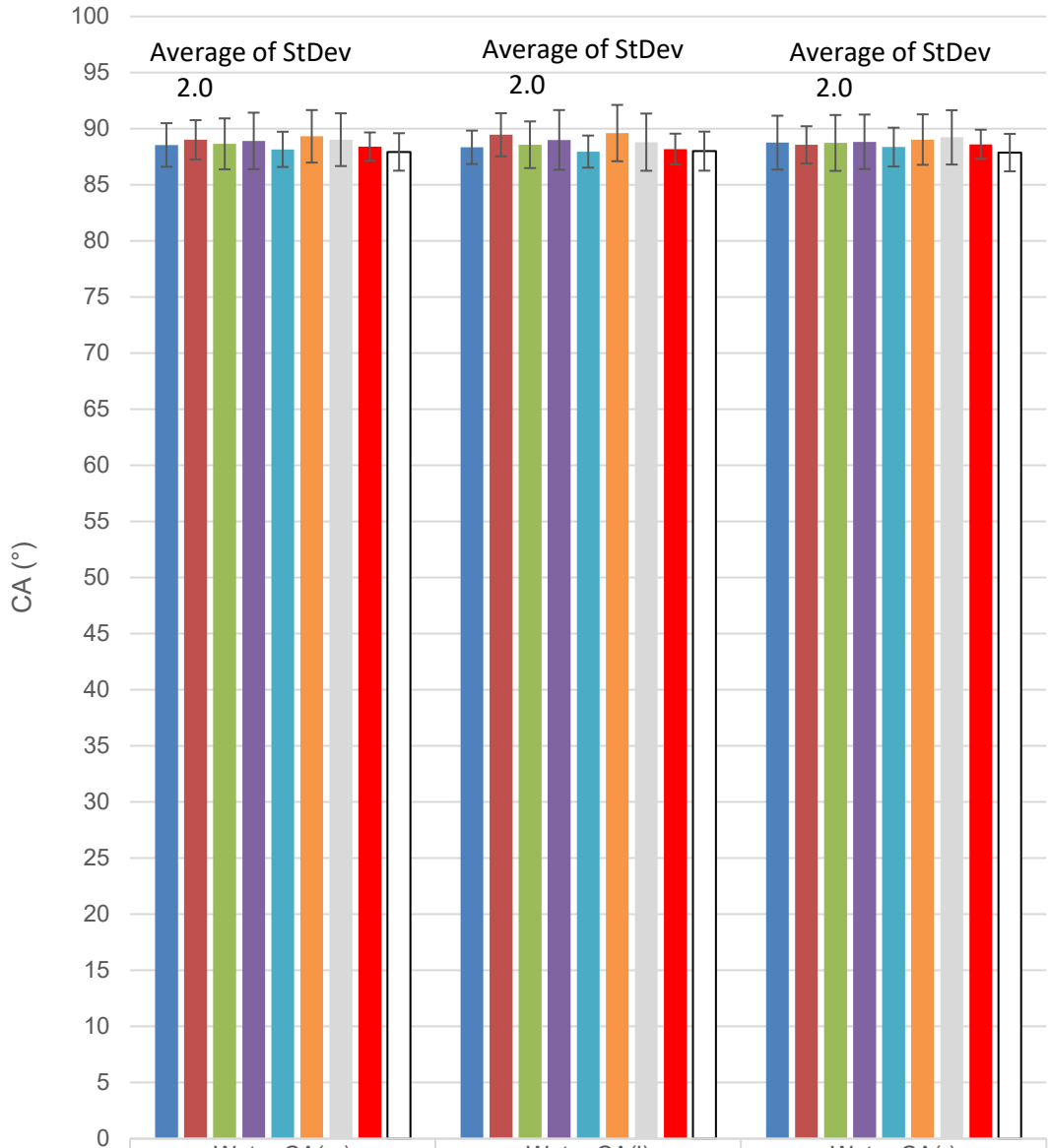

	Water CA(m)	Water CA(l)	Water CA(r)
0min	88.6	88.3	88.8
15min	89.0	89.5	88.6
30min	88.7	88.6	88.7
1h	88.9	89.0	88.8
2h	88.2	88.0	88.4
3h	89.3	89.6	89.0
4h	89.0	88.8	89.2
6h	88.4	88.2	88.6
8h	87.9	88.0	87.9

Figure A 5. *Screening 1, WCA, Open-air, B Med, T = 24 C, RH% = 57*

Sample B Wa with time intervals, a new droplet in each value

Measurement in practice: according to Protocol FIN-SW

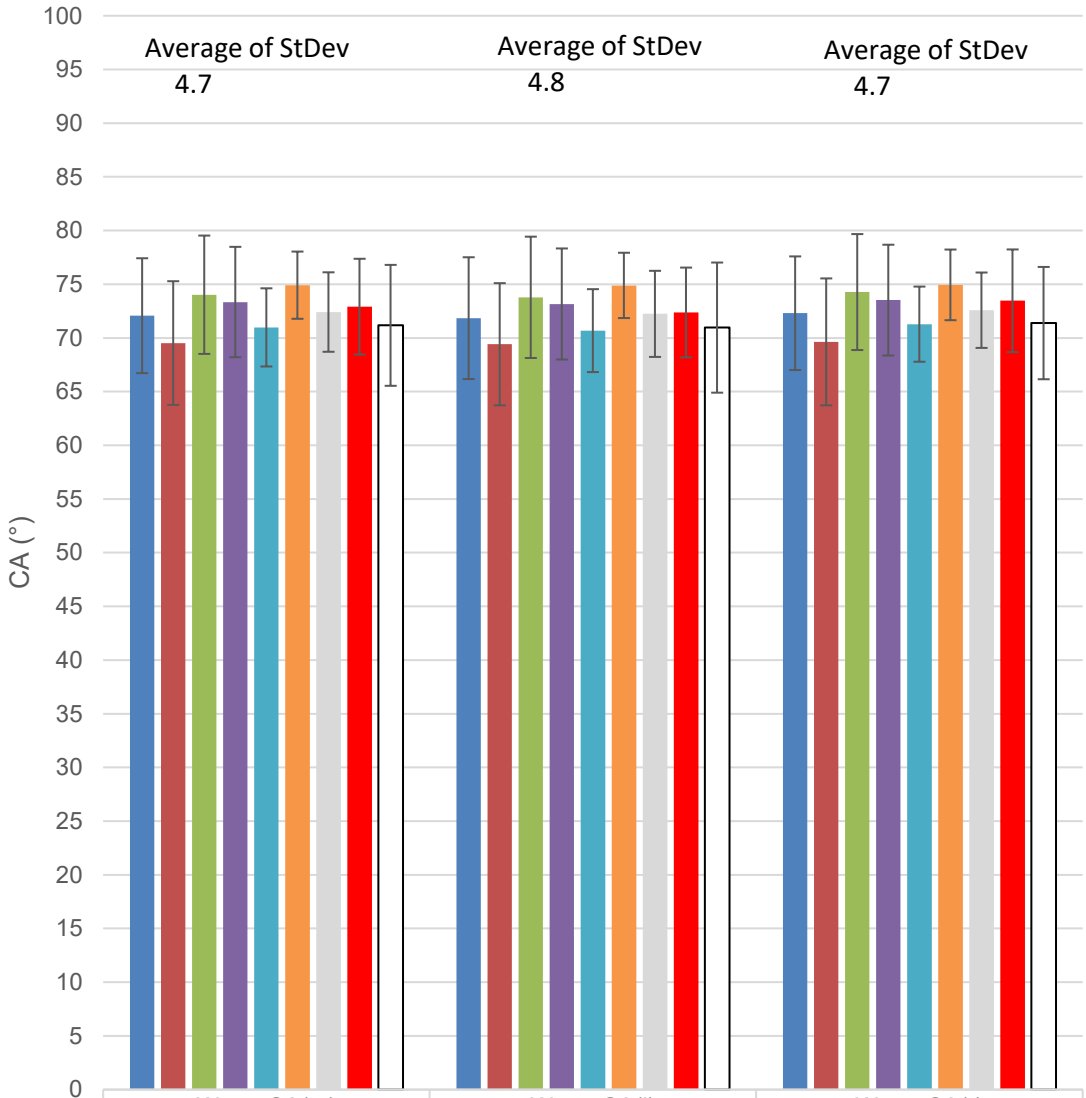

	Water CA(m)	Water CA(l)	Water CA(r)
0min	72.1	71.8	72.3
15min	69.5	69.4	69.6
30min	74.0	73.8	74.3
1h	73.3	73.2	73.5
2h	71.0	70.7	71.3
3h	74.9	74.9	74.9
4h	72.4	72.2	72.6
6h	72.9	72.4	73.5
8h	71.2	71.0	71.4

Figure A 6. *Screening 1, WCA, Open-air, B Wa, T = 24 C, RH% = 56*

Sample Grit Blast with time intervals, a new droplet in each value

Measurement in practice: according to Protocol FIN-SW

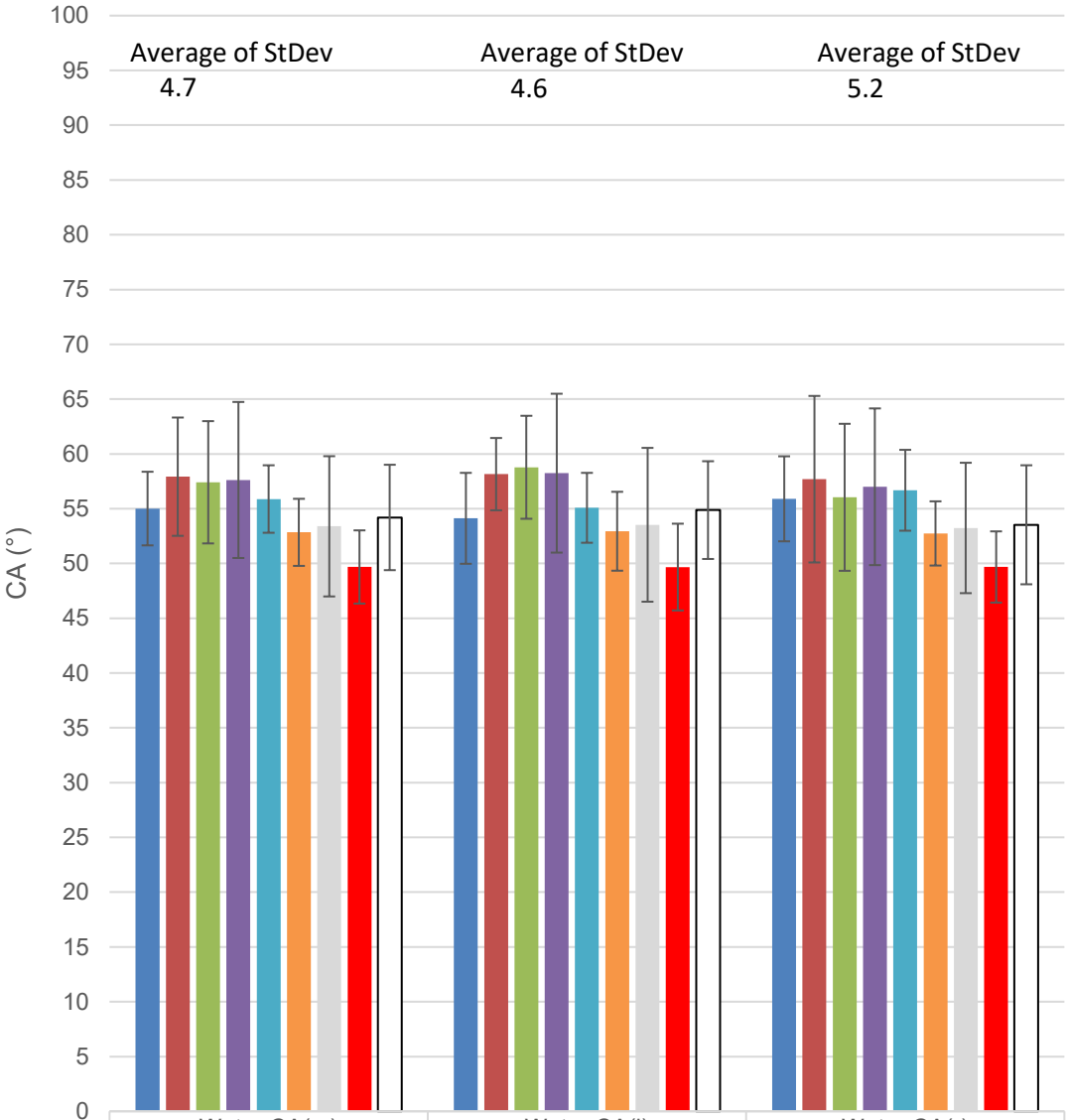

	Water CA(m)	Water CA(l)	Water CA(r)
0min	55.0	54.1	55.9
15min	57.9	58.2	57.7
30min	57.4	58.8	56.0
1h	57.6	58.2	57.0
2h	55.9	55.1	56.7
3h	52.8	52.9	52.7
4h	53.4	53.5	53.2
6h	49.7	49.7	49.7
8h	54.2	54.9	53.5

Figure A 7. *Screening 1, WCA, Open-air, Grit Blast, T = 24 C, RH% = 56*

APPENDIX B: SCREENING 2

CWP – FIN – 10.9.2021

Material: laminate based on prepreg 3501-6/AS4 UD (3M 300D disc)

Sample A Light 2 with time intervals, a new droplet in each value

Measurement in practice: according to Protocol FIN-SW

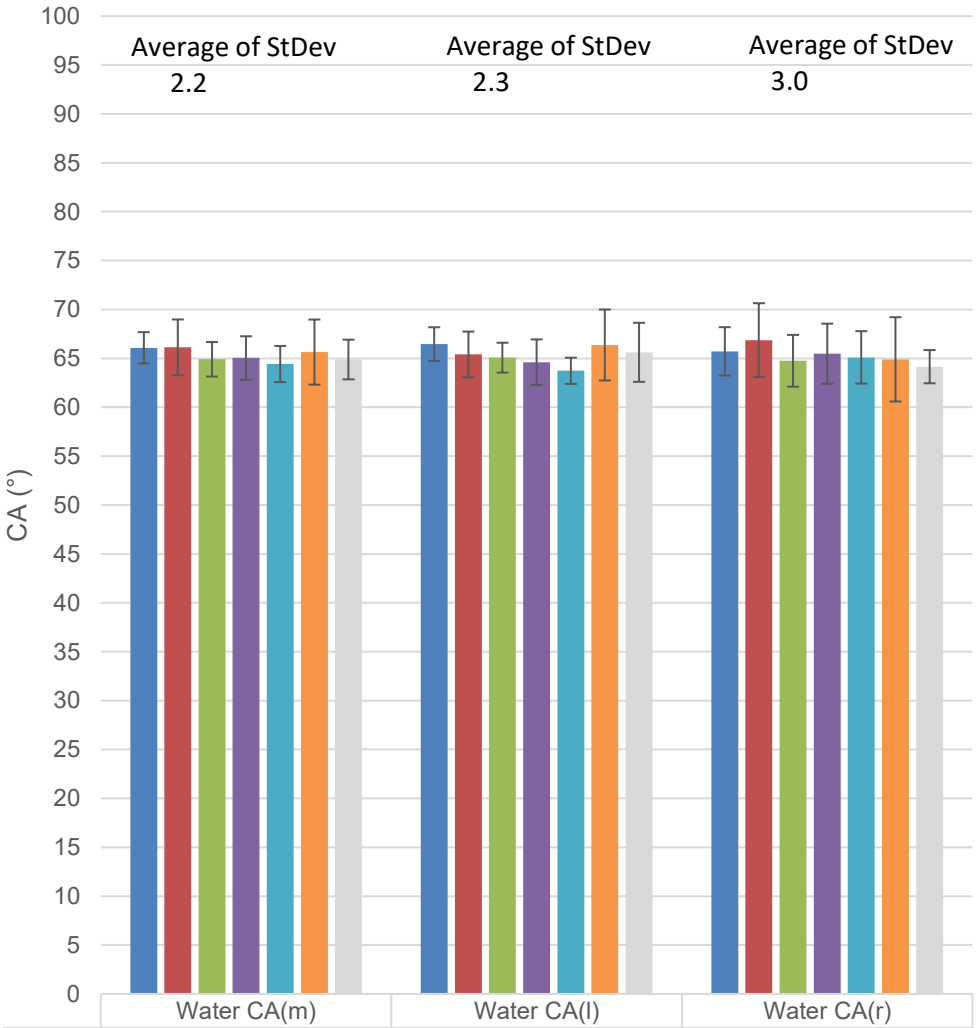

	Water CA(m)	Water CA(l)	Water CA(r)
0min	66.1	66.5	65.7
15min	66.1	65.4	66.9
30min	64.9	65.1	64.8
1h	65.0	64.6	65.5
2h	64.4	63.7	65.1
3h	65.6	66.4	64.9
4h	64.9	65.6	64.2

Figure B 1. *Screening 2, Water CA, Open-air, A Light 2, T = 24 C, RH% = 51*

Sample A Hard 2 with time intervals, a new droplet in each value

Measurement in practice: according to Protocol FIN-SW

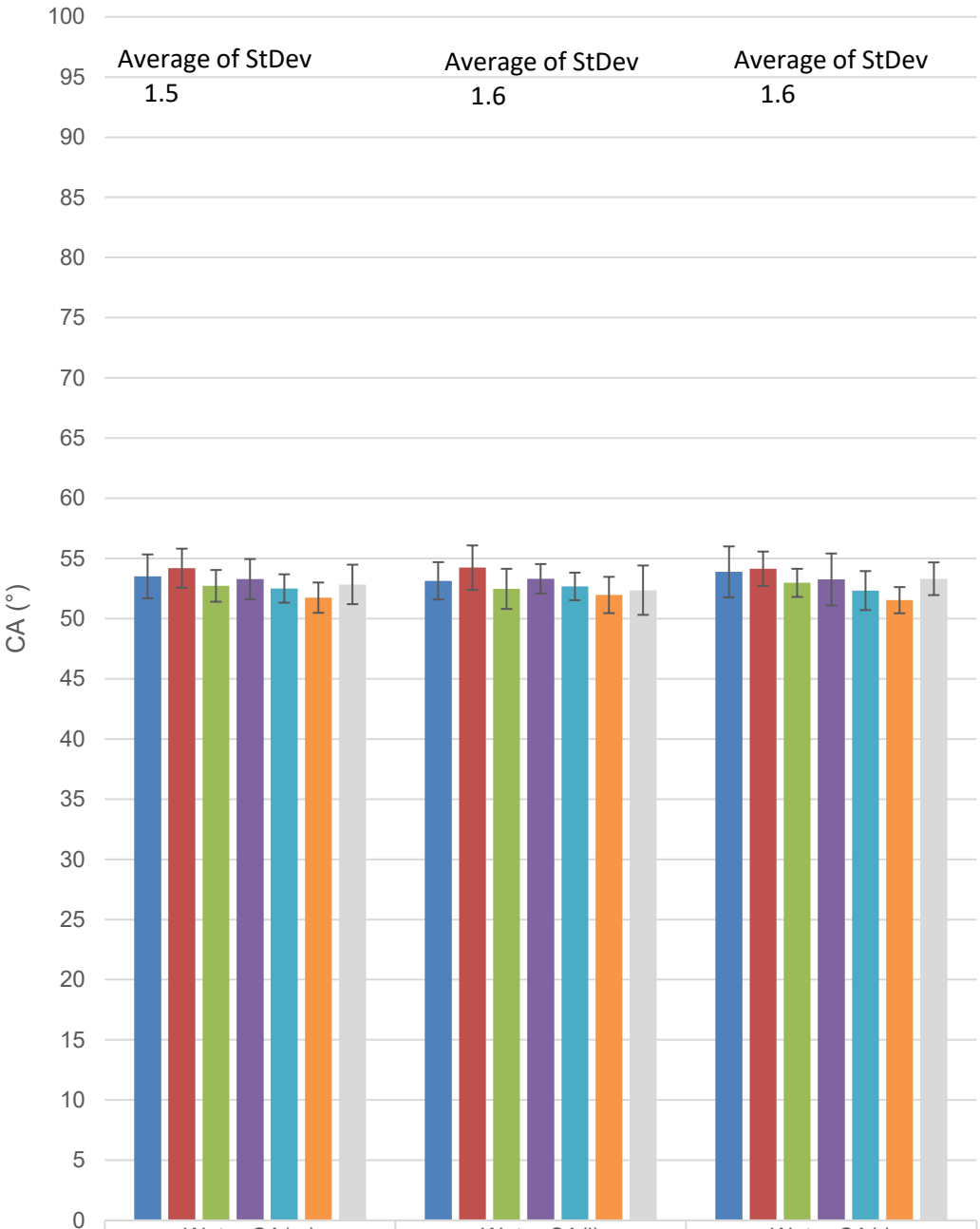

	Water CA(m)	Water CA(l)	Water CA(r)
0min	53.5	53.1	53.9
15min	54.2	54.2	54.1
30min	52.7	52.5	53.0
1h	53.3	53.3	53.3
2h	52.5	52.7	52.3
3h	51.7	52.0	51.5
4h	52.8	52.4	53.3

Figure B 2. *Screening 2, WCA, Open-air, AHard 2, T = 24 C, RH% = 51*

Sample A Med 2 with time intervals, a new droplet in each value

Measurement in practice: according to Protocol FIN-SW

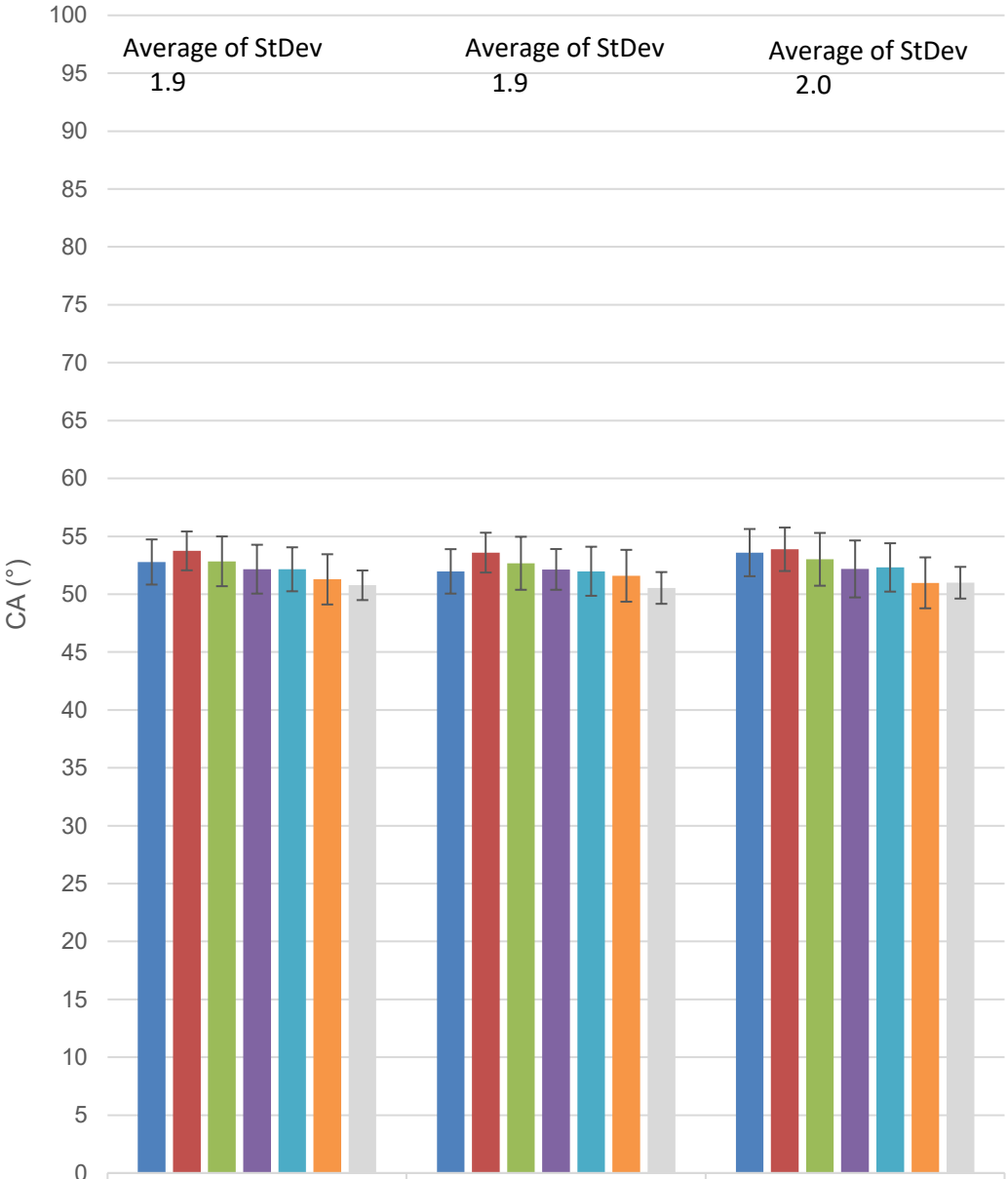

	Water CA(m)	Water CA(l)	Water CA(r)
0min	52.8	52.0	53.6
15min	53.7	53.6	53.9
30min	52.8	52.7	53.0
1h	52.2	52.1	52.2
2h	52.2	52.0	52.3
3h	51.3	51.6	51.0
4h	50.8	50.5	51.0

Figure B 3. *Screening 2, WCA, Open-air, A Med 2, T = 24 C, RH% = 50*

Sample B Med 2 with time intervals, a new droplet in each value

Measurement in practice: according to Protocol FIN-SW

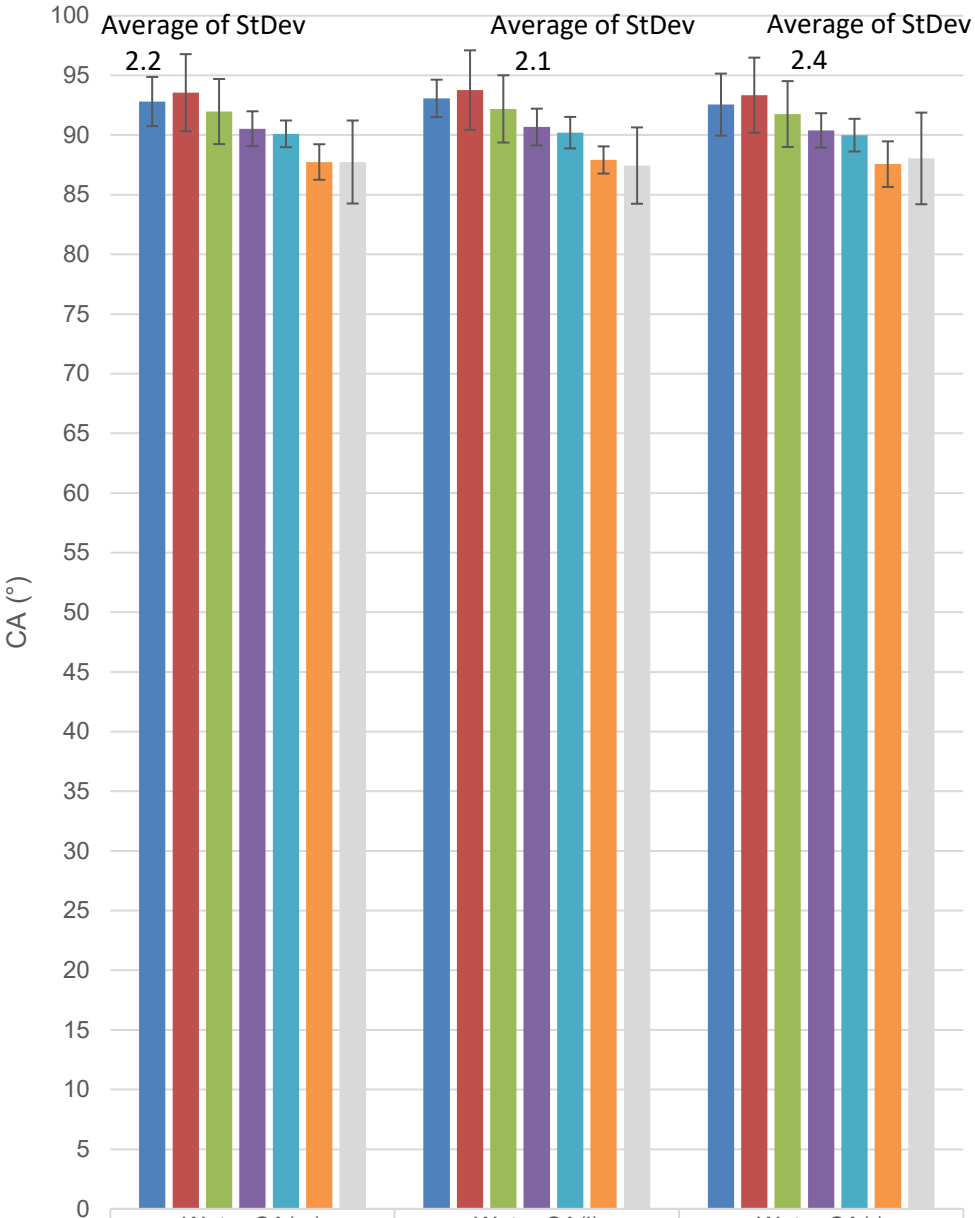

	Water CA(m)	Water CA(l)	Water CA(r)
0min	92.8	93.1	92.6
15min	93.6	93.8	93.3
30min	92.0	92.2	91.8
1h	90.5	90.7	90.4
2h	90.1	90.2	90.0
3h	87.7	87.9	87.6
4h	87.7	87.4	88.0

Figure B 4. *Screening 2, WCA, Open air, B Med 2, T = 24 C, RH% = 55*

Sample B Wa 2 with time intervals, a new droplet in each value

Measurement in practice: according to Protocol FIN-SW

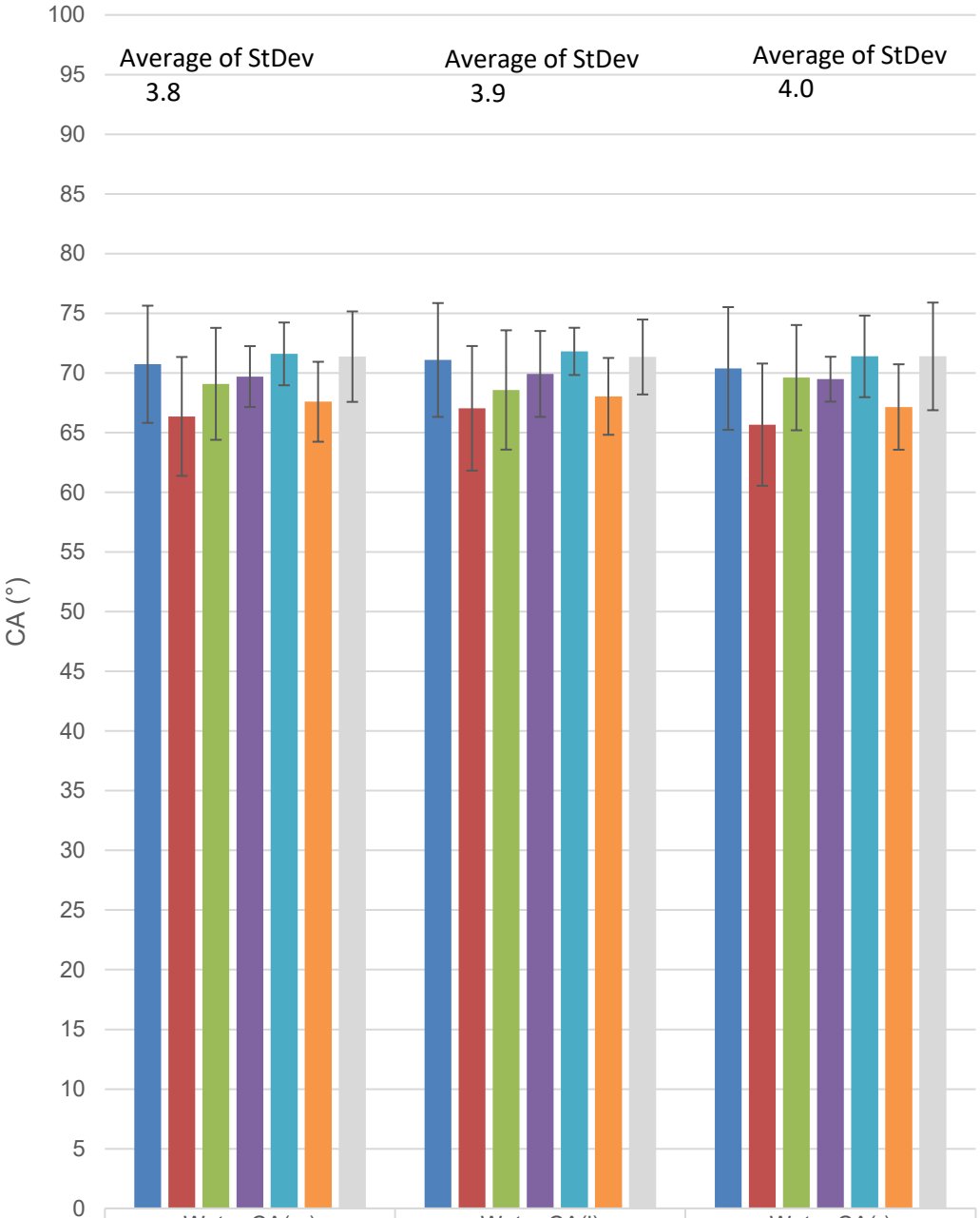

	Water CA(m)	Water CA(l)	Water CA(r)
0min	70.7	71.1	70.4
15min	66.4	67.0	65.7
30min	69.1	68.6	69.6
1h	69.7	69.9	69.5
2h	71.6	71.8	71.4
3h	67.6	68.0	67.2
4h	71.4	71.3	71.4

Figure B 5. *Screening 2, WCA, Open air, B Wa 2, T = 24 C, RH% = 55*

Sample Grit Blast 2 with time intervals, a new droplet in each value

Measurement in practice: according to Protocol FIN-SW

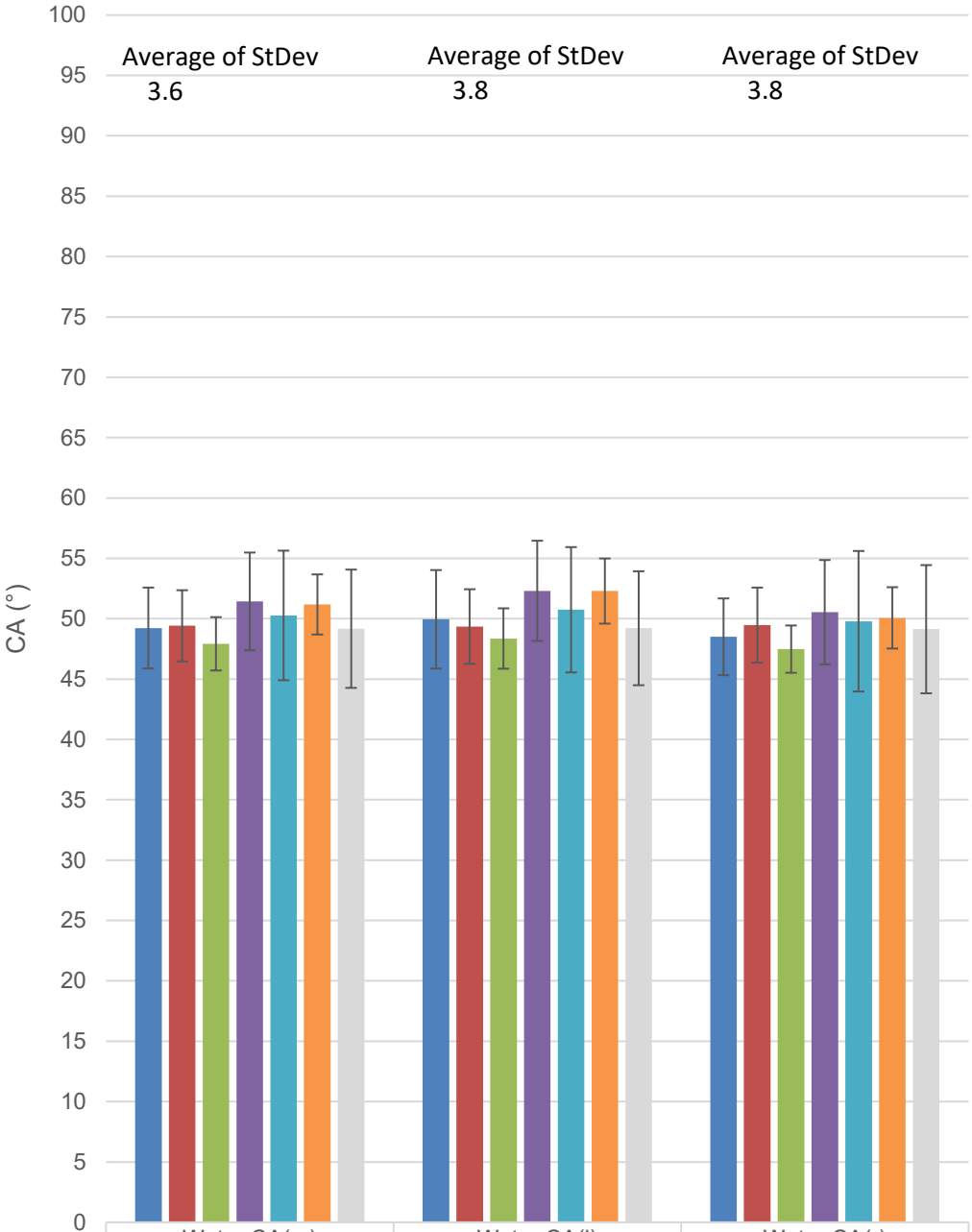

	Water CA(m)	Water CA(l)	Water CA(r)
0min	49.2	50.0	48.5
15min	49.4	49.4	49.5
30min	47.9	48.4	47.5
1h	51.4	52.3	50.5
2h	50.3	50.7	49.8
3h	51.2	52.3	50.1
4h	49.2	49.2	49.1

Figure B 6. *Screening 2, WCA, Open-air, Grit Blast 2, T = 24 C, RH% = 51*

APPENDIX C: FIGURES OF SAMPLES

This appendix contains figures of the samples used in the open-air screenings. The same type of treatment is represented in the same figure.

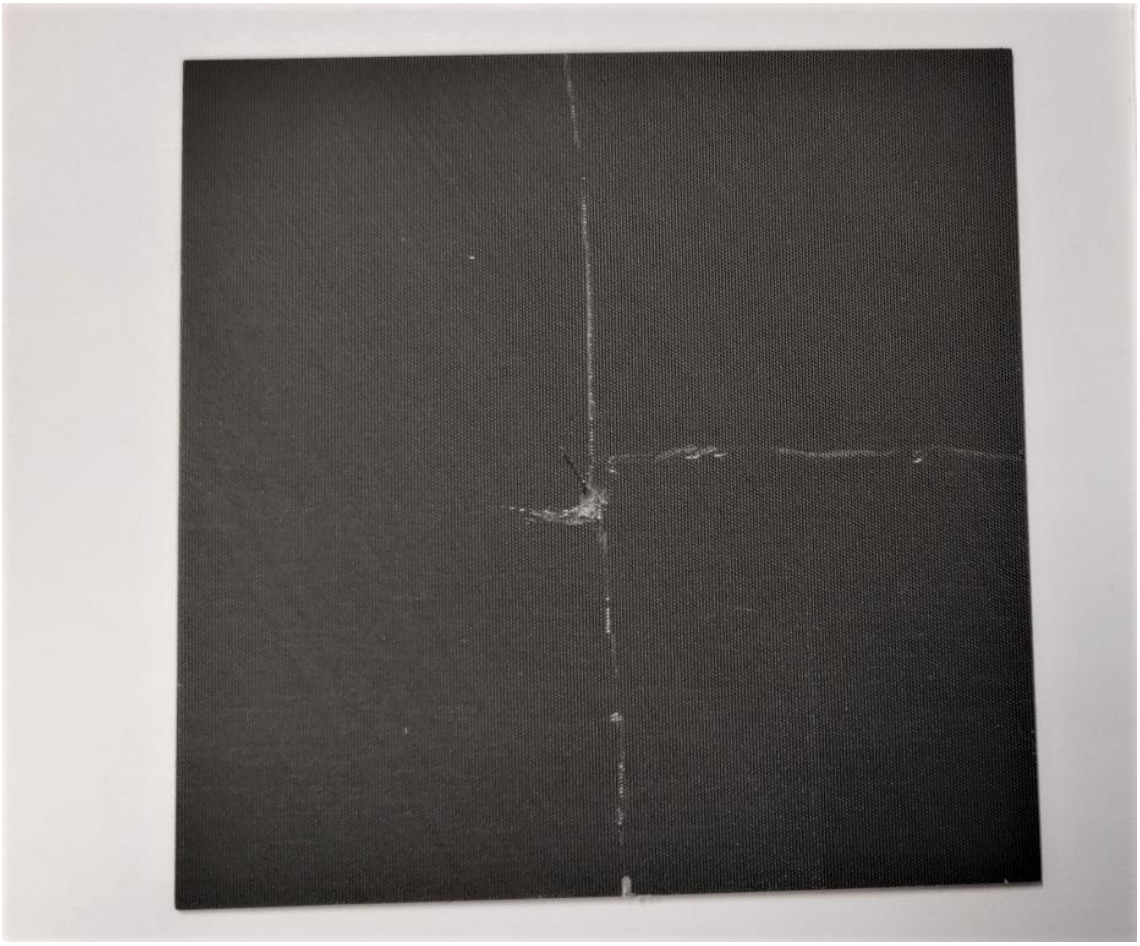

Figure C 1. *Screening 1, PPR0*

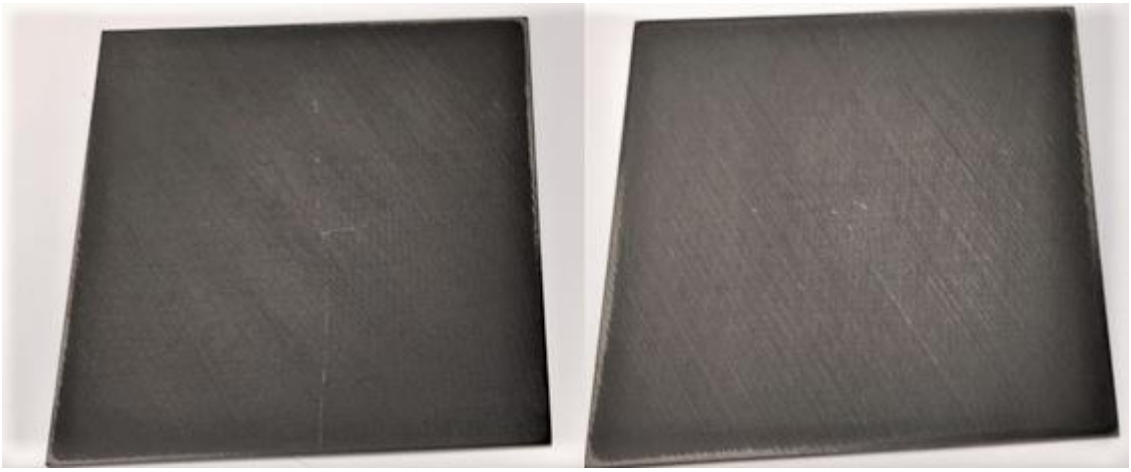

Figure C 2. *Screening 1, A Light (left). Screening 2, A Light 2 (right)*

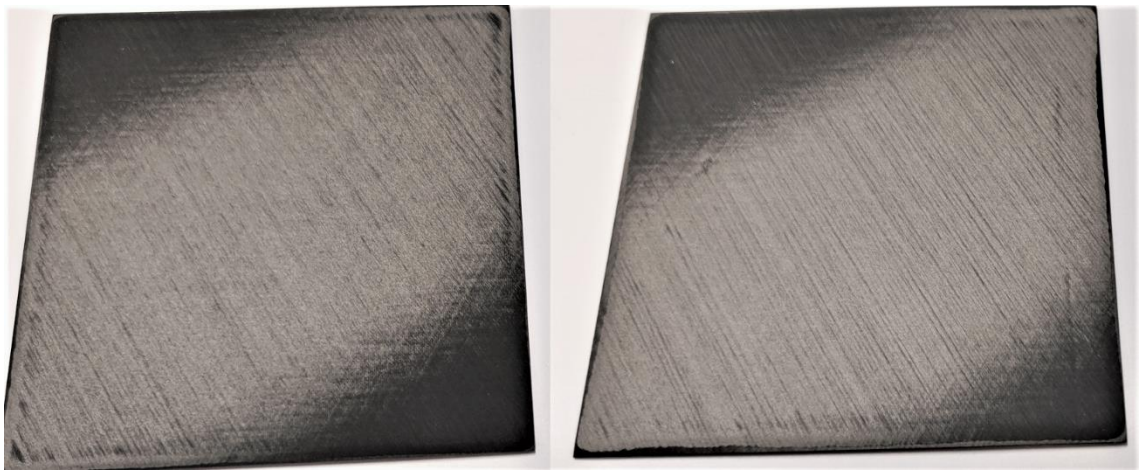

Figure C 3. *Screening 1, A Hard (left). Screening 2, A Hard 2 (right)*

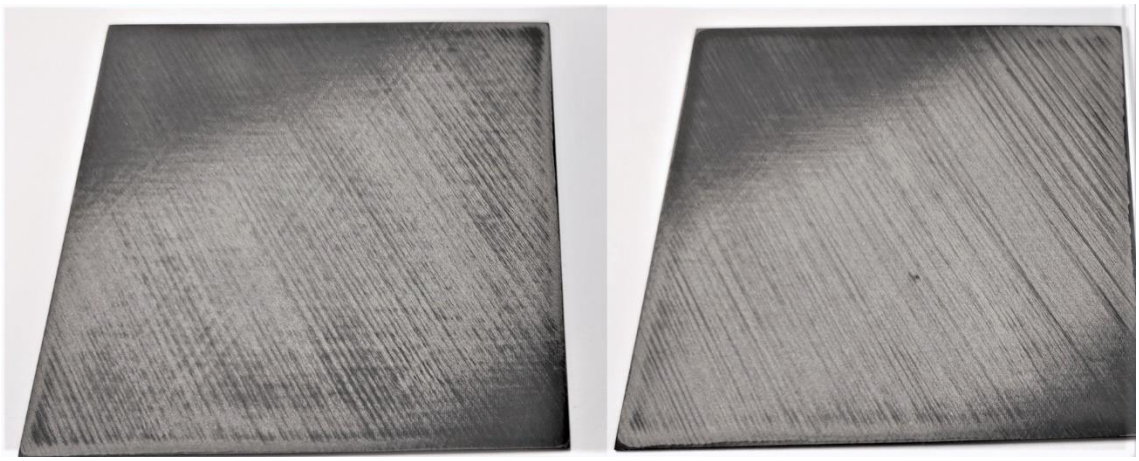

Figure C 4. *Screening 1, A Med (left). Screening 2, A Med 2 (right)*

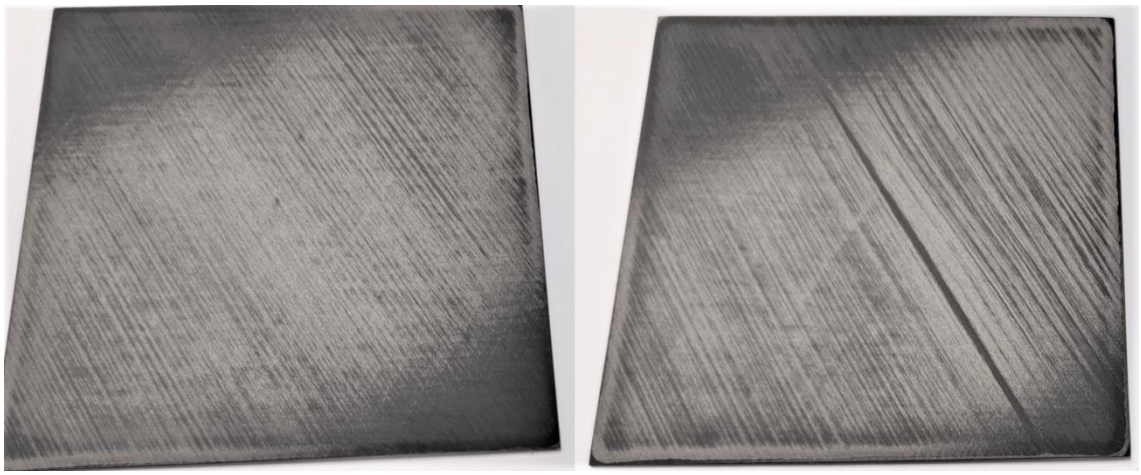

Figure C 5. *Screening 1, B Med (left). Screening 2, B Med 2 (right)*

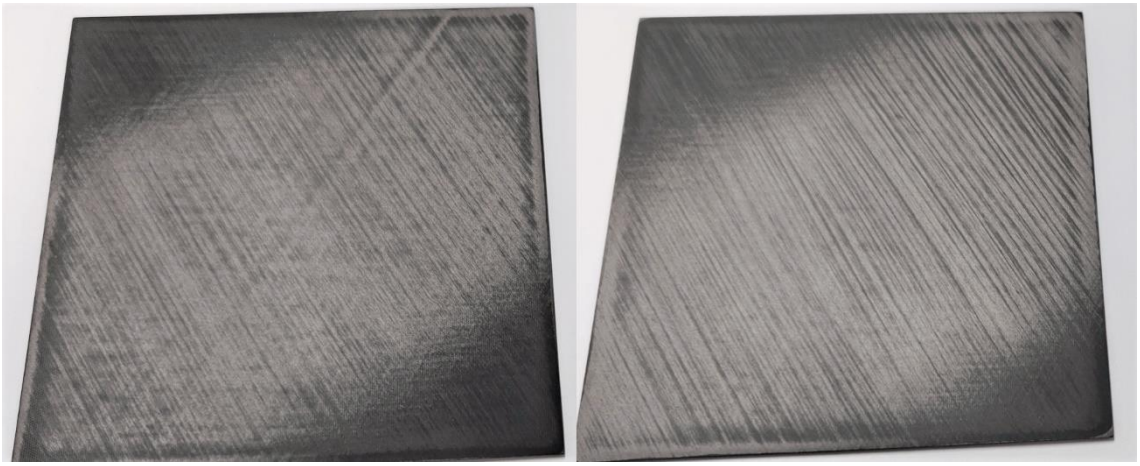

Figure C 6. *Screening 1, B Wa (left). Screening 2, B Wa 2 (right)*

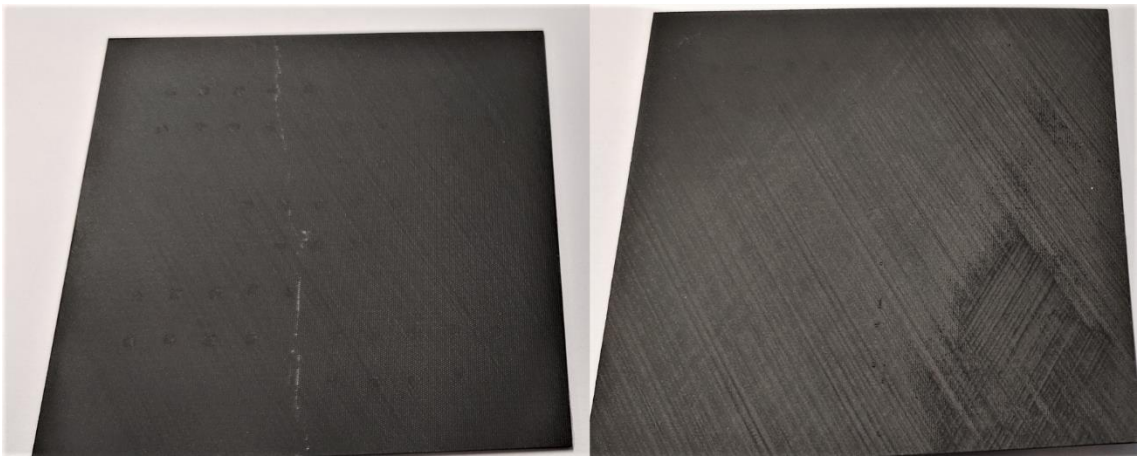

Figure C 7. *Screening 1, Grit Blast (left). Screening 2, Grit Blast 2 (right)*

APPENDIX D: STUDENT'S T-TESTS

This appendix contains the results of the t-tests. They are represented as confidence that there is a statistically significant difference between the measured values of the two samples.

Table D 1. *Confidence that there is a difference between the WCA values of different samples from SFE measurements using a t-test, a confidence of 95% should be reached for the difference to be statistically significant*

T-TEST	GritBlast	B Wa	B Med	A Hard	A Med	A Light
PPR0	100 %	100 %	100 %	100 %	100 %	93 %
A Light	100 %	100 %	100 %	100 %	100 %	
A Med	100 %	77 %	100 %	88 %		
A Hard	100 %	68 %	100 %			
B Med	100 %	100 %				
B Wa	100 %					

Table D 2. *Confidence that there is a difference between the Glycerol CA values of different samples from SFE measurements using a t-test, a confidence of 95% should be reached for the difference to be statistically significant*

T-TEST	GritBlast	B Wa	B Med	A Hard	A Med	A Light
PPR0	100 %	100 %	100 %	100 %	100 %	67 %
A Light	100 %	100 %	100 %	100 %	100 %	
A Med	77 %	100 %	100 %	27 %		
A Hard	83 %	100 %	100 %			
B Med	53 %	71 %				
B Wa	77 %					

Table D 3. *Confidence that there is a difference between the Ethylene glycol CA values of different samples from SFE measurements using T-test, a confidence of 95% should be reached for the difference to be statistically significant*

T-TEST	GritBlast	B Wa	B Med	A Hard	A Med	A Light
PPR0	100 %	100 %	100 %	100 %	100 %	100 %
A Light	100 %	100 %	100 %	100 %	100 %	
A Med	100 %	100 %	100 %	10 %		
A Hard	100 %	100 %	100 %			
B Med	100 %	72 %				
B Wa	100 %					

Table D 4. *Confidence that there is a difference between the Diiodomethane CA values of different samples from SFE measurements using a t-test, a confidence of 95% should be reached for the difference to be statistically significant*

T-TEST	GritBlast	B Wa	B Med	A Hard	A Med	A Light
PPR0	59 %	98 %	100 %	100 %	100 %	71 %
A Light	29 %	99 %	100 %	100 %	100 %	
A Med	85 %	100 %	100 %	100 %		
A Hard	78 %	100 %	100 %			
B Med	41 %	80 %				
B Wa	29 %					

Table D 5. *Confidence that there is a difference between the WCA values of different samples from Screening 1 using a t-test, a confidence of 95% should be reached for the difference to be statistically significant*

T-TEST	GritBlast	B Wa	B Med	A Hard	A Med	A Light
PPR0	100 %	99 %	99 %	100 %	100 %	100 %
A Light	100 %	96 %	100 %	100 %	100 %	
A Med	99 %	100 %	100 %	75 %		
A Hard	100 %	100 %	100 %			
B Med	100 %	100 %				
B Wa	100 %					

Table D 6. *Confidence that there is a difference between the WCA values of different samples from Screening 2 using a t-test, a confidence of 95% should be reached for the difference to be statistically significant*

T-TEST	GritBlast	B Wa	B Med	A Hard	A Med	A Light
PPR0	100 %	100 %	97 %	100 %	100 %	100 %
A Light	100 %	88 %	100 %	100 %	100 %	
A Med	90 %	100 %	100 %	43 %		
A Hard	95 %	100 %	100 %			
B Med	100 %	100 %				
B Wa	100 %					

Table D 7. *Open-air contamination samples, a confidence that there is a difference between 0min and 15min values compared to 3h and 4h values, 95% confidence needed for the difference to be statistically significant*

T-TEST	PPR0	A Light	A Med	A Hard	B Med	B Wa	GritBlast
Screening 1	42 %	83 %	86 %	63 %	40 %	97 %	83 %
Screening 2		37 %	95 %	98 %	100 %	50 %	34 %